NTNU

Norwegian University of
Science and Technology

Simultaneous precipitation of Calcium Sulfate and Calcium Carbonate during MEG regeneration

Therese Bache

Chemical Engineering and Biotechnology
Submission date: August 2016
Supervisor: Jens-Petter Andreassen, IKP
Co-supervisor: Xiaoguang Ma, IKP

Norwegian University of Science and Technology
Department of Chemical Engineering

Preface

This master thesis was performed during the spring 2016 and was given by the Department of Chemical Engineering (IKP) at the Norwegian University of Science end Technology (NTNU).

Firstly, I would like to thank my main advisor, professor Jens-Petter Andreassen, for support, whenever needed, great discussions and help understanding the complexity of crystallization. I have truly enjoyed working with you in this amazingly interesting field of study. Post.doc Xiaoguang Ma, my co-advisor, deserves a lot of gratitude. You have always been there for me, helping with everything from handling of large gas containers to great discussions of both scientific and non-scientific topics.

I would like to thank engineer Sergey Khromov for help with the SEM and Kristin Høydalsvik and Magnus Rotan for help with the XRD analyzes.

Seniz, thanks for keeping everything in order, in a somewhat chaotic environment in the labs. Ragnhild and Bjørnar, without you the crystallization group wouldn't be the same.

Thank you Silje, Siri Marthe, Gøril and Ole for keeping my motivation up in tough periods, and thank you Silje, Trond and dad for proofreading the work. Thank you mom, for listening and calming me down.

Trond, thank you for always beeing there for me.

This Master Thesis' was written on behalf of the Department of Chemical Engineering (IKP) at the Norwegian University of Science and Technology (NTNU) during spring 2016.

I hereby declare that this work is done independently and in accordance with the exam regulations at NTNU.

Trondheim, August 22, 2016

Therese Bache

Abstract

Simultaneous precipitation of calcium carbonate and calcium sulfate in supersaturated solutions containing a MEG-water concentration containing 0, 50 or 90 wt % MEG, was investigated in a bath setup at constant pressure and two different temperatures, T = 30 and T = 65 °C. The pH and temperature was monitored and logged automatically during the experiments, samples were taken out to titrate to find the concentration of calcium in the bulk solution, and samples were filtered out, first after precipitation had occured, and then at the end of the experiment, to determine the content of the crystals by XRD and SEM. Experiments to determine whether calcium sulfate precipitation was dependent on pH decrease was also done.

The pH was found to only decrease with precipitation of calcium carbonate, and not for calcium sulfate, making it a good indicator for which salt precipitates at a given time. It was further found that 0 and 50 wt % MEG concentrations favors precipitation of gypsum at both temperatures. Solvents with 90 wt % MEG favored precipitation of anhydrite for both temperatures.

The presence of MEG in the solvent was found to inhibit nucleation and growth of both calcium sulfate and calcium carbonate crystals. The size of the crystals found with increasing concentration of MEG were found to decrease. The amount of crystals found in the bulk solution at the end of an experiment was also decreased with increasing MEG concentration.

The amount and size of the precipitated crystals increased with increasing temperature.

The transition between gypsum and anhydrite was found to favor anhydrite at 90 wt % MEG, and gypsum for lower MEG concentrations. For T = 65 °C and T = 30 °C the transition occurred between 90 and 50 wt % MEG. Anhydrite was only found at 90 wt % MEG for both temperatures, and not at lower MEG concentrations.

High saturation ratios gave large crystals of calcium sulfate, and only small amounts of calcium carbonate. Low saturation ratios, $SR_{CaSO_4} = 1$ only resulted in calcium carbonate precipitation.

Both calcium and sulfate concentrations affect the expected amount of precipitation of both calcium sulfate and calcium carbonate. Further, both calcium and sulfate concentrations must be sufficiently high to give a desired yield of precipitate.

Sammendrag

Simultan utfelling av kalsiumkarbonat og kalsiumsulfat i løsninger inneholdende en konsentrasjon av MEG og vann på 0, 50 eller 90 vekt % MEG, ble undersøkt i et batchoppsett ved konstant trykk og ved to forskjellige temperaturer, T = 30 og T = 65 °C. pH og temperatur ble monitorert og registrert automatisk under forsøkene, prøver ble tatt ut for titrering for å finne konsentrasjonen av kalsium i bulkløsning, og prøver ble først filtrert ut etter at utfelling hadde skjedd, og så ved slutten av eksperimentet for å bestemme innholdet i krystallene ved bruk av XRD og SEM. Forsøk for å finne ut om pH ble redusert ved utfelling av kalsiumsulfat ble også gjort.

pH-verdien ble funnet til kun å avta ved utfelling av kalsiumkarbonat, og ikke for kalsiumsulfat, slik at pH målinger er en god indikator for hvilket salt som utfelles på et gitt tidspunkt. Det ble videre funnet at løsninger med 0 og 50 vekt % MEG favoriserer utfelling av gips (eng=gypsum) ved begge temperaturer. Løsninger med 90 vekt % MEG favoriserte utfelling av anhydritt for begge temperaturer.

Nærværet av MEG i løsningen, ble funnet å hemme nukleering og vekst av både kalsiumsulfat- og kalsiumkarbonat-krystaller. Størrelsen på krystallene ble funnet til å avta med økende konsentrasjon av MEG. Mengden av krystaller som ble funnet i bulkløsning ved slutten av et forsøk ble også redusert med økende konsentrasjon av MEG.

Mengde og størrelse av de utfelte krystallene økte med økende temperatur.

Overgangen mellom gips og anhydritt ble funnet å favorisere anhydritt ved 90 vekt % MEG, og gips for lavere MEG-konsentrasjoner. For T = 65 og T = 30 °C skjedde overgangen mellom 90 og 50 vekt % MEG. Anhydritt ble bare funnet i 90 vekt % MEG for begge temperaturer, og ikke ved lavere MEG konsentrasjoner.

Høye metningsforhold ga store krystaller av kalsiumsulfat, og bare små mangder av kalsiumkarbonat. Lavt metningsforhold, $SR_{CaSO_4} = 1$ resulterte kun i kalsiumkarbonat utfelling.

Både kalsium- og sulfat-konsentrasjonene påvirker mengden av forventet utfelling av både kalsiumsulfat og kalsiumkarbonat. Videre ble det funnet at både kalsium- og sulfat-konsentrasjonene må være høye nok for å gi et ønsket utbytte av de utfelte saltene.

Contents

List of Figures

List of Tables

CHAPTER 1

Introduction

In the production of oil and gas, some water containing different dissolved salts is also produced. Scale is the deposition of a mineral layer on a surface, and the precipitation of dissolved salts from the produced water, can act as a scale layer on equipment. Scaling may cause blocking of some pipelines, since the growth of the mineral layer may reduce the radius of the pipes. The blockage can lead to reduced production rate, and in some cases the production has to stop due to safety issues. A shut down in production is a huge cost, and understanding precipitation and scaling is of high interest [7].

For a salt to precipitate and form into a crystal, atoms have to arrange themselves into different arrangements, called polymorphs [3]. In order for scale to form, salts have to precipitate. To precipitate a salt, the solution must contain more dissolved ions present than what is needed at equilibrium, which gives a supersaturated solution. To achieve supersaturation, the temperature, alkalinity, pressure and concentration can be changed [9].

Gas hydrates formation is a problem in the oil and gas industry, and inhibiting the formation of gas hydrates is of importance. "A gas hydrate is a

crystalline solid with a gas molecule surrounded by a cage of water molecules" [7]. To inhibit the formation of these gas hydrates alcohols can be used. Mono Ethylene Glycol, MEG, is a commonly used inhibitor, which functions as an antifreeze agent, lowering the freezing point of the gas hydrates.

MEG is regenerated onshore, and reused in the production. Figure 1.1 show an illustration of the MEG-loop. Rich MEG which is consisting of high amounts of dissolved salts and water is regenerated to a lean MEG, consisting of only small amounts of water [1].

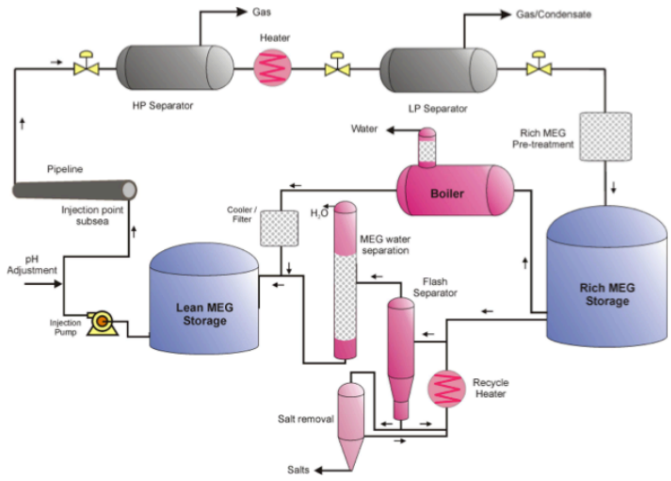

Figure 1.1 – Illustration of a MEG-loop [1].

Calcium carbonate is one of the most common salts contributing to the formation of scale. Calcium carbonate is a sparingly soluble salt, which favours precipitation on heat exchangers [10]. It crystallizes into three different polymorphs, with distinct crystal lattices, called calcite, vaterite and aragonite. Calcite is the most stable form, and aragonite is the least stable form. Studies of calcium carbonate precipitation in the presence of MEG has been previously studied by Flaten [11], [12].

Calcium sulfate is another salt contributing to scaling in the oil and gas industry [8] since it also is a sparingly soluble salt [10]. Calcium sulfate precipitates into anhydrite, hemihydrite and dihydrate [13]. Only anhydrite and gypsum will be precipitated in this work.

Simultaneous precipitation of calcium carbonate and calcium sulfate is not much studied. It is assumed that the mechanisms for precipitation and scaling might be different for different salts, and that the simultaneous precipitation of two salts might affect the thermodynamics and kinetics for a given salt, making it important to investigate the occurrence of any changes [10].

The experimental setup and procedure in this work is based on the specialization project work of fall 2015 by Bache [14]. In this work, both solutions containing ions, were preheated and bubbled before mixed at the start of the experiment. Both temperature and pH were automatically measured during the experiments.

Objective

The objective of this work is to investigate the simultaneous precipitations of two salts with a common cation in both MEG containing solvents and pure water solvent. Hopefully, during this work some of the complexity of simultaneous precipitation will be understood by analyzing the crystals by Powder X-ray Diffraction, XRD, Scanning Electron Microscope, SEM, titration and pH plotted curves. By combining the mentioned analyzing tools, polymorphism and morphology for precipitated calcium carbonate at different conditions will be investigated. It will also be tried to determining which phase of calcium sulfate precipitates at different conditions.

Knowing that both MEG concentration and temperature effect the precipitation of the salts, this work will give a clearer understanding of simultaneous precipitation.

CHAPTER 2

Theory

In this section relevant theory regarding basic crystalline matter, supersaturation, nucleation, crystal growth, the calcium carbonate system and the calcium sulfate system is presented. At the end of the section, different analyzing techniques used to determine polymorphism and morphology will be described.

2.1 Crystalline Matter

Solid matter can be characterized either as crystalline or amorphous. A crystalline matter consists of an arrangement of building blocks, which can either be atoms, ions or molecules. The building blocks have a high degree of internal regularity, hence the arrangement into a fixed lattice. This give rise to the structure of a crystal[3]. Amorphous materials however, do not arrange themselves in a regular pattern, giving the amorphous materials a high degree of randomness. The smallest repetitive arrangements in the crystal are called unit cells, and different unit cells give the crystals their specific crystal lattice. The crystal system can be split into seven groups, where the distinct relationship between the length of the axes and their corresponding angels differs from

group to group. The different systems; cubic, hexagonal, tetragonal, rhombohedral, orthorhombic, monoclinic and triclilnic, all have specific symmetries, appearances and packing capabilities [9].

Polymorphism and Morphology

Crystals rarely look exactly the same, even though they have the same internal structure. Different factors, such as which components are present and the growth conditions, contribute to the final appearance of the crystal. The crystal habit leads to a high degree of individuality in how the final appearance of the crystal turns out. Factors that contribute to the individuality is rapid growth in one direction, giving an elongated growth resulting in a needle-shaped crystal, or stunting (=reduced growth rate) in another direction [9].

A material that can be expressed by more than one crystal structure, is called a polymorph. These structures appear very different because of their different crystal structures. Different polymorphs might appear in different shapes, which is called morphology. At macro scale this appearance is due to different growth environment. Because the outer appearance of the crystal can be a result of different factors, such as local growth rate, polymorphism, nucleation, agglomeration, phase transformation, with more, X-ray diffraction (XRD) patterns are necessary to identify and distinguish between the possible polymorphs of the crystal [4]. A unit crystal is a crystal where the arrangement of the atoms is repeated throughout the entire structure without interruptions. Most crystalline matters are polycrystalline, they consist of many smaller crystals, or grains, with different crystallographic orientation [4].

The most stable polymorph is the one with the lowest free energy at a given time, which also has the lowest solubility product, K_{SP}. According to Ostwald's rule of stages, the most soluble polymorph, the least stable stage, precipitates first and then redissolves, before the next polymorph, which has a higher stability, precipitates. At the end, only the most stable polymorph can be found if all of the other polymorphs have dissolved [3]. An explanation to

this phenomena is that the reactions with the fastest growth/nucleation rate will dominate the deposition in the beginning, and that the system over time will move towards the most thermodynamical stable phase[3].

Defects and Dislocations

Crystalline defects, expressed as irregularities from the repeating structure, are present in most crystalline matter. These imperfections can be separated into point defects and line defects. Point defects impact only one local area of the unit cell. It can either be an atom missing from the unit cell, called vacancy, or a point where an atom has latched itself into a place in the regular lattice, that should have been unoccupied, called self-interstitial if the extra atom is of the same as the rest of the building blocks in the lattice [9]. Foreign atoms in the lattice structure can change the properties of the crystal.

The line defects cause the entire structure to be missaligned. A screw dislocation is the creation formed by an applied shear stress perpendicular to the direction of movement. The result is that a part of the crystal is being shifted one atomic distance relative to the rest of the crystal. When the shear stress is applied parallel to the direction of motion, an edge dislocation is formed. This is an existence of an extra plane, or a portion of one, where the edge of the plane terminates inside the crystal [4].

2.2 Supersolubility and Driving Force

In order for a crystal to form in a liquid the solution has to reach a supersaturated state, where there is more dissolved solid in the solution than at equilibrium conditions for a given temperature. Supersaturation is essential for crystallization. At low supersaturations however, it may not alone be effective enough to induce crystallization. Ostwald introduced terms such as "labile" and "metastable" to classify supersaturation in solutions that promote primary nucleation and solutions that do not promote primary nucleation, respectively[3]. The relationship between supersaturation and sponta-

neous crystallization is shown in figure 2.1. Figure 2.1 shows the metastable

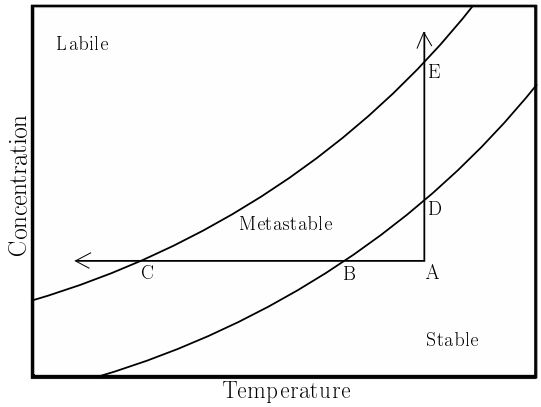

Figure 2.1 – The solubility-supersolubility diagram based on figure from [2].

zone in a solubility-supersolubility diagram. The stable zone is the unsaturated region, and represent the area where no thermodynamic drive for crystallization is present. This means that the supersaturation is less than one. The metastable region is supersaturated, and is where spontaneous crystallization may occur. If a seed or a crystal is placed in this region, it would grow. The labile zone is where crystallization will occur. From the figure we see that lowering the temperature makes it more likely to get into the metastable and labile zone, making crystallization more likely to happen. Increasing the concentration also makes it easier to reach the metastable and labile zone, making crystallization a possibility.

The solubility curve is determined thermodynamically and the supersolubility curve is related to the kinetics of the given system. The cooling/heating rate will have an influence on the width of the metastable area, and the curves will vary according to which components are present in the system.

The Driving Force

The difference in chemical potential of a substance in solution and in solid state is the fundamental driving force for crystallization[3]. The difference in chemical potential, $\Delta\mu$, can be written as equation 2.1

$$\Delta\mu = \mu_1 - \mu_2 \tag{2.1}$$

Here μ_1 and μ_2 are the chemical potentials for a molecule in the crystal and in the solution respectively. If $\Delta\mu > 0$, a driving force for crystallization is established and both nucleation and crystal growth can occur. The chemical potential can be defined as equation 2.2

$$\Delta\mu = \mu_0 + RT \ln a \tag{2.2}$$

Here, μ_0 is the standard potential, a is the activity, R is the universal gas constant, and T is the temperature. Rearranging the equation gives the dimensionless driving force for crystallization, which can be used to express a system where the solution is saturated by solute

$$\frac{\Delta\mu}{RT} = \ln \frac{a}{a^*} = \ln S \tag{2.3}$$

a^* is the activity of the saturated solution, and S is the fundamental supersaturation based on the activities. If $S > 1$ a driving force for crystallization is established. The concentration, c, and the activity are related through an experimentally dependent activity coefficient, γ, defined as equation 2.4

$$a = \gamma c \tag{2.4}$$

The activity coefficient is a measurement of how the solutions deviates from the ideality. An ideal solution will have an activity coefficient equal to 1, and the activity and the concentration will thus be equal. For very dilute system, the activities can be replaced by concentrations [3].

Electrolyte solutions

For electrolyte solutions, such as crystalline matter, the mean ionic activity, $a_{\pm}$ is more appropriate to use than the activity, since the interactions between the ions can be significant even at low concentrations [15].

$$a = a_{\pm}^{v} \tag{2.5}$$

Here $v(= v_+ + v_-)$ is the number of moles of ions in one mole of solute. The mean ionic activity can be written as equation 2.6, where (IAP) is the ion activity product.

$$a_{\pm} = (IAP)^{\frac{1}{v}} = (a_+^{v+} \cdot a_-^{v-})^{\frac{1}{v}} \tag{2.6}$$

The supersaturation for sparingly soluble electrolytes can be expressed in the terms of the ion activity product and the solubility product, $K_a = (a_+^x \cdot a_-^y)$.

$$S_a = \left(\frac{IAP}{K_a}\right)^{\frac{1}{v}} \tag{2.7}$$

By using equation 2.7, equation 2.3 can be rearranged into

$$\frac{\Delta\mu}{RT} = v \ln S_a \tag{2.8}$$

Where the number of ions are accounted for through the term v.

A mean ion activity coefficient, $\gamma_{\pm}$, has to be used for electrolytes, since the electrochemical potentials of ions in solution can't be separated and the activity of a given ion can't be directly measured [15]. This coefficient can be related to measurable quantities, and can thus be calculated through various models. For very dilute solutions, the Debye-Hückel equation can be used.

$$\gamma_{\pm} = -|z_+||z_-|A\sqrt{I} = -|z_+||z_-|A\sqrt{\left(\frac{1}{2}\sum_i c_i z_i^2\right)} \tag{2.9}$$

Where z is the charge number, c is the concentration, A is a solvent - dependent proportional coefficient and I is the ionic strength. Other models must be used in order to find the mean ion activity coefficient if the systems have high ionic strength or very sparingly soluble salts.

Saturation Ratio

The saturation ratio, SR, is another definition used for supersaturation [2], and is defined as:

$$SR = \frac{a_{salt}}{K_a} \tag{2.10}$$

Given salt AB, the saturation ratio can be calculated as equation 2.11 with ions A^+ and B^-

$$SR = \frac{a_{A^+} \times a_{B^-}}{K_{SP}(AB)} \tag{2.11}$$

Here $K_{SP}(AB)$ is the solubility product for the salt AB at equilibrium. The correlation between supersaturation, S, and the saturation ratio, SR, can be described with equation 2.12

$$S(AB) = \sqrt{SR(AB)} \tag{2.12}$$

If $SR > 1$ the salt will be supersaturated and might precipitate. If $SR = 1$ the solution is at equilibrium, and if $SR < 1$ the salt is under-saturated, and dissolution can occur if a solid is present.

2.3 Nucleation

Nucleation is the formation of a cluster of solid bodies, such as embryos, nuclei or seeds, that act as centers for the growth of a crystal[3]. After a supersaturated system is established, clusters of the new crystalline phase, must be formed. To form the clusters, an energy barrier has to be overcome. The formation of a solid phase is energetically stable, but before becoming a solid phase, the clusters need to transition from an interface that is energetically unfavorable. The formed clusters must resist the tendency to redissolve, and at the same time, the clusters need to find each other and form a well-structured lattice.

Nucleation can occur spontaneously or be artificially induced, and can be divided into two groups: primary nucleation and secondary nucleation. Figure 2.2 illustrates the mechanisms of nucleation. Primary nucleation describes a

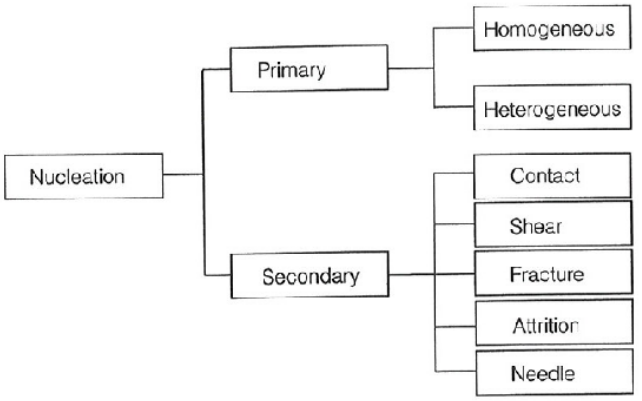

Figure 2.2 – Classification of nucleation [2].

system where no crystalline matter is present and nucleation occurs spontaneously, whereas secondary nucleation describes a system where some crystals are present in a supersaturated solution, and nucleation is induced by the presence of these crystals. Primary nucleation can be divided into homogeneous nucleation and heterogeneous nucleation. Homogeneous nucleation occurs in a pure solution, only consisting of solvent and solute molecules. Heterogeneous nucleation takes place in the presence of impurities, substrates or foreign particles that provide centers for nucleation. Secondary nucleation can be divided into five groups: Contact, Shear, Fracture, Attrition, and Needle nucleation [2].

Homogeneous Nucleation

Homogeneous nucleation can occur when formed clusters have reached a critical size, making them able to withstand the redissolution[3]. The number of molecules in a stable nucleus can vary, but how they organize themselves in a

strict lattice structure is important, and the organization is hard to understand. The molecules may collide with each other, but that is unlikely. A more likely scenario is the sequence of bimolecular additions, following the path shown in equation 2.13.

$$\begin{aligned} A + A &\rightleftarrows A_2 \\ A_2 + A &\rightleftarrows A_3 \\ A_3 + A &\rightleftarrows A_n \end{aligned} \tag{2.13}$$

Due to Brownian motions, solutions with sufficiently high supersaturation forms unstable molecular clusters [3]. When the clusters have reached the critical size, the behavior depends on the size reached. The critical size, r_c, represent the minimum size the nuclei need to reach in order to become stable. Particles smaller than the critical size will redissolve to obtain a reduction in their free energy. Particles larger than r_c will grow. Equation 2.14 shows the relationship between the critical size, the interfacial tension, γ, the volume excess free energy, ΔG_V, and the change in free energy [2].

$$\Delta G_{crit} = \frac{16\pi\gamma^3}{3(\Delta G_v)^2} = \frac{4\pi\gamma r_c^2}{3} \tag{2.14}$$

At the critical size, the change in free energy, ΔG, associated with nucleation is maximized, see figure 2.3. A further addition of ions will lower the free energy, and nucleation and growth will be further promoted. The number of nuclei formed per unit time, is called the rate of nucleation, symbolized with J, which can be expressed as equation 2.15

$$J = A\exp(\frac{-\Delta G}{\mathbf{k}T}) \tag{2.15}$$

A is the Arrhenius pre-exponential factor determined experimentally, $\mathbf{k}$ is the Boltzmann constant, and T is the temperature. Using the basic Gibbs - Thomson relationship for a non-electrolyte in equation 2.16 the free energy can be written with supersaturation as a term, see equation 2.17.

$$\ln S = \frac{2\gamma v}{\mathbf{k}Tr} \tag{2.16}$$

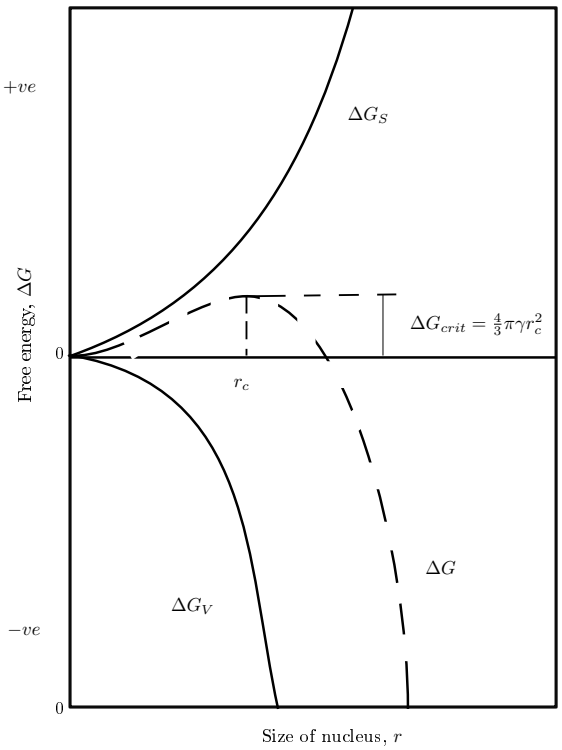

Figure 2.3 – Free energy diagram for homogeneous nucleation based on [2].

$$\Delta G_{crit} = \frac{16\pi\gamma^3 v^2}{3(\mathbf{k}T\ln S)^2} \tag{2.17}$$

The combination of equation 2.15 and 2.17 gives a new equation for the nucleation rate 2.18:

$$J = A\mathbf{exp}\Big[-\frac{16\pi\gamma^3 v^2}{3\mathbf{k}^3 T^3(\ln S)^2}\Big] \tag{2.18}$$

This equation indicates that the three most important variables for changing the nucleation rate is temperature, supersaturation and interfacial tension.

Figure 2.4 shows how the nucleation rate increase if a critical level of supersaturation is exceeded [2].

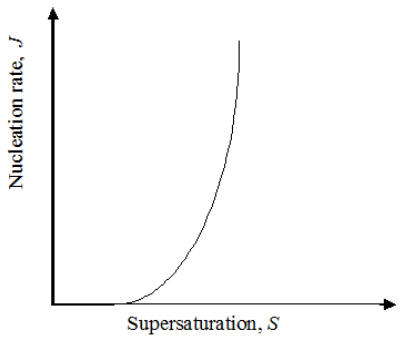

Figure 2.4 – Schematic illustration of the effect of supersaturation on the nucleation rate [2].

Heterogeneous nucleation

If the supersaturation is lower than required for homogeneous nucleation, the presence of foreign objects can induce nucleation. This is called heterogeneous nucleation [2]. The change in free energy for heterogeneous nucleation must be lower than for homogeneous nucleation. The foreign particles can be impurities from poor filtration and/or cleaning of the equipment. The impurities can act as both nucleation inhibitors and accelerators for nucleation and the presence of foreign particles contribute to solid surfaces that nucleate the crystallization processes. The availability of solid surfaces, make the critical energy for nucleation change with a factor of ϕ as seen in equation 2.19. When ϕ is one, homogeneous nucleation occurs, when ϕ equals zero, heterogeneous nucleation

(with seeding of a supersaturated solution), occurs [2].

$$\Delta G_{crit,het} = \phi \Delta G_{crit} \tag{2.19}$$

$\Delta G_{crit,het}$ is the overall free energy change associated with heterogeneous nucleation, and ϕ can be expressed as equation 2.20.

$$\phi = \frac{(2 + \cos\theta)(1 - \cos\theta)^2}{4} \tag{2.20}$$

θ is the contact angle shown in figure 2.5, where a crystalline matter is deposited onto a foreign particle. θ represent the angle between the crystalline matter and the impurity.

The contact angle, can be expressed by Young's equation 2.21, and is shown in figure 2.5. As seen from equation 2.18, interfacial tension impacts the nu-

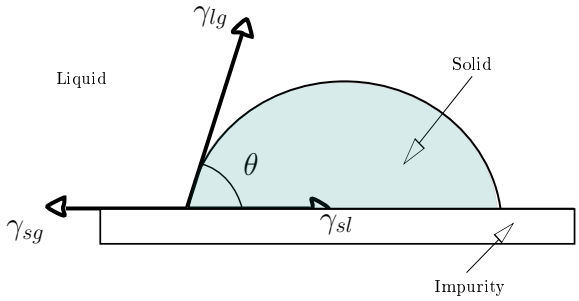

Figure 2.5 – The contact angle between the crystalline deposit and the foreign particle based on [2].

cleation rate. Introducing a foreign surface, that could have a lower interfacial tension between the crystallizing object and the surface, γ_{cs}, gives rise to a lower interfacial tension between the crystallizing object and the liquid, γ. From Young's equation 2.21 the contact angle can be expressed as:

$$cos\theta = \frac{\gamma_s - \gamma_{cs}}{\gamma} \tag{2.21}$$

From this equation it is known that for $0° < \theta < 180°$, the foreign surface will be wetted by the crystallizing object and thus give $\Delta G_{het} > \Delta G$, making heterogeneous nucleation easier, since the overall surface energy required is less than for homogeneous nucleation [4].

Secondary nucleation

Secondary nucleation can be described as contact between the crystallizing components and the supersaturated solution. Collision of particles with agitator blades, reactor wall and/or other particles are examples of how to induce secondary nucleation. The most accepted expression describing secondary nucleation is the one by Giulietti et al., 2001 [2], and can be written as equation 2.22.

$$B_0 = k_n \sigma^b \epsilon^k M_T^j \tag{2.22}$$

Where the secondary nucleation rate is defined as B_0, ϵ is the average power input form the agitator, and is usually associated with the energy for collision. k is in the range of 0.6 to 0.7, M_T is the concentration of the solids, and describes the collision between crystals (j=2) or the collision between crystal and either wall or impeller(j=1). b is usually in the range of 1 to 3, and is the supersaturation dependence.

High supersaturations give rise to more edges and corners on the crystal surface, where attrition can take place, since the surface of the crystal is altered to be more rough. With a rough crystal surface, more steps and dendritic growth can occur. Slow integration into the lattice formes a layer close to the crystal surface. If this layer is partly swept away due to contact or hydrodynamic forces, the torn layer might act as a nuclei for the formation of new crystals.

Induction Time

The induction time is the time elapsed between when supersaturation is achieved and the appearance of detectable crystals [2]. The induction time is influenced

by the level of supersaturation, presence of impurities and other forces promoting nucleation/crystallization. The induction period, t_{ind} may be written as

$$t_{ind} = t_r + t_n + t_g \tag{2.23}$$

The relaxation time, t_r, is the time the system requires to reach a quasi-steady-state distribution of molecular clusters, the nucleation time, t_n, is the time the formation of stable nucleus takes, and the growth time, t_g, is the time when a nucleus grows to a detectable size. Figure 2.6 shows a de-supersaturated curve, where also the latent period, t_{lp}, is shown.

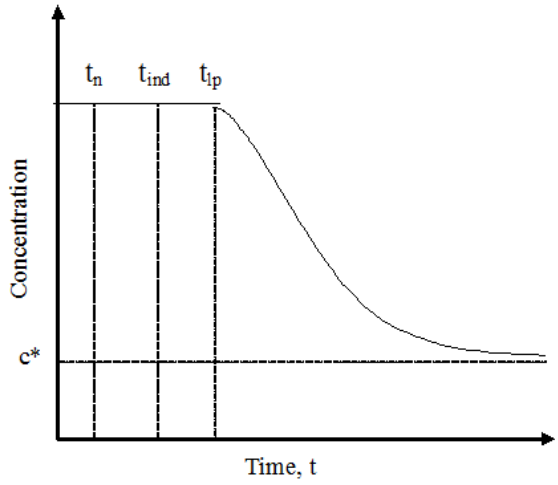

Figure 2.6 – De-supersaturated curve for a batch experiment where t_n is the nucleation time, t_{ind} is the induction time, t_{lp} is the latent period and c^* is the equilibrium saturation. [2].

The latent period is the occurrence of a significant change in the system. The change can be characterized as a lot of nucleation occurrence or some clear evidence that the solution has had an decrease in supersaturation.

2.4 Crystal Growth

When the critical size is reached and the nuclei have become stable, the nuclei enlarge themselves into particles of a detectable size [4]. Several methods for particle growth exist. The diffusion-reaction theory and the adsorption layer theory are two of the most mentioned. A characteristic dimension for the growth of a particle can be identified. The linear growth rate, G, with L as the chosen characteristic length, can be expressed as [2]:

$$G = \frac{dL}{dt} \tag{2.24}$$

Growth Models

The adsorption layer theory is a crystal growth mechanism postulated by Volmer, and is based on an adsorbed layer of solute atoms on a crystal surface [4]. The solute atoms arrive at a crystalline substance and migrate freely over the surface of the crystal, the adsorption layer. Eventually the solute atoms link themselves into the crystal lattice at the active centers. The attractive forces are the strongest at the active centers. The arrival of building units is repeated until the whole surface of the crystal is covered with solute atoms. When no more active sites are present on the surface of the crystal, new "centers of crystallization" must be formed [3]. Secondary nucleation might occur if the adsorbed layer is ripped away from the crystal surface making it act as a new nucleation cite.

The diffusion-reaction model was suggested by Berthoud and Valeton, and suggests a two step process for crystal growth [4]. The first step includes the diffusion of molecules or ions from the bulk solution being transported to the crystal surface. The second step, the surface integration, is a reaction with the surface into the lattice through a first-order reaction and happens at the end of the first step. The principle of mass transfer is presented in figure 2.7.

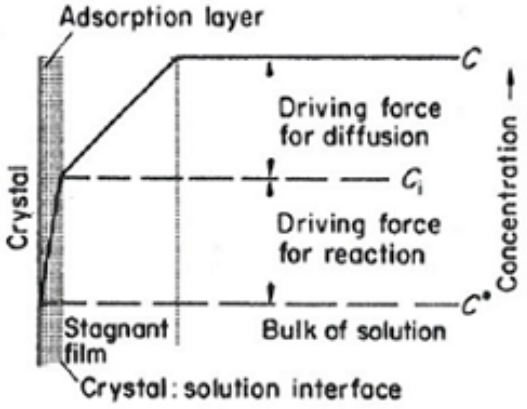

Figure 2.7 – A simple diffusion - reaction model [3]

By combining equation 2.25 for diffusion mass transfer and equation 2.26 for the reaction mass transfer, the general equation for mass transfer by the diffusion - reaction model can be expressed as equation 2.27.

$$\frac{dm}{dt} = k_d A(c - c_i)\textbf{(diffusion)} \tag{2.25}$$

$$\frac{dm}{dt} = k_r A(c_i - c^*)\textbf{(reaction)} \tag{2.26}$$

$$\frac{dm}{dt} = k_G A(c - c^*)^g \tag{2.27}$$

Here m is the mass of solid deposited, t is the time, k_d is the mass transfer by diffusion coefficient, k_r is a rate constant for surface integration and k_G is the overall crystal growth coefficient. c, c_i, and c^* are the solute concentration, the solute concentration in the solution at the crystal - solution interface and the concentration at equilibrium, respectively. A is the surface area of the crystal, and g is usually referred to as the order of the overall crystal growth process, and is either 1, 2 or >2. An assumption for equation 2.27 is that the deposition rate at the surface of the crystal is proportional to the difference in concentration between the deposition point on the crystal and the bulk solution [4].

Equation 2.28 describes the crystal growth controlled by surface integration, where S is the supersaturation defined by equation 2.7, g is the growth order and k_G is the growth rate constant [2]

$$G = k_G(S-1)^g \tag{2.28}$$

Growth rate mechanisms

For growth to occur at the crystal surface, a step or kink must be formed, acting as an active center where the attractive forces are the greatest. Different mechanisms operate to form these active centers, such as nucleation at the surface, or defects in the lattice structure. In total three mechanisms can be used to describe the growth of a crystal.

Nucleation at the surface, where building blocks latch themselves to the steps, or kinks formed on the crystal surface is one of the mechanisms proposed for crystal growth. Nucleation at the surface can be distinguished between 2D-nucleation, also called the birth-and-spread model, and the spiral growth, which is a result of dislocations on the surface as mentioned earlier. The birth-and-spread nucleation can be described as a growth where one layer is completely built on top of another before a new nucleus appear on the new surface. The three growth mechanisms can be seen in figure 2.8 where the growth will be a result of a sequence of steps. These steps include mass transfer of reactants to the crystal surface, controlled by diffusion, adsorption at the surface followed by diffusion at the surface, and finally surface reaction and integration into the lattice [3].

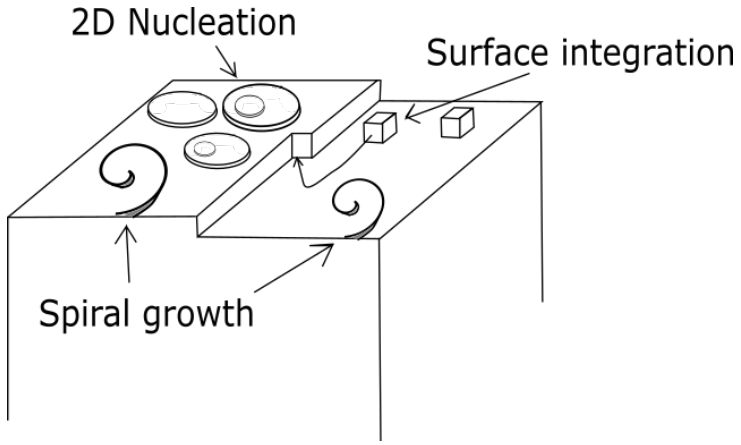

Figure 2.8 – Growth models; surface diffusion, 2D-nucleation and spiral growth. Based on figures found in [4].

When crystal growth is controlled by diffusion of building blocks toward the surface of the crystal, the growth order in equation 2.24 depends only on the difference in concentration and $g = 1$. In the case of spiral growth with high supersaturation, $g = 1$ and low supersaturation, $g = 2$. High supersaturation results in a lower growth rate, because of an increase in the resistance in the film near the crystal surface, since the reactants at the film increase and the diffusion is slower [4].

If the supersaturation is high, growth can occur anywhere on the crystal surface, and the surface becomes rough. A rough surface can have kink sites, terraces and steps everywhere, and results in different types of morphologies. Nucleation and growth can occur simultaneously and the growth order might be larger than two, $g > 2$. The rate of nucleation versus the rate of growth will determine if the final crystal surface will become smooth or rough [4].

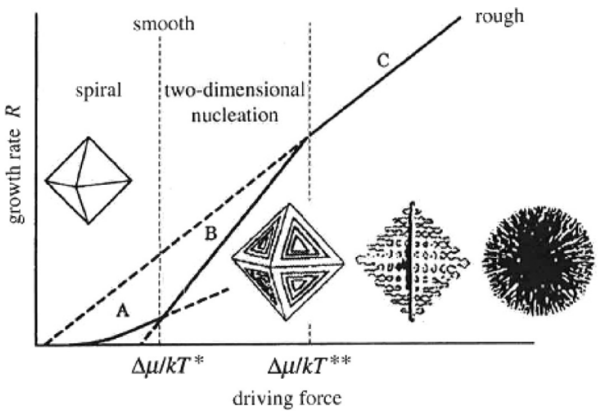

Figure 2.9 – Rough growth; morphology of crystals as a function of the driving force.[5]

Figure 2.9 shows the growth rate as a function of driving force, the supersaturation, and the resulting growth mechanisms and expected morphology in each of the different routes of crystal growth. A in the figure represents a growth primarily described by spiral growth. B represents a two-dimensional nucleation, the birth-and-spread mechanism. In both A and B the crystal surface is smooth. The crystal becomes rough when we reach point C, where the crystal growth is controlled by diffusion, giving a crystal without flat faces - spheres or dendrites.

2.5 The Calcium Carbonate System

Calcium carbonate precipitating in an aqueous solution, can be described by the following equations 2.29 - 2.32.

$$CO_2(g) = CO_2(l) \tag{2.29}$$

$$CO_2(aq) + H_2O = H^+ + HCO_3^{2-} \tag{2.30}$$

$$HCO_3^{2-} = H^+ + CO_3^{2-} \tag{2.31}$$

$$Ca^{2+}(aq) + CO_3^{2-}(aq) = CaCO_3(s) \tag{2.32}$$

CO_2 is in contact with water, and with the addition of bicarbonate(HCO_3^-), equation 2.30 is shifted to the right according to Le Chatelier's principle. Le Chatilier's principle tells us that if a system with a dynamic equilibrium is disturbed by changing the conditions, the equilibrium shifts to counteract the change [15]. In other words, the addition of bicarbonate shifts the equilibrium in 2.30 to the right and in equation 2.31 to the left, so that more bicarbonate is used up.

The definition of pH is the negative logarithm of the concentration of hydronium ions, H_3O^+, or the concentration of protons, H^+, [4] see equation 2.33.

$$pH = -\log[H^+] \tag{2.33}$$

As seen from equations 2.29-2.32, the carbonate activity is linked to the activity of H^+, and thus the pH. The pH increases if the activity of carbonate increases, and therefore, the pH decreases with precipitation of calcium carbonate. Figure 2.10 shows the preferred pH for each of the carbonate products in equations 2.29 - 2.32.

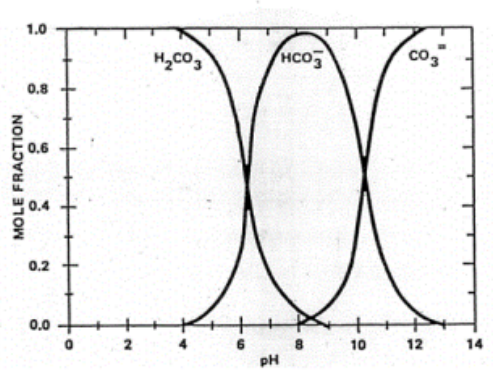

Figure 2.10 – Bicarbonate - carbonate distribution as function of pH [4].

To determine the concentration of sodium (bi)carbonate required to maintain a given supersaturation, the alkalinity of the system must be known [4]. Alkalinity is a measure of the ability for a system to resist a change in pH. To resist the pH change, the equivalent point of carbonate or bicarbonate must be set at a given value, and this can be done by neutralizing the solution with hydronium up to the given value. Species contributing to alkalinity can be identified by setting up an electron balance for the sodium carbonate and calcium chloride system, as presented in equation 2.34.

$$C_{Na^+} + 2C_{Ca^{2+}} + C_{H^+} = C_{HCO_3^-} + 2C_{CO_3^{2-}} + C_{OH^-} + C_{Cl^-} \tag{2.34}$$

Ignoring weak acids, basic species, and the dissociation product of neutral species, equation 2.34 can be reduced to

$$C_{Na^+} = C_{HCO_3^-} + C_{CO_3^{2-}} \tag{2.35}$$

Equation 2.35 shows that the alkalinity required to maintain a desired supersaturation ratio can be calculated based on the concentration of the sodium ions. This calculation can be done in a simulation program such as MultiScale.

Calcium carbonate is characterized as an inverse soluble salt, a salt in which the solubility product decreases with increasing temperature. This means that calcium carbonate will precipitate when the temperature rises, opposite from most precipitating salts [4]. Figure 2.11 illustrates the phenomena of invers solubility.

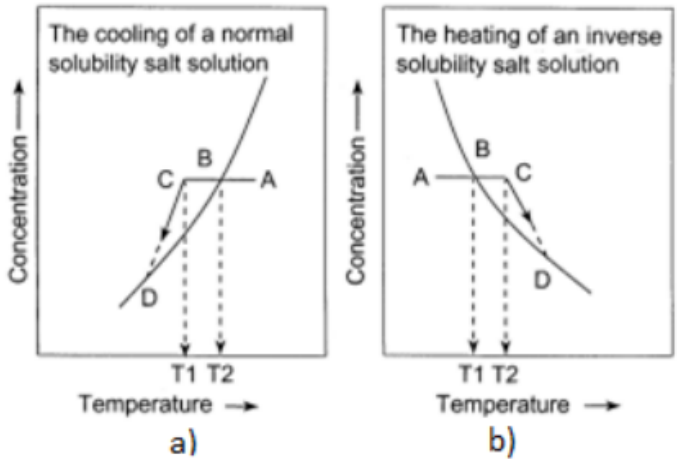

Figure 2.11 – The solubility of a normal salt (left) and an invers soluble salt(right)[4].

Calcium carbonate has three different polymorphs: calcite, aragonite and vaterite, listed with decreasing solubility respectively. Calcite precipitates as rombohedral structured cubes, aragonite as orthorhombic, often needle shapes, and vaterite as a polycrystalline, hexagonal structure. Vaterite can easily transform to stable polymorphs due to its high solubility product.

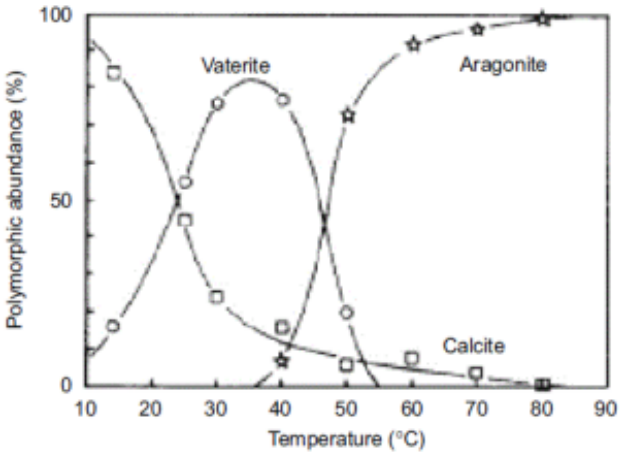

Figure 2.12 – Temperature dependent polymorphic abundance [6].

Figure 2.12 shows which polymorphs it is expected to find in a given temperature interval. Calcite is the dominant polymorph at lower temperatures when calcium carbonate precipitated from amorphous calcium carbonate. Aragonite is the dominant polymorphs at higher temperatures, and vaterite is most usually found at high supersaturation.

2.6 The Calcium Sulfate System

The precipitation of calcium sulfate in an aqueous solution follows the equations 2.36 - 2.37 below.

$$Ca^{2+}(aq) + SO_4^{2-}(aq) = CaSO_4(s) \tag{2.36}$$

$$CaSO_4(s) + 2H_2O = CaSO_4 * 2H_2O(s) \tag{2.37}$$

Calcium combines with sulfate, making calcium sulfate precipitate. Calcium sulfate has six different solid forms; 3 anhydrates, 2 hemihydrates and 1 dihydrate. The dihydrate is called gypsum, $CaSO_4 * 2H_2O$, and precipitates as

monoclinic needles and plate like shapes [16]. Both the anhydrite, $CaSO_4$ and the gypsum is the termodynamically stable phases at the chosen conditions for this work. The reaction between the two stable phases is seen in equation 2.37. Hemihydrate, $CaSO_4 * 0.5H_2O$, is a metastable phase in aqueous solutions. By drying gypsum at 140 - 150 °C hemihydrate can be made.

The transition temperature in pure water between gypsum and anhydrite has been found by several authors, but in the work by Sandengen [7], it is predicted that the gypsum - anhydrite phase stability shifts at about 46,7 °C. The temperature denotes at what temperature which calcium sulfate phase modification is stable, and hence which state it is most likely to find as precipitated crystals. If the temperature in pure water is $>$ 45 °C, equation 2.37 is shifted to left, and anhydrite is most stable. At temperatures lower than the transition temperature, gypsum is the most stable phase.

Addition of MEG decrease the water activity, and if some of the water is exchanged with MEG, equation 2.37 shifts to the left, and anhydrite is more stable at lower temperatures as well. The crystal water in gypsum gives rise to an increase in the solubility for gypsum in MEG and it might start to dissolve instead of precipitating [7]. At temperatures below 45 °C figure 2.13 shows the solubility of gypsum and anhydrite and the mole fraction of MEG where the stable phase shifts.

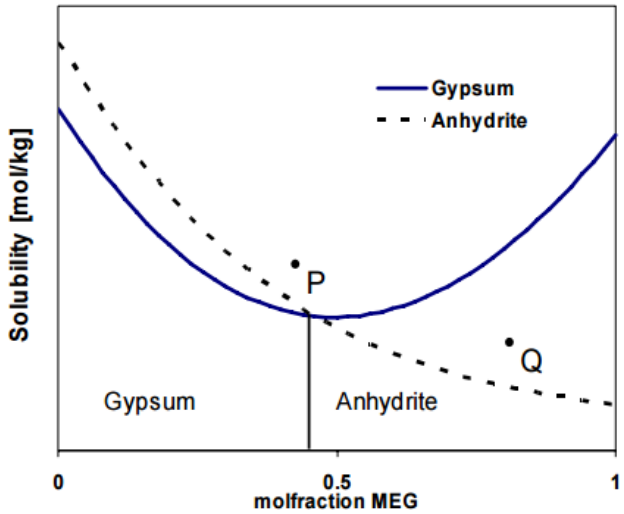

Figure 2.13 – Schematic of $CaSO_4$ solubility versus molefraction of MEG at T $<$ 45 °C[7].

From figure 2.13 it is shown that gypsum is the stable phase with MEG concentrations below 50 % and anhydrite is the stable phase above at T $<$ 45 °C. The solubility of $CaSO_4$ in mixed solvents at 25 °C [8] is shown in figure 2.14 and shows a shift in the stable phase at approximately 70 wt % of MEG. The solubility product, K_{SP} for both anhydrite, A, and gymsum, G, is shown in equation 2.38 and 2.39.

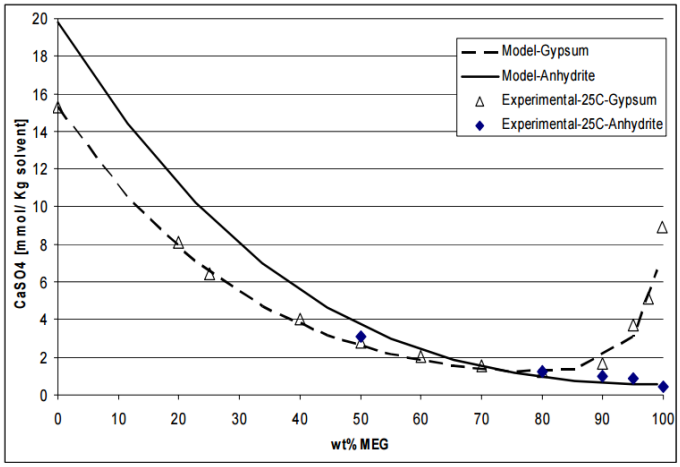

Figure 2.14 – Solubility of $CaSO_4$ in mixed solvent at T= 25 °C[8].

$$K^0_{SP}(G) = m_{Ca^{2+}} m^{2-}_{SO_4} \gamma^S_{Ca^{2+}} \gamma^S_{SO_4^{2-}} (a^S_{H_2O})^2 \dot{\gamma}^N_{CaSO_4(A)} \tag{2.38}$$

$$K^0_{SP}(A) = m_{Ca^{2+}} m^{2-}_{SO_4} \gamma^S_{Ca^{2+}} \gamma^S_{SO_4^{2-}} \dot{\gamma}^N_{CaSO_4(G)} \tag{2.39}$$

2.7 Analyzing Methods

Analyzing the crystals obtained is an important part of discovering what actually have reacted and determining the polymorphism and morphology.

Powder X-ray Diffraction

The powder X-ray diffraction (XRD) is used to characterize the crystal structures of the crystalline material in a prepared sample. X-rays are diffracted by the crystalline matter in the sample, and give a pattern with peaks of intensity at different positions, specific for a given compound. The positions of the peaks

are referred to as 2θ-values, where θ is the Bragg angle in the Bragg's equation 2.40:

$$\lambda = 2d \sin\theta \tag{2.40}$$

Where λ is the X-ray wavelength and d is the distance between atomic planes in a crystalline phase. Polymorphs will have different diffractive patterns, because they have different arrangements in the crystal lattice. The intensity of the peaks will differ for polymorphs and increase with increasing degree of crystallinity [17]. The results from the XRD contains information about intensity, shape and position of the peaks, and can be used to identify the content of the sample.

Scanning Electron Microscope

The pictures obtained from the Scanning Electron Microscope (SEM) are taken of the surface of the sample and are created by scanning the sample surface with an electron beam. The interaction between the atoms in the sample and the electrons produces signals containing information about the topography and composition of the sample. With a non-concuctive sample, the possibility of electron charge build up in the sample can be hindered by coating the sample. The problem with coating the sample is the loss of small topographic details [17].

The SEM pictures can be obtained by using different kinds of electrons. Secondary electrons (SE) are reflected from the matter closest to the surface of the sample, and thus give better information of the sample surface. The SE are more sensitive to charging than the back scattering electrons (BSE). The BSE are reflected from deeper inside the sample, and makes heavier elements appear lighter, because heavier atoms have more electrons and hence more electrons are reflected, giving rise to a larger contrast between the elements in the sample [17].

CHAPTER 3

Experimental

A total of 38 experiments were conducted. All experiments were executed in the same experimental setup and had the same procedure. The first 8 experiments were based on the work of the specialization project work of fall 2015 by Bache [14], and are the initial test of the setup and procedure in this work. 6 experiments were performed to determine the effect of pH on calcium sulfate precipitation. The remaining 24 experiments are considered the main group for investigating the simultaneously precipitation of two salts. The experimental setup has been improved during the experiments.

3.1 Experimental Procedure

The experiments were performed in a 1 L reactor, and stirred with a digital stirrer engine (IKA) equipped with a 50 mm three-bladed impellar of propellar type, operating at a constant stirrer rate of 500 ± 5 rpm. The reactor was jacketed for temperature control, and all experiments were operated at at a constant CO_2 partial pressure, ensured by constant bubbling with CO_2 for the entire duration of the experiments. The calcium containing and the carbonate

and sulfate containing solutions were preheated as well as bubbled with CO_2 to reach a stable pH before mixing in the vessel. The pH in both solutions were measured before mixing. The CO_2 was saturated with the different solvent mixtures used in the experiments, by running it through the mixture before entering it in the vessel to minimize the evaporation of solvent during the experiments. The solvent mixtures were either 0 wt % MEG + 100 wt % distilled water, 50/50 wt % MEG and distilled water, or 90 wt % MEG + 10 wt % distilled water. For a figure of the experimental setup, see figure 3.1. The amount of chemicals needed to reach a specific supersaturation ratio

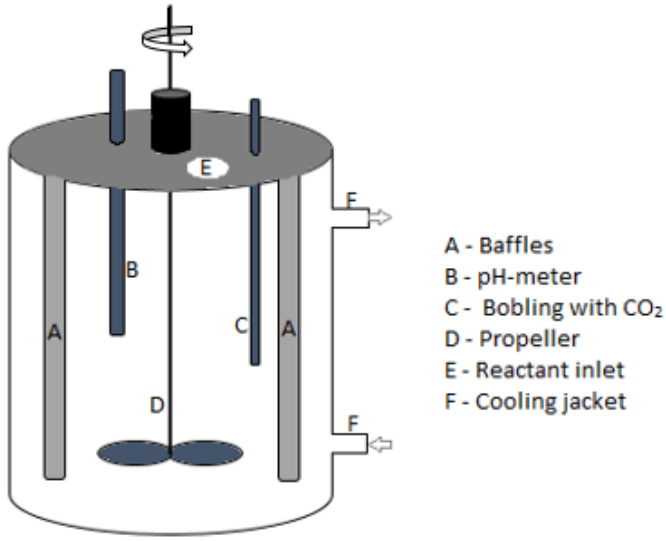

Figure 3.1 – The experimental setup with a reactor with a heated glass jacket, a lid containing places for pH - meter, bubbling with CO_2 and an opening to pour reactant solutions, a stirrer engine with propeller blades, and baffles.

was calculated using MultiScale. For a complete list of chemicals used in the experiments, see table A.1 in appendix A.

Calcium chloride dihydrate was measured out on a four digit Mettler Toledo AB204-S scale, and dissolved in a volumetric flask until a total weight of 300 g were reached, either with 100 % distilled water, 50 wt % of MEG and 50 wt % of distilled water or 90 wt % of MEG and 10 wt % of distilled water. Sodium bicarbonate and sodium sulfate were measured out and dissolved in an Erlend Meyer flask containing 300 g in total of either distilled water, 50 wt % of MEG and 50 wt % of distilled water or 90 wt % of MEG and 10 wt % of distilled water.

An InLab Expert pH - meter probe connected to a Metler Toledo MultiEasy pH - meter, which was connected to a computer, was used to determine the pH decrease in the reactor solution, making it possible to determine the precipitation of calcium carbonate. pH experiments were run to determine if the pH was affected by the precipitation of calcium sulfate. To further determine the total calcium decrease in the reactor, samples were taken out with a Millipore 0.22mm attachable filter in front of a syringe, weighted on a scale, diluted with distilled water, and run through titration with ethylenediaminetetraacetic acid, EDTA.

After a detectable pH decrease or a change of transparency in the reactor, a 10 mL sample were taken out with a syringe and filtered through a Büchner funnel with a 47 mm Durapore 0.22 mm filterpaper. The filterpaper was washed with ethanol to stop further growth and dried over night. At the end of each experiment, the bulk precipitate was filtered out on 47 mm Durapore 0.22 mm filter, washed with ethanol and left to dry over night. The filtered samples were analyzed using XRD and a SEM.

The reactor vessel and the lid with the propeller were washed with a mixture of water and hydrochloric acid for 10 minutes. Before the reactor and the lid were set to dry over night they were rinsed thoroughly with distilled water.

3.2 Experimental Conditions

All experiments were conducted at constant temperature and pressure. In table 3.1 the operating conditions for both water baths for both temperatures are shown, as well as the approximately weight of each solution.

Table 3.1 – Operating conditions

Condition	At T = 30 °C	At T = 65 °C	unit
$T_{waterbath_1}$	30,0	65,5	$°C$
$T_{waterbath_2}$	31,0	66,5	$°C$
$T_{Solution_1}$	30,0	65,0	$°C$
$T_{Solution_2}$	31,3	66,0	$°C$
p	1	1	bar
$V_{Solution_1}$	300	300	g
$V_{Solution_2}$	300	300	g
$V_{reactor}$	600	600	g

The experimental conditions were found from calculations in MultiScale and can be seen in table 3.2 to 3.4. The pH experiments had $SR_{CaCO_3} \approx 1$ in all experiments, to ensure undersaturated solution for precipitation of calcium carbonate. The calcium sulfate however, had saturation ratio, $SR_{CaSO4_g} \approx 4$, to ensure precipitation. All pH experiments were run at both temperatures and with varying MEG concentration to investigate which form of the salt that would precipitate, gypsum or anhydrite, and the effect of pH. The initial tests were performed for the same conditions as in the work by Bache [14], with the new procedure where both solutions were bubbled with CO_2 and preheated, as well as pH being measured before mixing. For both the initial and the main group of experiments, the saturation ratio was approximately 50, $SR_{CaCO_3} \approx 50$. The main group of experiments were run at both temperatures, all three concentrations of MEG and all four saturation ratios for calcium sulfate, SR_{CaSO_4}.

T °C	wt% MEG	SR_{CaCO_3}	SR_{CaSO4_g}	Ca^{2+} [mmol kg^{-1}]	Alkalinity [mmol kg^{-1}]	SO_4^{2-} [mmol kg^{-1}]
65	0	1,4012	4,0305	53	7,15	65
65	50	1,0210	4,0949	20	3,3	5,2
65	90	1,0277	4,0735	100	1,7	4
30	0	1,0619	4,0818	100	10,5	47
30	50	1,0949	4,0846	100	6	4,6
30	90	1,0368	4,0556	100	4	4,3

Table 3.2 – Experimental conditions for the pH experiments.

T °C	wt% MEG	SR_{CaSO4_g}	Ca^{2+} [mmol kg^{-1}]	Alkalinity [mmol kg^{-1}]	SO_4^{2-} [mmol kg^{-1}]
65	0	10,0774	96	55,5	300
65	0	4,0893	60	45,7	75
65	0	2,5182	40	33,6	48,5
65	0	1,0905	50	36,3	13,5
65	50	10,1477	40	22,9	14,2
65	50	4,0846	20	27	6,8
65	50	2,5044	20	26	3,9
65	50	1,0404	10	33,7	2,3

Table 3.3 – Experimental conditions for the initial experiments.

3.3 Analyzing the Products

During and after the experiments the bulk solution and the crystals formed were analyzed using different tools. pH measurements were used to determine at what time calcium carbonate precipitated, titration was used to find the calcium concentration in the bulk solution at a given time, and XRD and SEM were used to investigate the polymorphs and morphology of the crystals. The combination of titration and pH measurements are believed to give a better understanding of which salt precipitates first.

T °C	wt% MEG	SR_{CaSO4_g}	Ca^{2+} [mmol kg^{-1}]	Alkalinity [mmol kg^{-1}]	SO_4^{2-} [mmol kg^{-1}]
65	0	10,0553	100	51,55	250
65	0	4,0038	100	34,25	43,4
65	0	2,5057	100	32,3	25
65	0	1,0261	100	30,55	9,7
65	50	10,0607	100	18,27	11
65	50	4,223	100	17,87	4,3
65	50	2,5084	100	17,78	2,67
65	50	1,0373	100	17,68	1,1
65	90	10,0197	40	15,9	11,8
65	90	4,0798	40	14,89	4,2
65	90	2,4969	40	14,67	2,5
65	90	1,0226	40	14,46	1
30	0	10,0953	140	98,4	243,5
30	0	4,0034	140	68,3	45,8
30	0	2,5049	140	64,9	26,5
30	0	1,0137	140	62,1	10,1
30	50	10,0871	100	44,15	12,9
30	50	4,0159	100	42,85	4,9
30	50	2,5089	100	42,55	3,03
30	50	1,0029	100	42,25	1,2
30	90	10,0838	100	31,1	14,6
30	90	4,0657	100	30,12	5,4
30	90	2,5094	100	29,85	3,27
30	90	1,0920	100	29,63	1,4

Table 3.4 – Experimental conditions for the main group of experiments.

pH Measurements

During the experiments the pH was automatically measured in the reactor to determine when calcium carbonate precipitates. The pH-values, as well as the temperature measurements for the inside of the reactor, were saved in an Excel-workbook to be further analyzed. The pH - meter measures the decreasing alkalinity, due to loss of carbonate ions, and the corresponding curve tells when the precipitation occurs.

Titration

All experiment in the main group were analyzed with titration. Titration was used to determine the calcium concentration in the bulk solution. Samples of approximately 2 $\pm$ 0,2 mL were drawn using a filter in front of a syringe from the bulk solution. The samples were transfered to a measuring cup containing approximately 40 $\pm$ 10 mL of DI water, and weighted on a scale. Hydrochloric acid was added to the samples to further dissolve any precipitated calcium. Ammonia/ammonium buffer solution was added to reach a pH about 10, before the samples were titrated with EDTA in a Metler Toledo DL53 titrator unit. EDTA was added in relative small amounts to the samples during the titration. EDTA binds up the calcium ions stoichiometrically. Two electrodes measure the voltage in the samples and at the end point of the titration, where the voltage drops significantly, indicating that all the calcium ions have been bound to EDTA and only free EDTA is available. From the amount of EDTA used as well as the weight of the samples, the concentration of calcium in the sample can be calculated, and then presented in a plot.

Scanning Electron Microscopy

Whenever a pH drop was noticed, or a change of transparency in the reactor, samples were taken out and filtrated using a Büchner funnel with a filter paper. At the end of each experiment, the remaining liquid in the reactor was filtrated with the same procedure as the small samples taken earlier in the experiment.

The samples were left to dry over night before analyzed with a Hitachi S-3400 N scanning electron microscope. Samples were prepared for SEM by adding a small amount of crystals to a double sided carbon tape placed on a sample holder. The samples were coated with gold in an Edwards Sputter Coater SB150B before entering the SEM. Secondary electrons (SE) was used in low-vacuum mode. Typical settings for the SEM were pressure of 40 Pascal, voltage of 15 - 20 kV, emission current of 40 mA and working distance of approximately 7 ± 2 mm.

Powder X-ray Diffraction

Samples were prepared for the DaVinci 1 unit for Powder X-ray diffraction, XRD, from the filtered samples taken at the end of the experiments. The powder was prepared for XRD by crushing the crystals into fine powder using a pestle and mortar, and ethanol was added until the powder was wetted. A drop of the wetted, fully pulverized crystal sample was transfered to a single crystal silicon sample holder. When the ethanol had evaporated, the sample was analyzed. The samples were scanned using scanning angels between 5 and 75 degrees and a step size of 0.01 ° and eventually analyzed using the Diffrac EVA application.

CHAPTER 4

Results and discussion

This work has focused on investigating simultaneous precipitation of two salts, calcium carbonate and calcium sulfate.

4.1 Development of Experimental Setup

The experimental setup in this work was based on the development done in the specialization project work of fall 2015 by Bache [14]. A further development was necessary to get more correct answers. Where the work done in the previous project only bubbled one of the ion containing solutions with CO_2 before the start of the experiment, this work has had both solutions bubbled with CO_2 before starting. One solution was heated and bubbled in the reactor with constant stirrer rate, the other was heated and bubbled in a second water bath, in an Erlend Meyer flask. In addition the pH was measured in both solutions two assure steady state and desired temperature before the experiment was started. According to the initial tests, the new setup worked well, and further experiments for investigating the simultaneous precipitation of calcium carbonate and calcium sulfate in MEG were performed.

4.2 Effect of pH

From the specialization project work performed by Bache fall 2015, it was assumed that pH only was effected by the precipitation of calcium carbonate, and that the precipitation of calcium sulfate was not related to the decrease in pH. To make sure this is the case, experiments with precipitation of calcium sulfate in presence of carbonate were performed. Experiments with saturation ratio for gypsum, $SR_{CaSO_4 g}$, equal to approximately 4 for calcium sulfate and 1 for calcium carbonate at temperature T = 65 °C and T = 30 °C were run with the same operating conditions as every other experiments. The MEG concentration varied from 0 to 50 and 90 wt % MEG, and the experiments were run until and beyond the point of precipitation, marked by visible crystals appearing in the reactor. In table 4.1 the experimental conditions for the experiments are listed. In figure 4.1 and figure 4.2 the pH plots for both temperatures are shown, as well as the pH for the different MEG conditions.

T °C	wt% MEG	SR_{CaCO_3}	SR_{CaSO4_g}	Ca^{2+} [mmol kg^{-1}]	Alkalinity [mmol kg^{-1}]	SO_4^{2-} [mmol kg^{-1}]	Initial pH	Equilibrium pH
65	0	1,4012	4,0305	53	7,15	65	5,8674	5,9184
65	50	1,0210	4,0949	20	3,3	5,2	6,0560	6,0667
65	90	1,0277	4,0735	100	1,7	4	6,2488	6,2453
30	0	1,0619	4,0818	100	10,5	47	6,3309	6,3252
30	50	1,0949	4,0846	100	6	4,6	5,8851	5,8672
30	50	1,0368	4,0556	100	4	4,3	5,7109	5,7312

Table 4.1 – Experimental conditions for the pH experiments.

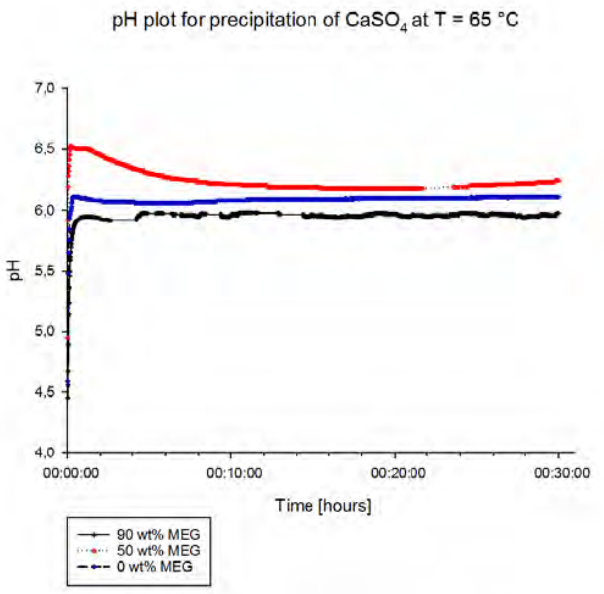

Figure 4.1 – pH plot for precipitation of calcium sulfate for 90, 50 and 0 wt % MEG at 65 °C.

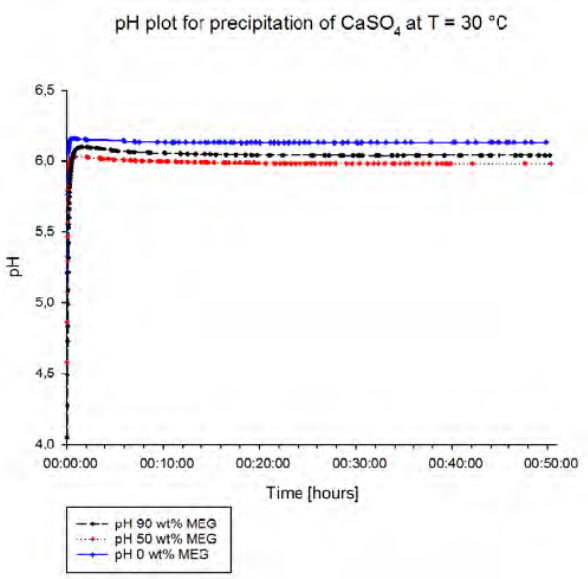

Figure 4.2 – pH plot for precipitation of calcium sulfate for 90, 50 and 0 wt % MEG at 30 °C.

From figure 4.1 and figure 4.2 it is not possible to observe any significant change in pH when calcium sulfate precipitates. The slight decrease in pH for 50 wt % MEG at T=65 °C might be due to change in temperature. The temperature for the experiment was higher than desired at the start of the experiment, and to reach a steady state, it had to be decreased, which resulted in an decrease also in pH-values measured. For a pH and temperature plot over time for the experiments with 50 wt % MEG and $T = 65°C$ see figure 4.3.

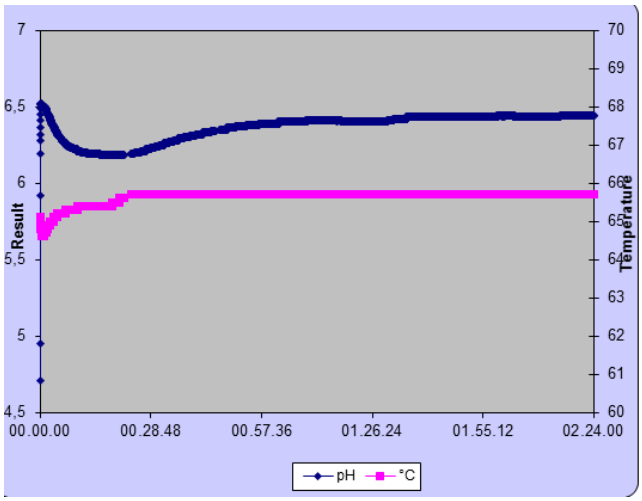

Figure 4.3 – pH and temperature plot for experiments with 50 wt % MEG at T = 65 °C.

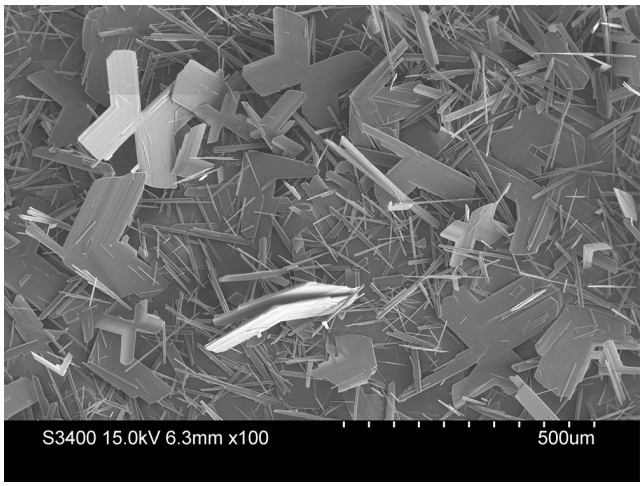

Figure 4.4 – SEM picture of pH experiments with 0 wt % MEG at T = 65 °C. Scale bar is 500µm and the magnification is 100.

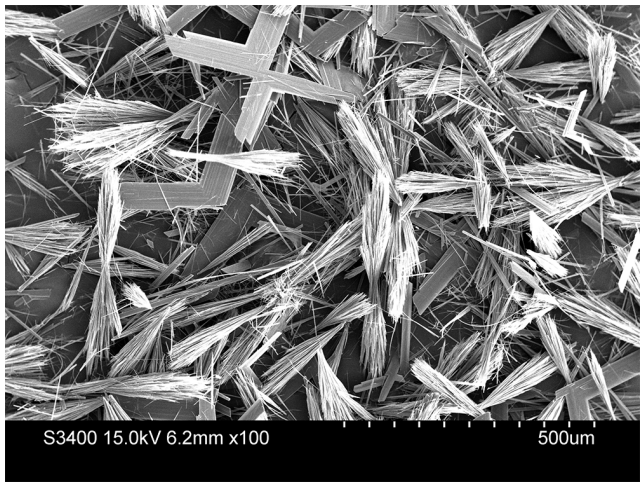

Figure 4.5 – SEM picture of pH experiments with 50 wt % MEG at T = 65 °C. Scale bar is 500µm and the magnification is 100.

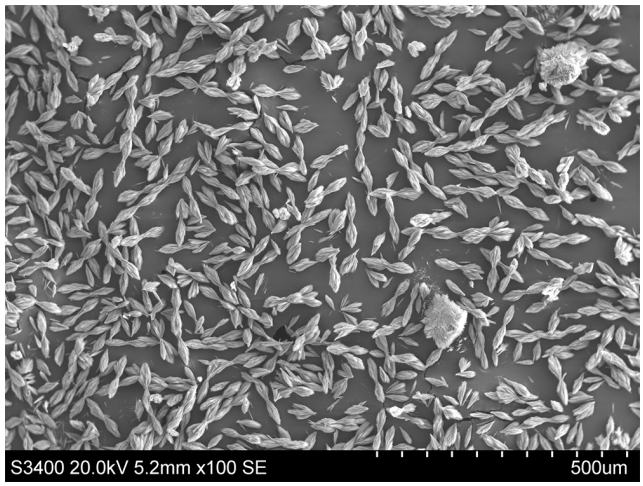

Figure 4.6 – SEM picture of pH experiments with 90 wt % MEG at T = 65 °C. Scale bar is 500µm and the magnification is 100.

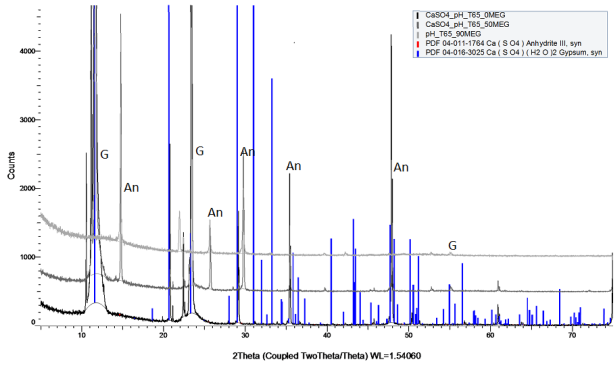

Figure 4.7 – XRD for T=65 °C and all MEG concentrations for the pH experiments.

Figures 4.4, 4.5 and 4.6 show SEM pictures of the precipitated crystals from the experiments with temperature, T = 65°C and varying MEG concentration. There are no calcium carbonate crystals visible, which the XRD plots confirms in figure 4.7. At this temperature the calcium sulfate gypsum crystals take the form of needles, plates and a combination of the two and anhydrite take the form of small thin needles lumped together in a "peanut shape". From the XRD - plots in figure 4.7, it can be seen that for MEG concentration at 50 wt % and 90 wt % anhydrite can be found, as well as gypsum can be found at 0 wt % MEG. This corresponds well with the pictures from SEM, figure 4.4, 4.5 and 4.6, where large plates and thick needles can be found in figure 4.4, both plates and thinner needles in figure 4.5, which can be a previous stage in the growth for anhydrite, and in figure 4.6 small thin needles formed together as larger crystals is shown, indicating anhydrite. The size of the crystals can be seen to be larger at lower MEG concentration, indicating that MEG might hinder or slow down the precipitation rate. A fast nucleation rate results in more nuclei formed, and the crystals precipitated are small, but many. As the MEG concentration increases, the size and amount of crystals found in the SEM pictures decrease.

In figures 4.8, 4.9 and 4.10 the SEM pictures of the pH experiments at

$T = 30°C$ and varying MEG concentration is shown. No calcium carbonate can be found in these experiments, confirmed by both SEM pictures and XRD-plots in figure 4.11. At lower temperatures, T = 30 °C, gypsum is the dominating form of calcium sulfate, and can be found in both 0 and 50 wt % MEG. At 0 wt % of MEG, gypsum precipitates as plates in the form of stars, at 50 wt % the crystals found resemble broken plates and small uniform needles. At 90 wt % MEG the crystals consist of many small needles grown together forming a larger rough crystal, see figure 4.12. With no MEG in the solution, more and larger crystals precipitate than in the solutions with MEG present.

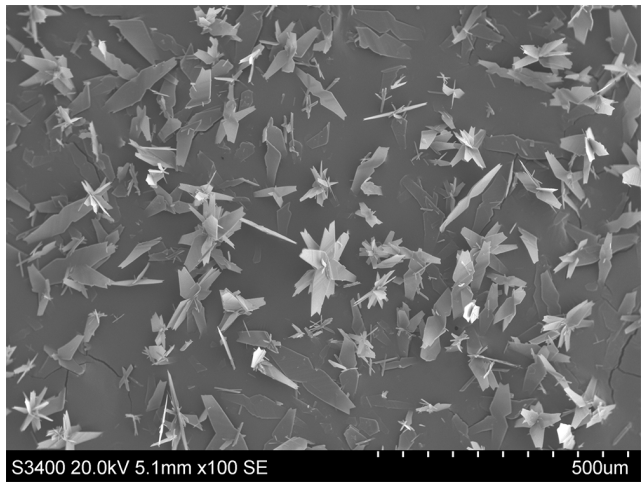

Figure 4.8 – SEM picture of pH experiments with 0 wt % MEG at T = 30 °C. Scale bar is 500µm and the magnification is 100.

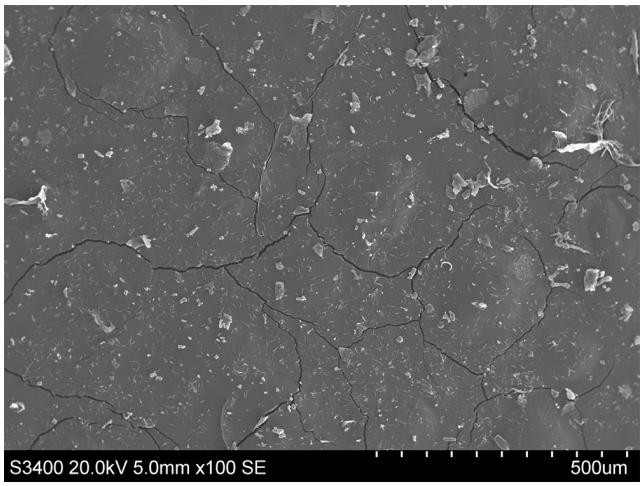

Figure 4.9 – SEM picture of pH experiments with 50 wt % MEG at T = 30 °C. Scale bar is 500µm and the magnification is 100.

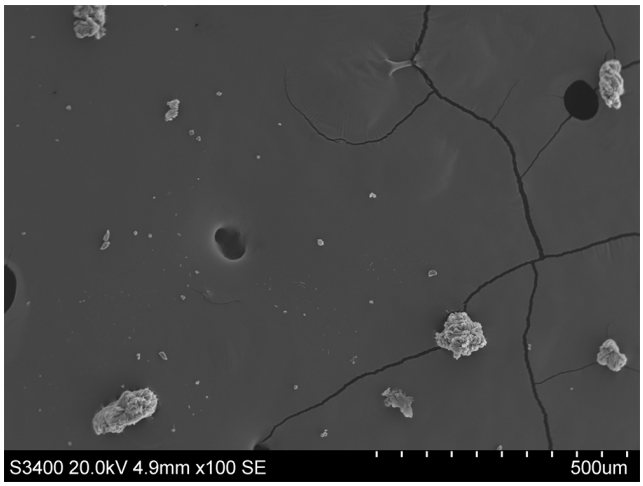

Figure 4.10 – SEM picture of pH experiments with 90 wt % MEG at T = 30 °C. Scale bar is 500µm and the magnification is 100.

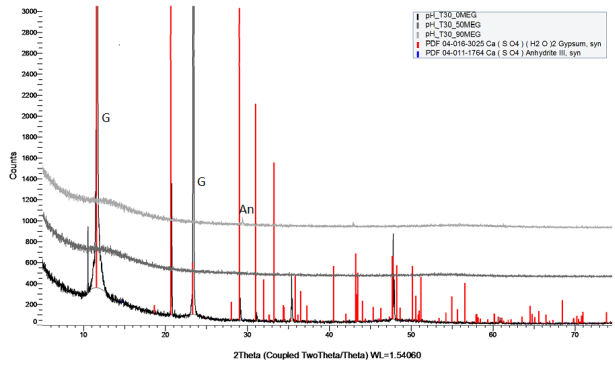

Figure 4.11 – XRD for T=65 °C all MEG concentrations for the pH experiments.

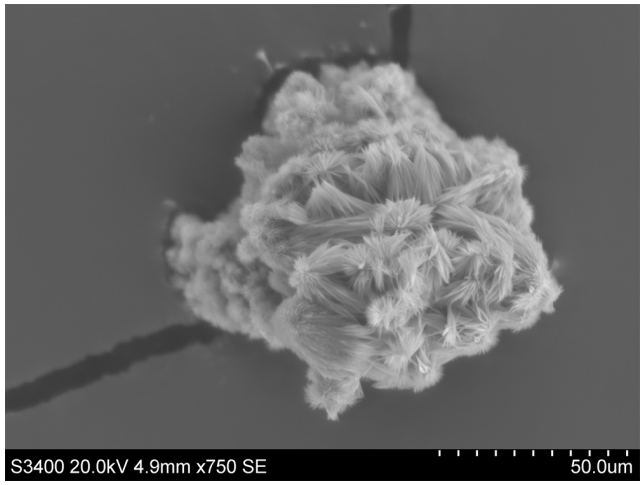

Figure 4.12 – SEM picture of pH experiments with 90 wt % MEG at T = 30 °C. Scale bar is 50µm and the magnification is 750.

Comparing pH-plots to XRD plots and SEM pictures, indicates that pH does not change with precipitation of calcium sulfate at these operating conditions.

It can be seen that the measured pH-values for the experiments in figures 4.1 and 4.2 are lower than the ones calculated in MultiScale, see table 4.1. Reasons for this might be that the experiments hadn't reached steady state before mixing, or that the pH-electrode wasn't calibrated for a MEG containing solution, and might therefore be lower. The exact pH-value in these experiments weren't of interest, since they didn't effect the overall picture. In this work, only the behavior of pH was interesting, not the exact value. Further work should focus on measuring the exact values for pH when salts precipitate in MEG containing solutions.

4.3 Effect of Temperature

The effect of temperature was investigated by performing every experiment at two temperatures, T= 65 °C and T= 30 °C. In figure 4.13 the XRD plot for $SRCaSO_4$ = 10 and 0 wt% MEG for both temperatures is shown. The figure shows that gypsum is the dominating phase of calcium sulfate for both temperatures, T=65 °C (red) and T=30 °C (black). The difference in the plot is the intensity of the peaks. At 65 °C the peaks are more intense, and the amount of gypsum might be greater than at 30 °C.

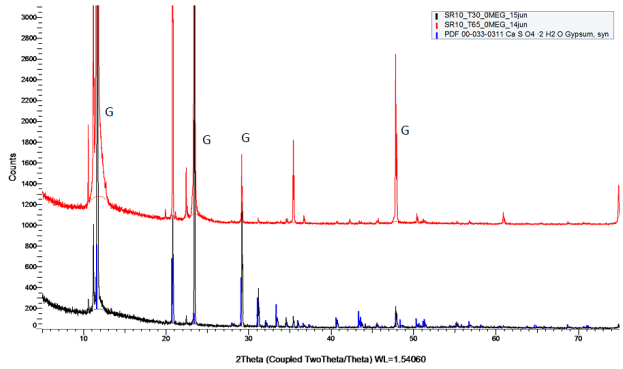

Figure 4.13 – XRD plot for $SRCaSO_4$ = 10, 0 wt % MEG and both temperatures for the main group of experiments.

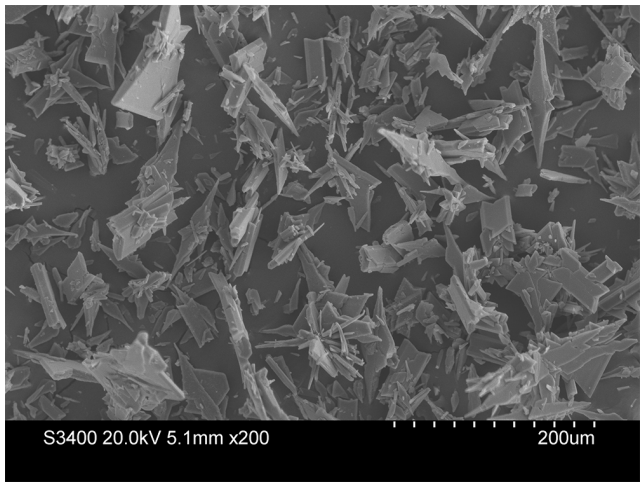

Figure 4.14 – SEM picture of experiment with $SRCaSO_4 = 10$ and 0 wt % MEG at T = 30 °C. Scale bar is 200µm and the magnification is 200.

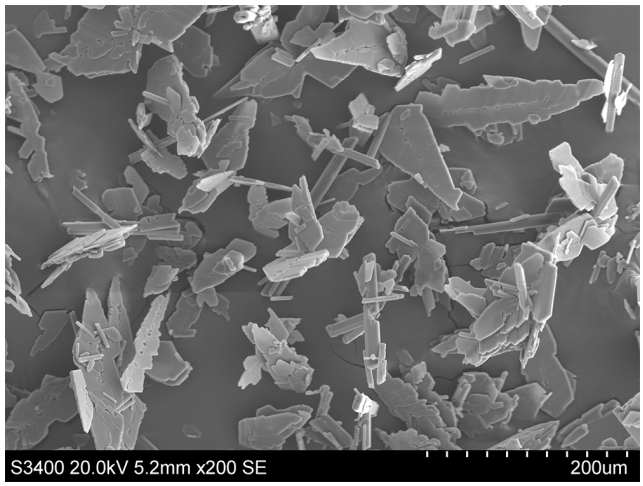

Figure 4.15 – SEM picture of experiment with $SRCaSO_4 = 10$ and 0 wt % MEG at T = 65 °C. Scale bar is 200µm and the magnification is 200.

In figure 4.16 the XRD plot for $SRCaSO_4 = 10$ and 50 wt% MEG for both temperatures is shown. The figure shows that gypsum is the dominating phase of calcium sulfate for both temperatures, T=65 °C (red) and T=30 °C (black). For this wt % of MEG, the peaks for both temperatures are relatively equal, and the crystals precipitated for both temperatures are mostly large plates in a x- like shape. For T = 65 °C some small crystals are also seen, these crystals might be smaller calcium sulfate crystals or calcium carbonate in the form of aragonite.

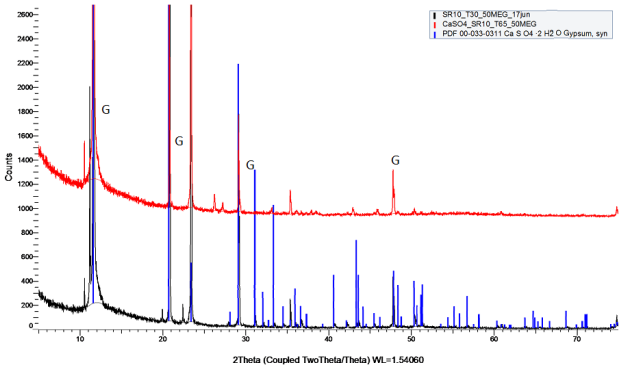

Figure 4.16 – XRD plot for $SRCaSO_4 = 10, 50$ wt % MEG and both temperatures for the main group of experiments.

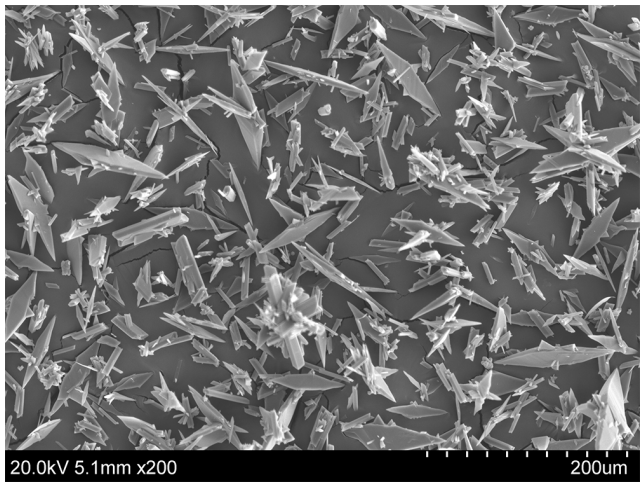

Figure 4.17 – SEM picture of experiment with $SRCaSO_4 = 10$ and 50 wt % MEG at T = 30 °C. Scale bar is 200µm and the magnification is 200.

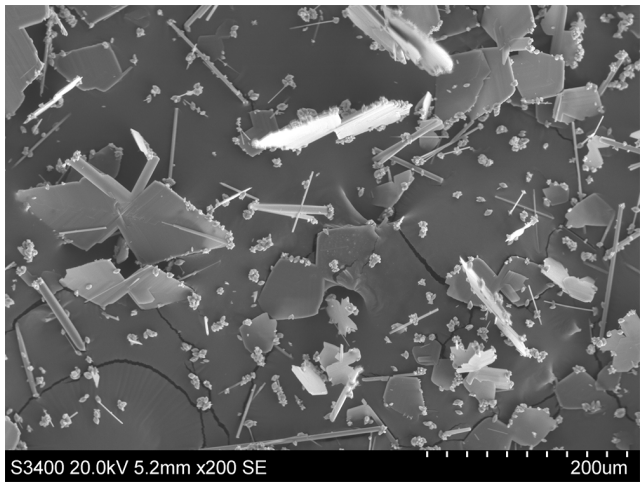

Figure 4.18 – SEM picture of experiment with $SRCaSO_4 = 10$ and 50 wt % MEG at T = 65 °C. Scale bar is 200µm and the magnification is 200.

In figure 4.19 the XRD plot for $SRCaSO_4 = 10$ and 90 wt% MEG for both temperatures is shown. The figure shows that anhydrite is the dominating phase of calcium sulfate for both temperatures, T=65 °C (red) and T=30 °C (black). The difference in the plot is the intensity of the peaks. For 65 °C the peaks are more intense, and the amount of anhydrite might be greater than for 30 °C.

The anhydrite takes the form of small uniform needles and larger rough crystals consisting of many of theses needles together. The size of the needles are larger at lower temperature, indicating that a lower temperature lowers the nucleation rate, making fewer, but larger crystals than at higher temperatures. A low nucleation rate results in fewer nuclei formed above the critical radius, hence giving the nuclei formed time to grow before other nuclei is formed and "steal" building blocks. For a figure of the two types of anhydrite needles, se figures 4.20 and 4.21.

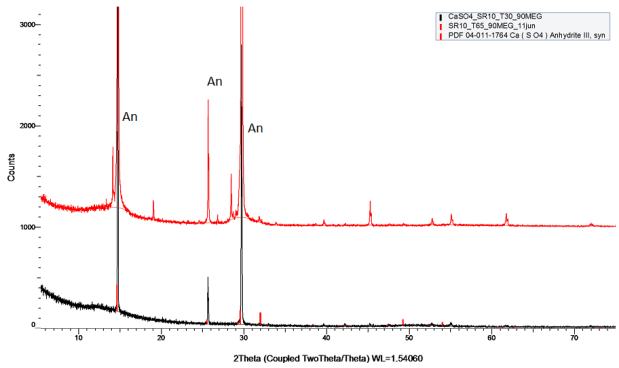

Figure 4.19 – XRD plot for $SRCaSO_4 = 10, 90$ wt % MEG and both temperatures for the main group of experiments.

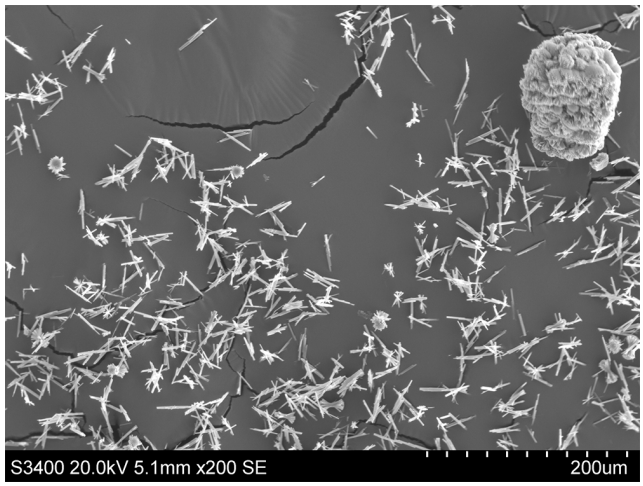

Figure 4.20 – SEM picture of experiment with $SRCaSO_4 = 10$ and 90 wt % MEG at T = 30 °C. Scale bar is 200µm and the magnification is 200.

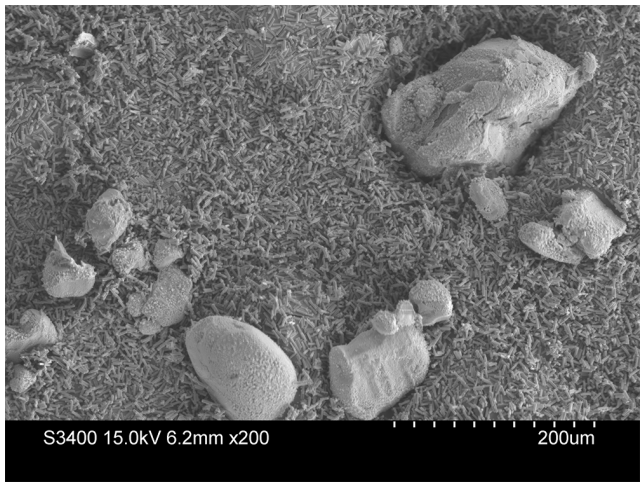

Figure 4.21 – SEM picture of experiment with $SRCaSO_4 = 10$ and 90 wt % MEG at T = 65 °C. Scale bar is 200µm and the magnification is 200.

From table 4.2 it can be seen that the temperature impacts the supersaturation of anhydrite. The saturation ratio for anhydrite, gypsum and hemihydrate is calculated in MultiScale. Only for 0 and 50 wt % MEG and T = 65 °C have higher saturation ratio for anhydrite than for gypsum. Kaasa et al [8] found that the shift in what phase of calcium sulfate is dominating at 25 °C is found at 70 wt % MEG, and since T = 30 °C is close to this temperature, it is assumed that the shift occurs around the same MEG concentration value in this work. Sandengen [7] found that for T > 45 °C gypsum was the dominating phase in pure water. At 90 wt % and T = 30 °C however, see table 4.2, the anhydrite has a higher value for saturation ratio than gypsum, indicating that anhydrite might be a stable phase at these conditions. From table 4.2 the saturation ratio for anhydrite is higher than the saturation ratio for gypsum for all MEG concentrations for T = 65 °C, which is above the transition temperature of 45 °C, and anhydrite might precipitate at these conditions. Only $SR_{CaSO_4 g} = 10$ is shown in table 4.2.

T °C	wt% MEG	$SR_{CaSO_{4a}}$	$SR_{CaSO_{4g}}$	Ca^{2+} [mmol kg^{-1}]	Alkalinity [mmol kg^{-1}]	SO_4^{2-} [mmol kg^{-1}]
65	0	16,2	10,0	100	51,55	250
65	50	17,9	10,0	100	18,27	11
65	90	240,8	10,0	40	15,9	11,8
30	0	8,45	10,0	140	98,4	243,5
30	50	9,38	10,0	100	44,15	12,9
30	90	164,2	10,0	100	31,1	14,6

Table 4.2 – Table showing experimental conditions calculated from MultiScale for all MEG concentrations, $SR_{CaSO_4} = 10$ and both temperatures.

From the XRD-plots in figures 4.13, 4.16 and 4.19 and the SEM pictures, anhydrite is the only precipitate at 90 wt % MEG for both temperatures. Even though T > transition temperature (45 °C) when T = 65 °C anhydrite precipitates only in 90 wt % MEG and not in 0 and 50 wt % of MEG.

4.4 Effect of MEG

The effect of MEG was investigated by performing experiments at different MEG concentrations. It is known that MEG decreases the solubility of both salts [8], which gives rise for less reactants needed to saturate the solutions. Because of the decreased solubility, fewer ions can be found in the mixed solutions in the reactor, and fewer building blocks for nucleation are found. Less nucleation results in slower growth, and the precipitated crystals are smaller and fewer than with lower MEG concentrations.

Figure 4.22 shows XRD-plots for experiments at T = 30 °C for SR_{CaSO_4} = 10 and varying MEG concentrations. It can be seen that gypsum is the dominating phase at lower MEG concentrations, 0 and 50 wt %, and that anhydrite is the dominating phase at 90 wt % MEG. Figure 4.23 shows large gypsum crystals, figure 4.24 shows smaller gypsum crystals and figure 4.25 shows needle shaped anhydrite.

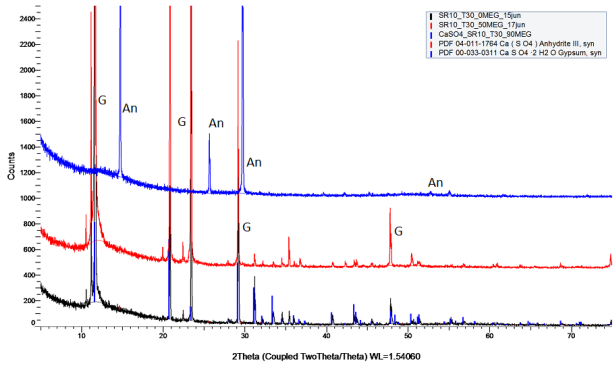

Figure 4.22 – XRD plots for SR_{CaSO_4} = 10 for T = 30 °C and all wt % of MEG

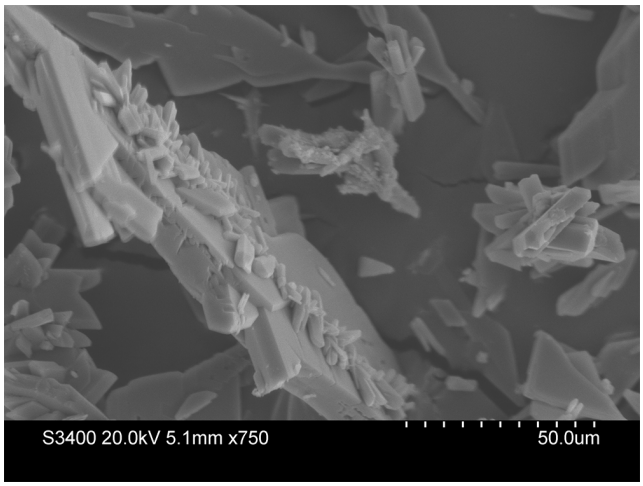

Figure 4.23 – SEM pictures of $SR_{CaSO_4} = 10$ at 0 wt% MEG and 30 °C. Scalebar is 50µm and magnification is 750.

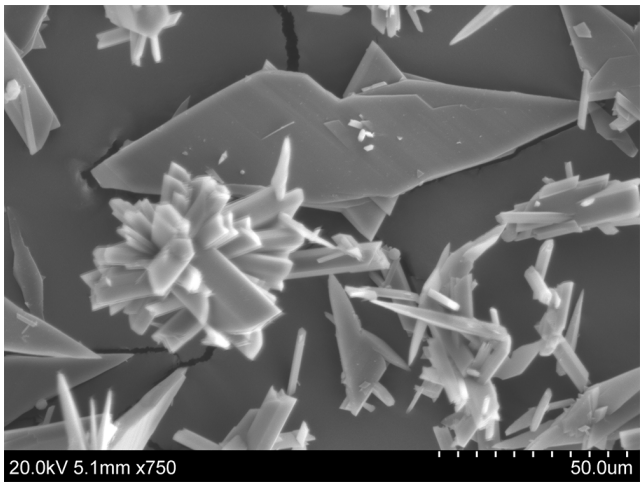

Figure 4.24 – SEM pictures of $SR_{CaSO_4} = 10$ at 50 wt% MEG and 30 °C. Scalebar is 50µm and magnification is 750.

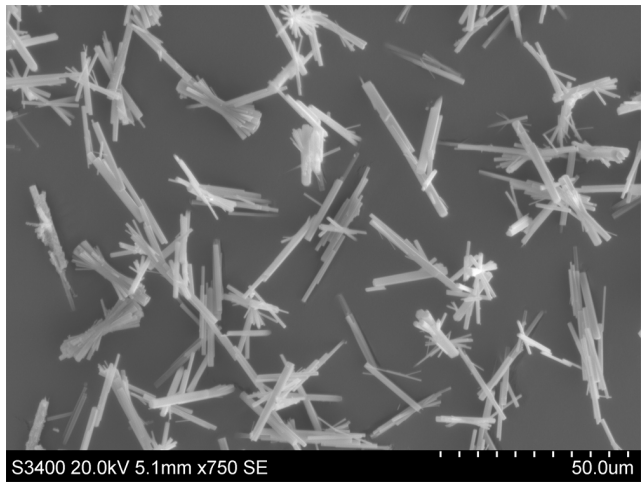

Figure 4.25 – SEM pictures of $SR_{CaSO_4} = 10$ at 90 wt% MEG and 30 °C. Scalebar is 50µm and magnification is 750.

Figure 4.26 shows XRD-plots for experiments at T = 65 °C for $SR_{CaSO_4} = 10$ and varying MEG concentrations. It is seen that gypsum is the dominating phase at lower MEG concentrations, 0 and 50 wt %, and that anhydrite is the dominating phase at 90 wt % MEG. Figure 4.27 shows large gypsum crystals, figure 4.28 shows smaller gypsum crystals and figure 4.29 shows small uniform needle shaped anhydrite.

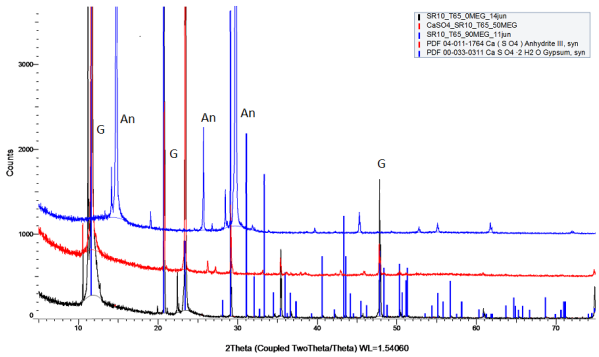

Figure 4.26 – XRD plots for $SR_{CaSO_4} = 10$ for T = 65 °C and all wt % of MEG.

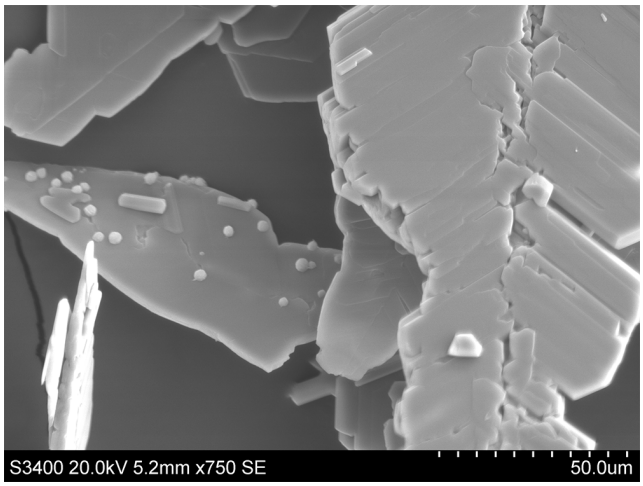

Figure 4.27 – SEM pictures of $SR_{CaSO_4} = 10$ at 0 wt% MEG and 65 °C. Scalebar is 50µm and magnification is 750.

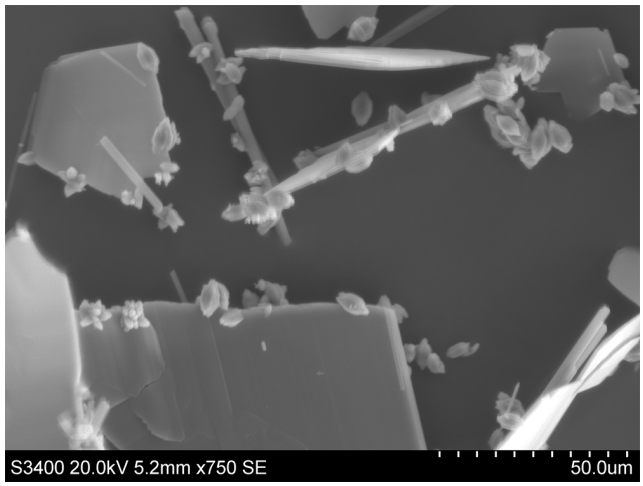

Figure 4.28 – SEM pictures of $SR_{CaSO_4} = 10$ at 50 wt% MEG and 65 °C. Scalebar is 50µm and magnification is 750.

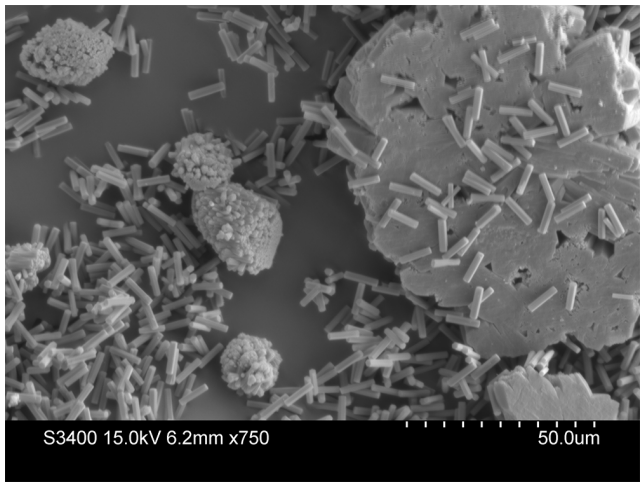

Figure 4.29 – SEM pictures of $SR_{CaSO_4} = 10$ at 90 wt% MEG and 65 °C. Scalebar is 50µm and magnification is 750.

Figure 4.30 shows XRD-plots for experiments at T = 30 °C for $SR_{CaSO_4} = 1$ and varying MEG concentrations. Only calcium carbonate precipitates in these experiments. At 0 wt % MEG all polymorphs of calcium carbonate, calcite, vaterite and aragonite can be found. However the dominating polymorphs are calcite and aragonite as seen in figure 4.31. For 50 wt % of MEG calcite is the dominating polymorph, but some vaterite and aragonite can also be seen in figure 4.32. Vaterite and calcite are the dominating polymorphs at 90 wt % MEG at these conditions, as seen in figure 4.33. The effect of MEG on the size of the crystals is clearly seen in the SEM pictures. The crystals found in no MEG are larger and more complex, they are formed from many smaller crystals with different polymorphs, than the crystals found in 50 wt % MEG. The crystals in 50 wt % MEG consist of some complex crystals, but it can clearly be seen monoclinic calcite and spheric vaterite as smaller crystals. At 90 wt % MEG the crystals consist mainly of small vaterite spheres and some calcite cubes, which are much smaller than the crystals found in experiments with lower MEG concentrations.

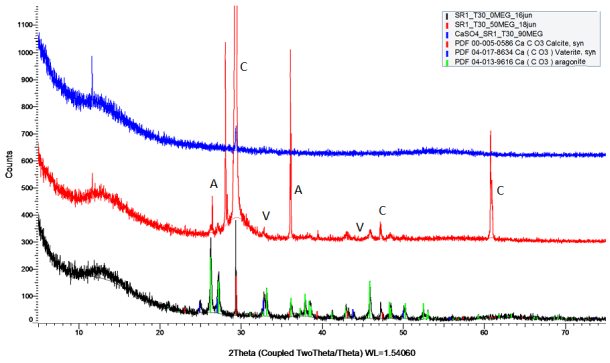

Figure 4.30 – XRD plots for $SR_{CaSO_4} = 1$ for T = 30 °C and all wt % of MEG.

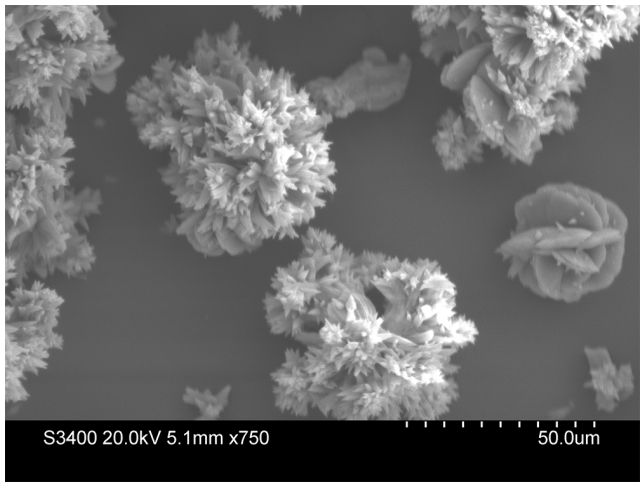

Figure 4.31 – SEM pictures of $SR_{CaSO_4} = 1$ at 0 wt% MEG and 30 °C. Scalebar is 50µm and magnification is 750.

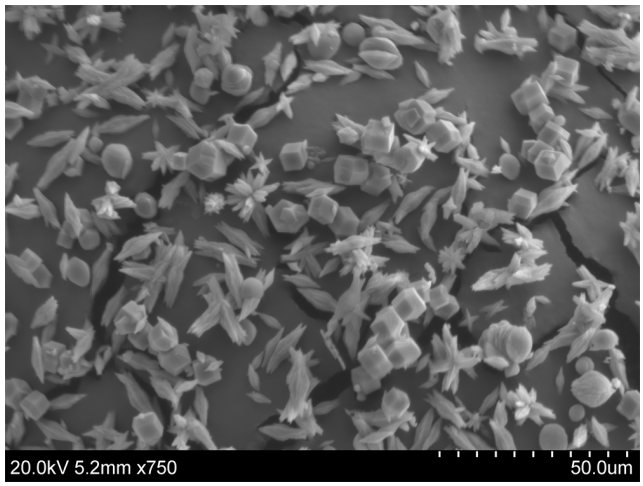

Figure 4.32 – SEM pictures of $SR_{CaSO_4} = 1$ at 50 wt% MEG and 30 °C. Scalebar is 50µm and magnification is 750.

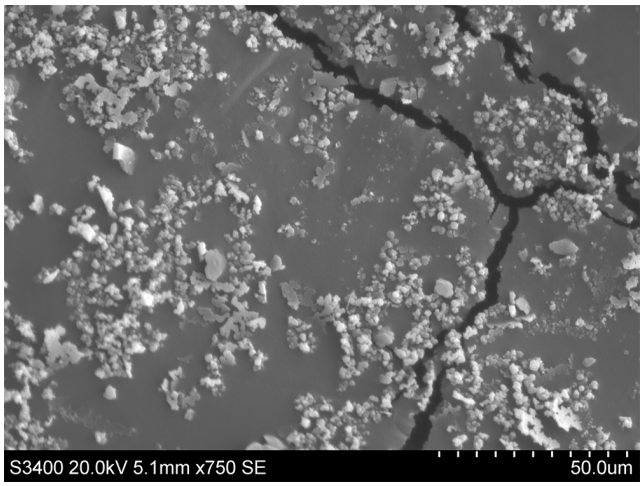

Figure 4.33 – SEM pictures of $SR_{CaSO_4} = 1$ at 90 wt% MEG and 30 °C. Scalebar is 50µm and magnification is 750.

Figure 4.34 shows XRD-plots for experiments at T = 65 °C for $SR_{CaSO_4} = 1$ and varying MEG concentrations. Only calcium carbonate precipitates in these experiments. At 0 wt % MEG all polymorphs of calcium carbonate, calcite, vaterite and aragonite can be found. However the dominating polymorph is aragonite as seen in figure 4.35 where aragonite spikes grow out of a vaterite flower. For 50 wt % calcite is the dominating polymorph, but some vaterite and aragonite can also be seen in figure 4.36 where complex crystals consisting of all polymorphs can be seen. The dominating polymorphs at 90 wt % MEG at these conditions are harder to determine. As seen in figure 4.37 the crystals have formed in a filter cake that has been broken. It can however be assumed that aragonite and calcite can be found because of the polymorphic abundance at this temperature, see figure 2.12. The effect of MEG on the size of the crystals is also seen in the SEM pictures. The crystals found in no MEG are larger and more complex, than the crystals found in 50 wt % MEG.

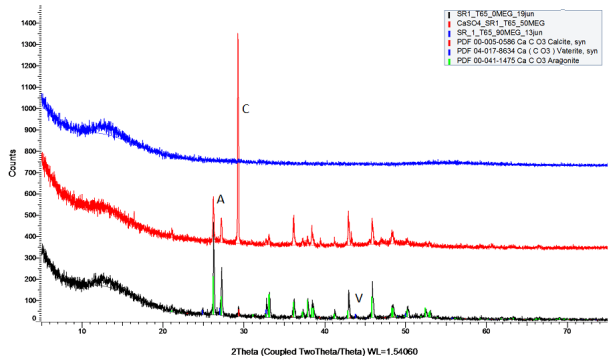

Figure 4.34 – XRD plots for $SR_{CaSO_4} = 1$ for T = 65 °C and all wt % of MEG.

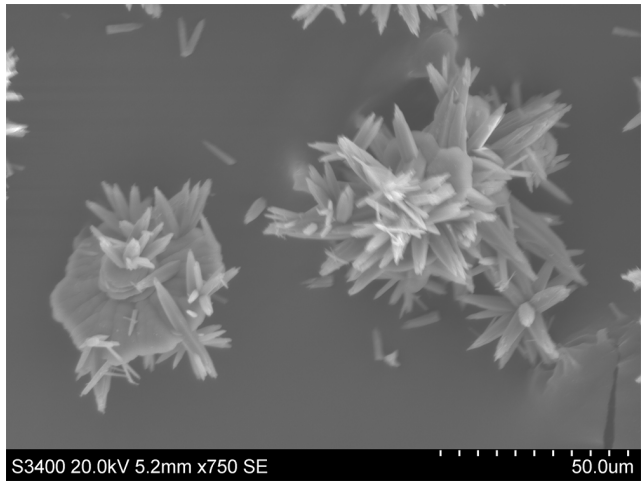

Figure 4.35 – SEM pictures of $SR_{CaSO_4} = 1$ at 0 wt% MEG and 65 °C. Scalebar is 50µm and magnification is 750

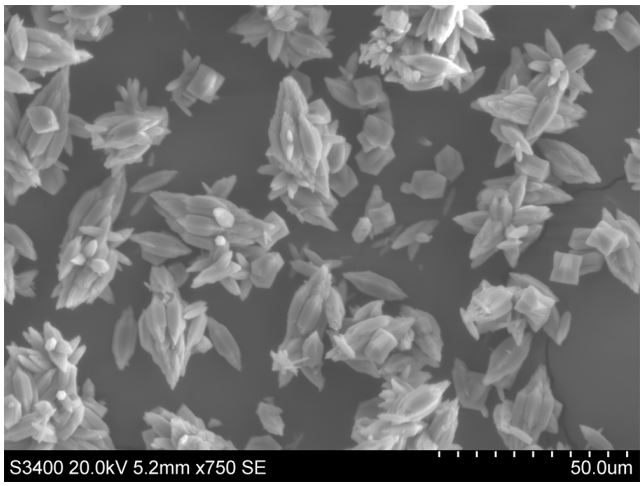

Figure 4.36 – SEM pictures of $SR_{CaSO_4} = 1$ at 50 wt% MEG and 65 °C. Scalebar is 50µm and magnification is 750.

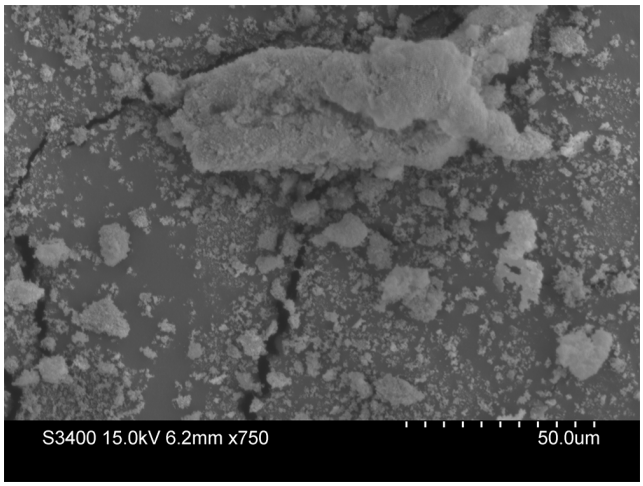

Figure 4.37 – SEM pictures of $SR_{CaSO_4} = 1$ at 90 wt% MEG and 65 °C. Scalebar is 50µm and magnification is 750.

The gypsum-anhydrite shift is at approximately 45 °C in pure water, and at ≈ 50 wt % MEG at T < 45 °C. For 90 wt % MEG at T = 65 °C the phase of calcium sulfate found is anhydrite. A reason for this is that gypsum consist of two crystal water in its structure, and with high MEG concentration, it is not enough water in the solution to favor gypsum precipitation, and thus anhydrite is the most stable phase at these conditions [7].

4.5 Effect of Supersaturation

The effect of supersaturation was investigated by performing experiments with four different saturation ratios at all conditions, varying MEG concentration and temperature. Saturation ratios were chosen to favour both precipitation of only calcium carbonate in the presence of sulfate, $SR_{CaSO_4} = 1$, and fast precipitation of calcium sulfate, $SR_{CaSO_4} = 10$. Two saturation ratios between the outer points were chosen to get a better understanding of which salt precipitates first of calcium carbonate and calcium sulfate. The temperatures, T = 35 °C and T = 65 °C were chosen based on thermodynamical scale calculations from Total, seen in appendix D. The MEG concentrations were chosen to ensure understanding of simultaneous precipitation with and without MEG, and the high 90 wt % MEG concentration was chosen in the hope of precipitating anhydrite.

Experiments with 0 wt % MEG and T = 30 °C

Figure 4.38 and figure 4.39 show the measured pH values for experiments with $SR_{CaSO_4} = 1, 2.5, 4 \text{and} 10$ for 0 wt % MEG and T = 30 °C, and the titration curve for the same experiments, respectivly.

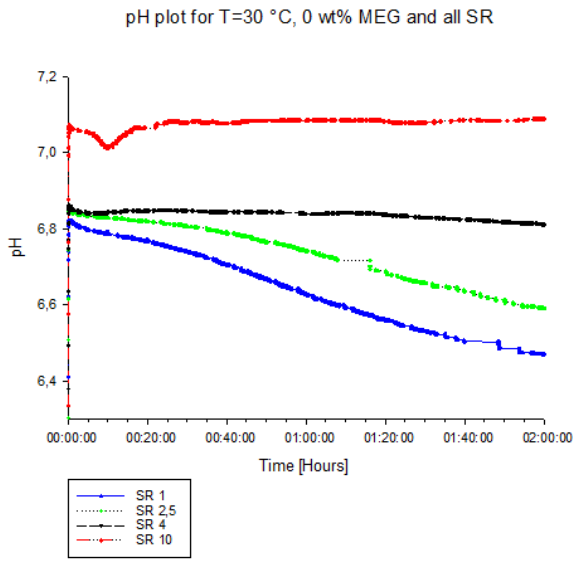

Figure 4.38 – pH-plot for experiments with T = 30 °C and 0 wt & MEG for all SR_{CaSO_4}.

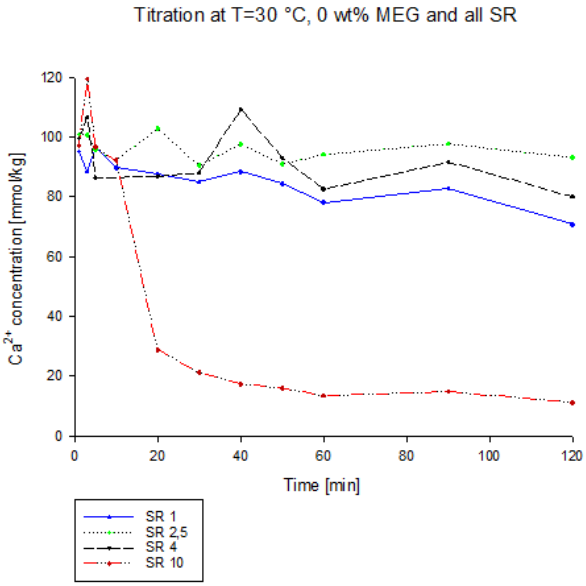

Figure 4.39 – Titration curves for experiments with T = 30 °C and 0 wt & MEG for all SR_{CaSO_4}.

A decrease in the pH for the two lowest saturation ratios is clearly seen in figure 4.38, which indicates that calcium carbonate has precipitated. The decrease in pH for the experiments with the two highest saturation ratios is small, or non existent, which indicates that calcium sulfate has precipitated. Comparing figure 4.38 and figure 4.39 gives a better understanding of what has happened in the reactor. For $SR_{CaSO_4} = 10$ a non existing pH decrease, is followed by a large drop in calcium concentration, indicating that a lot of calcium has precipitated 20 minutes into the experiment. As seen from figure 4.40, XRD analysis of the crystals for $SR_{CaSO_4} = 10$ is found to consist only of calcium sulfate, gypsum.

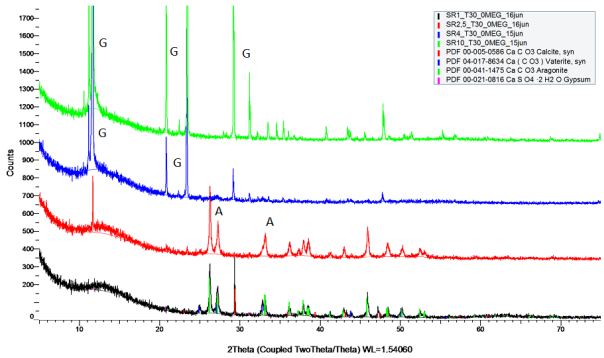

Figure 4.40 – XRD-plots for T = 30 °C and 0 wt & MEG for all SR_{CaSO_4}.

Figures 4.41 to 4.48 show the development of crystals for all experiments at 0 wt % MEG, T = 30 °C and all saturation ratios. It is clearly seen that the crystals formed after 27 minutes for $SR_{CaSO_4} = 1$ in figure 4.41 is a combination of all polymorphs of calcium carbonate. The presence of calcium carbonate crystals at 27 minutes in the reactor, corresponds well to the pH decrease seen in figure 4.38 and the decrease in calcium concentration seen in figure 4.39. After 2 hours, the crystals have developed into more complex systems as seen in figure 4.42, but no gypsum has precipitated, which corresponds well to the XRD-plot.

It is further seen that the crystals formed after 19 minutes for $SR_{CaSO_4} = 2.5$ in figure 4.43 is a combination of different polymorphs of calcium carbonate. This corresponds well to the measured pH decrease, which is steeper than the one for $SR_{CaSO_4} = 1$. After 2 hours, the crystals in the reactor have developed into more complex crystals consisting of different polymorphs of calcium carbonate, seen in figure 4.44. The amount of crystals has also increased.

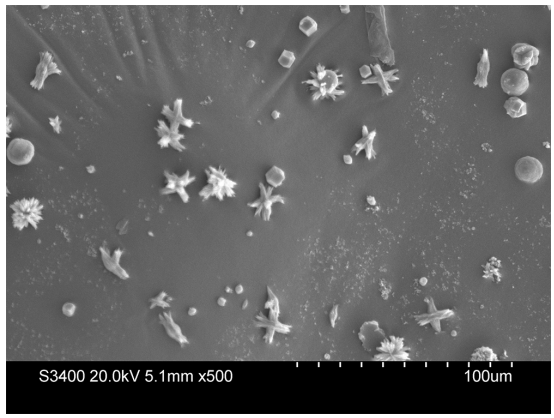

Figure 4.41 – SEM picture of the experiment with 0 wt % MEG, T = 30 °C at $SR_{CaSO_4} = 1$ after 27 minutes. Scalebar is 100 µm and magnification is 500.

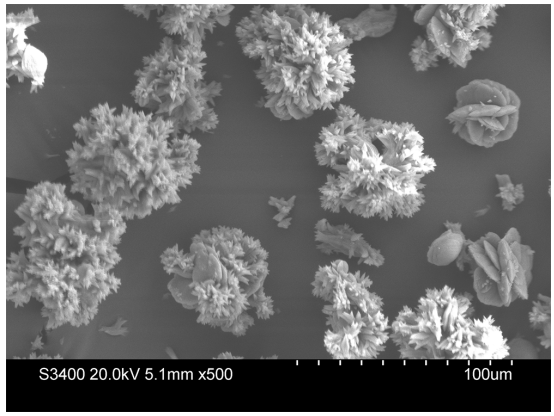

Figure 4.42 – SEM picture of the experiment with 0 wt % MEG, T = 30 °C at $SR_{CaSO_4} = 1$ after 2 hours. Scalebar is 100 µm and magnification is 500.

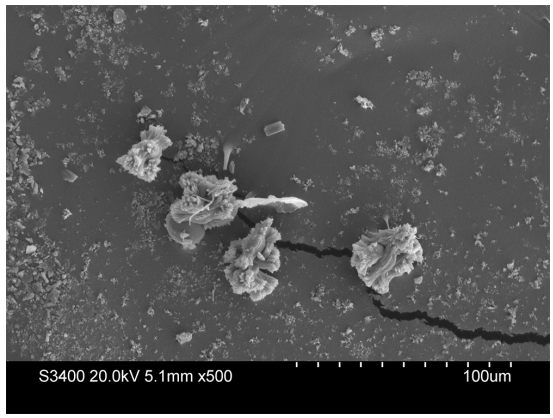

Figure 4.43 – SEM picture of the experiment with 0 wt % MEG, T = 30 °C at $SR_{CaSO_4} = 2.5$ after 19 minutes. Scalebar is 100 µm and magnification is 500.

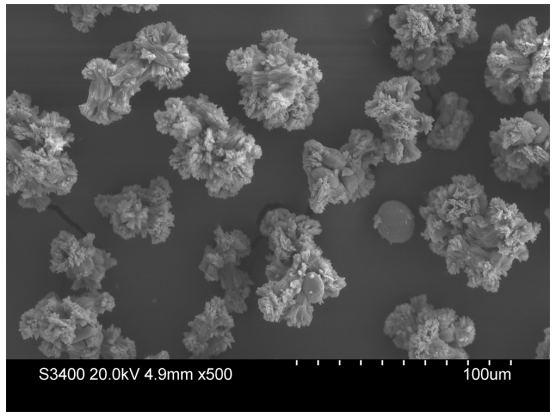

Figure 4.44 – SEM picture of the experiment with 0 wt % MEG, T = 30 °C at $SR_{CaSO_4} = 2.5$ after 2 hours. Scalebar is 100 µm and magnification is 500.

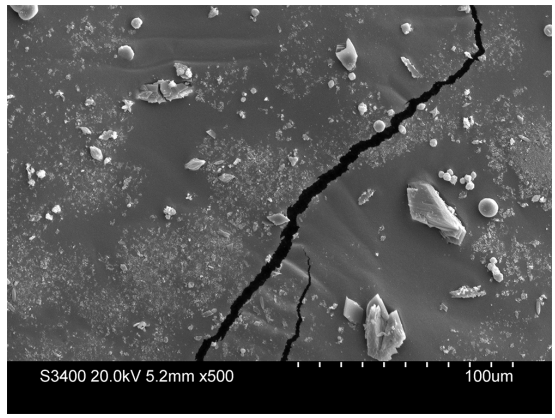

Figure 4.45 – SEM picture of the experiment with 0 wt % MEG, T = 30 °C at $SR_{CaSO_4} = 4$ after 51.5 minutes. Scalebar is 100 µm and magnification is 500.

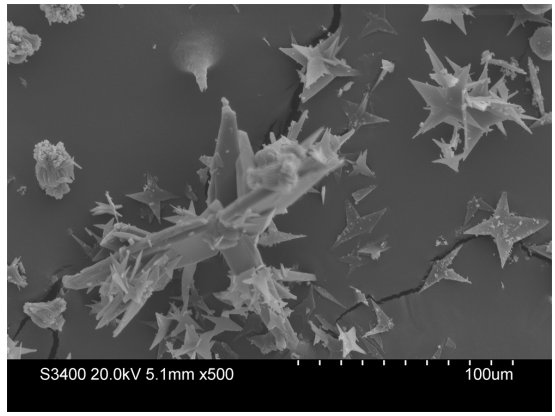

Figure 4.46 – SEM picture of the experiment with 0 wt % MEG, T = 30 °C at SR_{CaSO_4} = after 2 hours. Scalebar is 100 µm and magnification is 500.

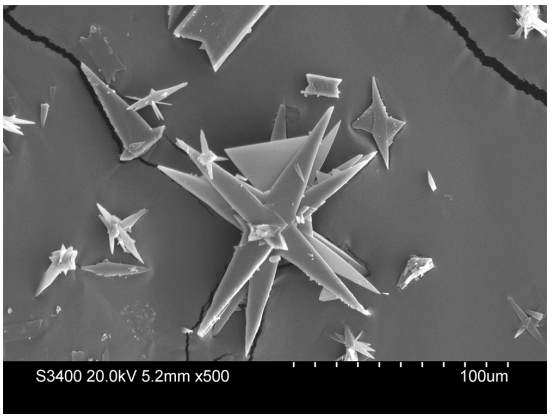

Figure 4.47 – SEM picture of the experiment with 0 wt % MEG, T = 30 °C at $SR_{CaSO_4} = 10$ after 7 minutes. Scalebar is 100 µm and magnification is 500.

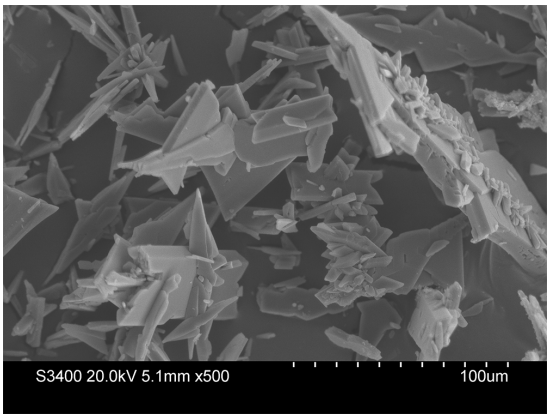

Figure 4.48 – SEM picture of the experiment with 0 wt % MEG, T = 30 °C at $SR_{CaSO_4} = 1$ after 2 hours. Scalebar is 100 µm and magnification is 500.

The crystals formed after 51,5 minutes for $SR_{CaSO_4} = 4$ in figure 4.45 are a combination of plate like gypsum and spheric vaterite. The presence of gypsum

crystals at 51,5 minutes in the reactor, corresponds well to the almost non existing pH decrease seen in figure 4.38. The decrease in calcium concentration seen in figure 4.39 tells that calcium has precipitated, and comparing pH and titration plots results in an assumption that gypsum has precipitated. After 2 hours, the crystals have developed into more complex systems of gypsum formed as rough stars, as seen in figure 4.46, which corresponds well to the XRD-plot showing gypsum as the dominating phase at these conditions.

The crystals formed after 7 minutes for $SR_{CaSO_4} = 10$ in figure 4.47 are large gypsum star shaped crystals of calcium sulfate. This corresponds well to the non exicting pH decrease. The titration curve shows a large drop in calcium concentration, indicating that gypsum has precipitated fast. After 2 hours, the crystals in the reactor has grown into more complex crystals, seen in figure 4.48.

Experiments with 50 wt % MEG and T = 30 °C

Figure 4.49 and figure 4.50 show the measured pH values for experiments with $SR_{CaSO_4} = 1, 2.5, 4 and 10$ for 50 wt % MEG and T = 30 °C, and the titration curve for the same experiments, respectivly.

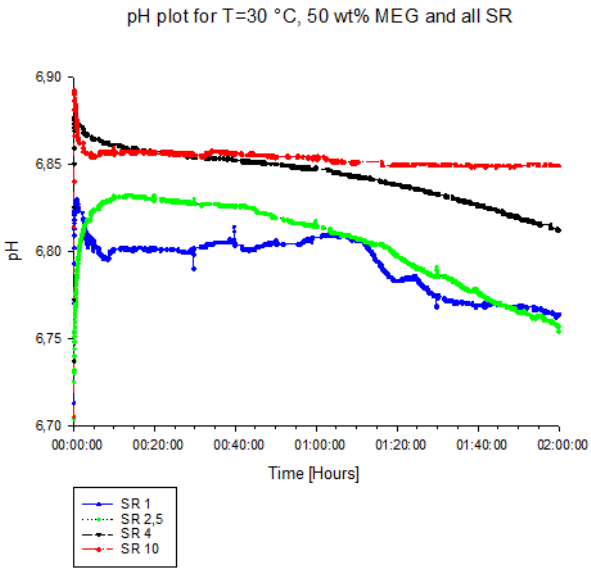

Figure 4.49 – pH-plot for experiments with T = 30 °C and 50 wt & MEG for all SR_{CaSO_4}.

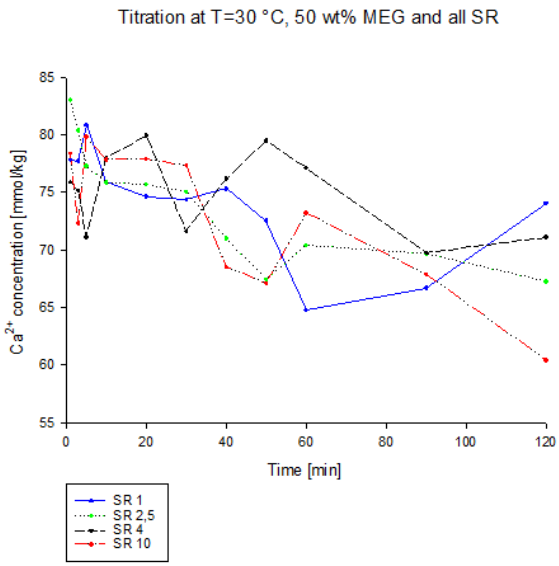

Figure 4.50 – Titration curves for experiments with T = 30 °C and 50 wt & MEG for all SR_{CaSO_4}.

It is clearly a decrease in the pH for the three lowest saturation ratios, which indicates that calcium carbonate has precipitated. The decrease in pH for the experiments with the highest saturation ratios is small, or non existent, which indicates that calcium sulfate has precipitated. Comparing figure 4.49 and figure 4.50 gives a better understanding of what has happend in the reactor. For $SR_{CaSO_4} = 10$ a non existing pH decrease, is followed by a quite large drop in calcium concentration, indicating that a lot of calcium has precipitated in the first 45 minutes of the experiment. As seen from figure 4.51, XRD analysis of the crystals for $SR_{CaSO_4} = 10$ is found to consist only of calcium sulfate.

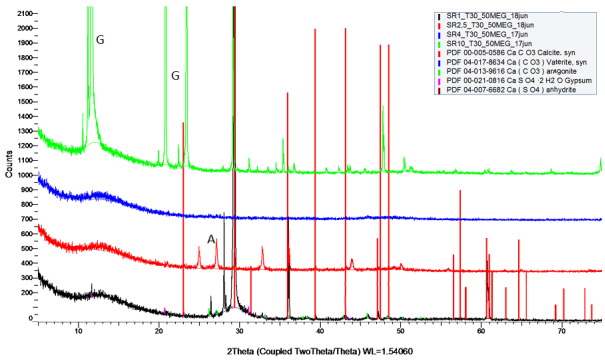

Figure 4.51 – XRD-plots for T = 30 °C and 50 wt & MEG for all SR_{CaSO_4}.

Figures 4.52 to 4.59 show the development of crystals for all experiments at 50 wt % MEG, T = 30 °C and all saturation ratios. It is clearly seen that the crystals formed after 72,5 minutes for $SR_{CaSO_4} = 1$ in figure 4.52 are a combination of all polymorphs of calcium carbonate. The presence of calcium carbonate crystals at 72,5 minutes in the reactor, corresponds well to the pH decrease seen in figure 4.49 and the decrease in calcium concentration seen in figure 4.50. After 2 hours, the crystals have developed into more complex systems as seen in figure 4.53, but no gypsum has precipitated, which corresponds well to the XRD-plot. Some crystals are still in a pure polymorphic form, as it is clearly observed vaterite spheres and calcite cubes.

It is further seen that the crystals formed after 38 minutes for $SR_{CaSO_4} = 2.5$ in figure 4.54 are a combination of different polymorphs of calcium carbonate. This corresponds well to the measured pH decrease, which starts earlier than the one for $SR_{CaSO_4} = 1$. After 2 hours, the crystals in the reactor have developed into more complex crystals consisting of different polymorphs of calcium carbonate, seen in figure 4.55. Some calcite cubes and vaterite spheres can still be observed. The amount of crystals have also increased.

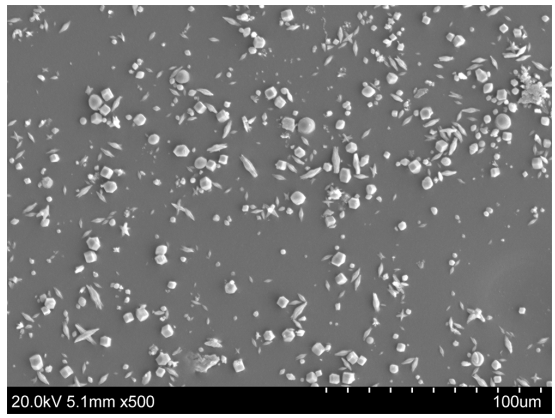

Figure 4.52 – SEM picture of the experiment with 50 wt % MEG, T = 30 °C at $SR_{CaSO_4} = 1$ after 72.5 minutes. Scalebar is 100 µm and magnification is 500.

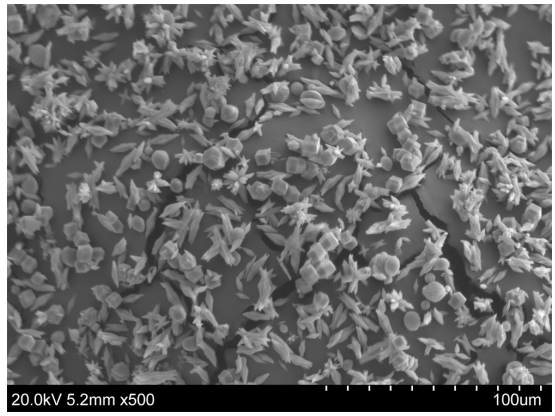

Figure 4.53 – SEM picture of the experiment with 50 wt % MEG, T = 30 °C at $SR_{CaSO_4} = 1$ after 2 hours. Scalebar is 100 µm and magnification is 500.

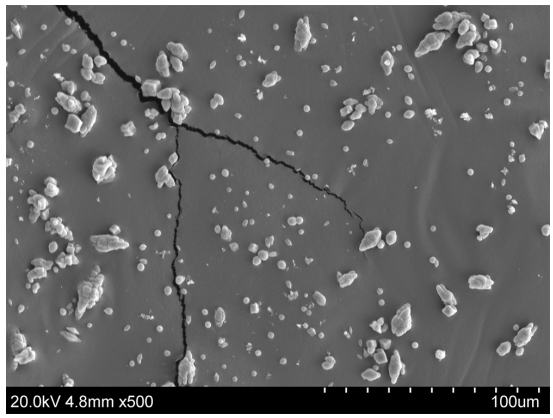

Figure 4.54 – SEM picture of the experiment with 50 wt % MEG, T = 30 °C at $SR_{CaSO_4} = 2.5$ after 38 minutes. Scalebar is 100 µm and magnification is 500.

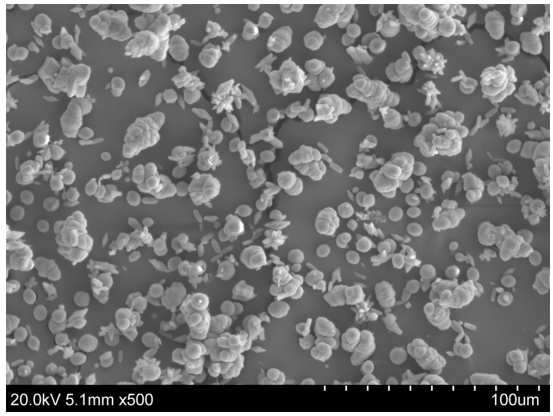

Figure 4.55 – SEM picture of the experiment with 50 wt % MEG, T = 30 °C at $SR_{CaSO_4} = 2.5$ after 2 hours. Scalebar is 100 µm and magnification is 500.

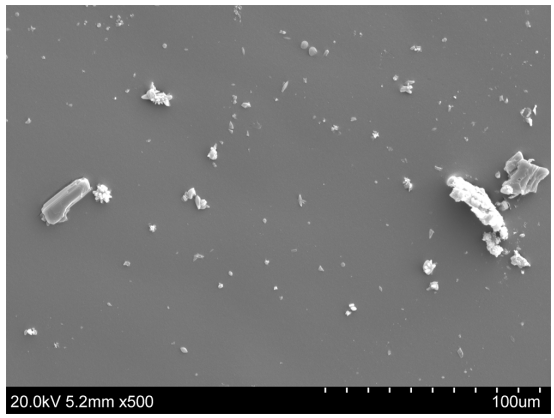

Figure 4.56 – SEM picture of the experiment with 50 wt % MEG, T = 30 °C at $SR_{CaSO_4} = 4$ after 42 minutes. Scalebar is 100 µm and magnification is 500.

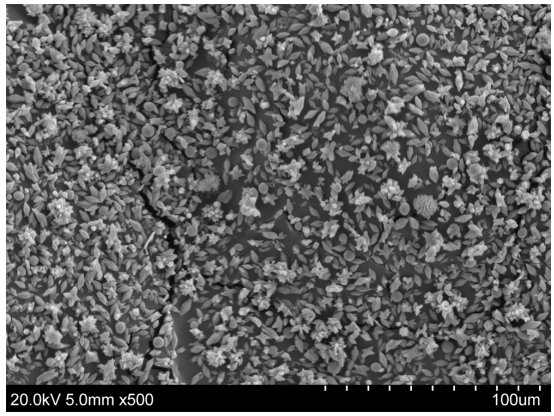

Figure 4.57 – SEM picture of the experiment with 50 wt % MEG, T = 30 °C at $SR_{CaSO_4} = 4$ after 2 hours. Scalebar is 100 µm and magnification is 500.

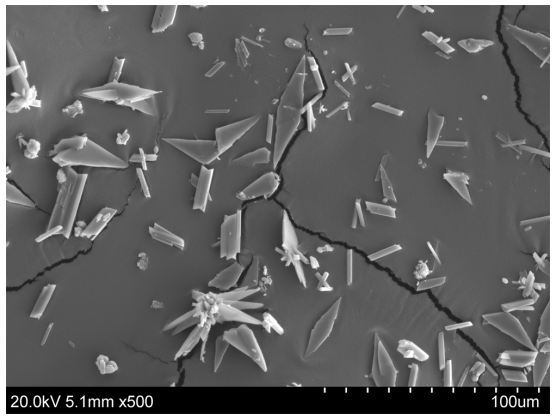

Figure 4.58 – SEM picture of the experiment with 50 wt % MEG, T = 30 °C at $SR_{CaSO_4} = 10$ after 42 minutes. Scalebar is 100 µm and magnification is 500.

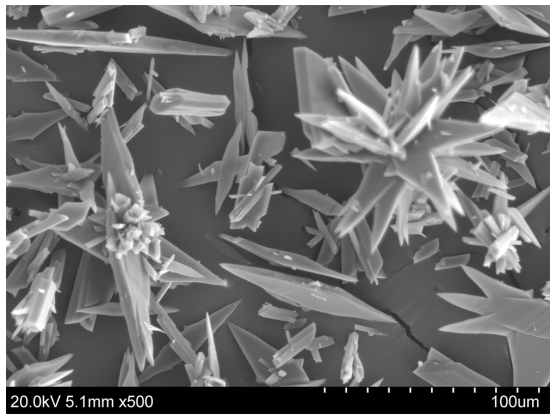

Figure 4.59 – SEM picture of the experiment with 50 wt % MEG, T = 30 °C at $SR_{CaSO_4} = 10$ after 2 hours. Scalebar is 100 µm and magnification is 500.

The crystals formed after 42 minutes for $SR_{CaSO_4} = 4$ in figure 4.56 are mostly plate like gypsum. The presence of gypsum crystals at 42 minutes in

the reactor, corresponds well to the stable pH curve up until this point as seen in figure 4.49. The decrease in calcium concentration seen in figure 4.50 tells that calcium has precipitated, and comparing pH and titration plots gives an assumption that gypsum has precipitated. After 2 hours, more crystals have become visible, and some calcium carbonate is also seen in figure 4.57, which corresponds well to the XRD-plot for these conditions.

The crystals formed after 42 minutes for $SR_{CaSO_4} = 10$ in figure 4.58 are gypsum star shaped crystals of calcium sulfate. This corresponds well to the non existing pH decrease. The titration curve shows a large drop in calcium concentration, indicating that gypsum has precipitated fast. After 2 hours, the crystals in the reactor have grown into more complex crystals, seen in figure 4.48 and the amount of crystals have increased.

Experiments with 90 wt % MEG and T = 30 °C

Figure 4.60 and figure 4.61 show the measured pH values for experiments with $SR_{CaSO_4} = 1, 2.5, 4 \text{and} 10$ for 90 wt % MEG and T = 30 °C, and the titration curve for the same experiments, respectivly.

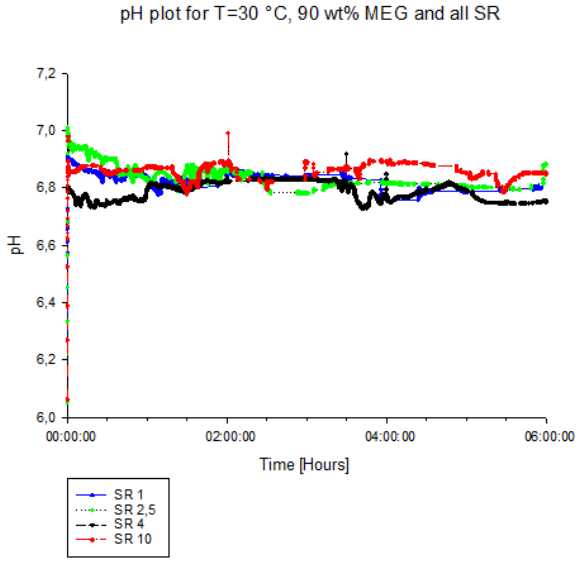

Figure 4.60 – pH-plot for experiments with T = 30 °C and 90 wt & MEG for all SR_{CaSO_4}.

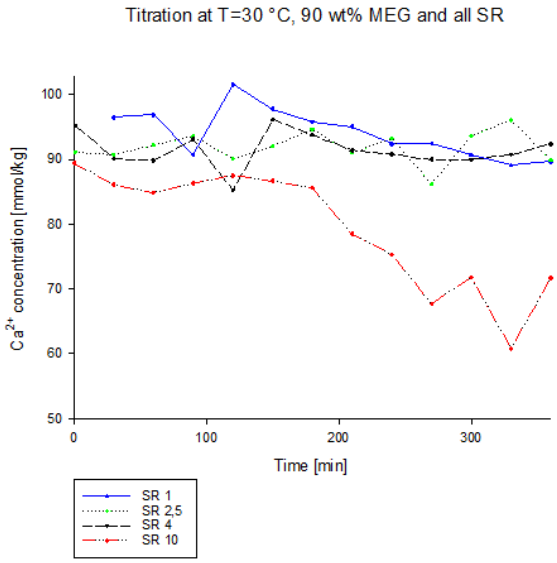

Figure 4.61 – Titration curves for experiments with T = 30 °C and 90 wt & MEG for all SR_{CaSO_4}.

It is hard to observe a decrease in the pH for different saturation ratios, which indicates that calcium sulfate might have precipitated. Comparing figure 4.60 and figure 4.61 gives a better understanding of what has happened in the reactor. For $SR_{CaSO_4} = 10$ a non existing pH decrease, is followed by a quite large drop in calcium concentration, indicating that a lot of calcium has precipitated during the 360 minute long experiment. As seen from figure 4.62, XRD analysis of the crystals for $SR_{CaSO_4} = 10$ is found to consist only of calcium sulfate anhydrite, and lower saturation ratio experiments consists of anhydrite, gypsum and different polymorphs of calcium carbonate.

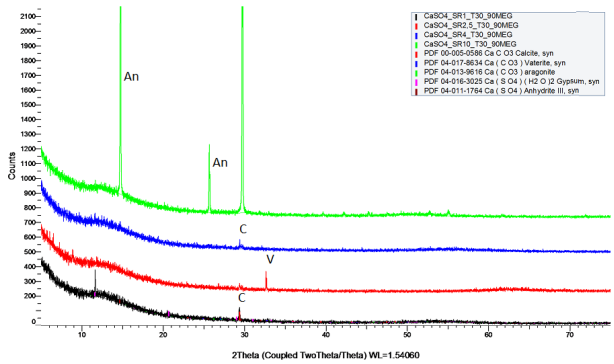

Figure 4.62 – XRD-plots for T = 30 °C and 90 wt & MEG for all SR_{CaSO_4}.

Figures 4.63 to 4.66 show the development of crystals for all experiments at 90 wt % MEG, T = 30 °C and all saturation ratios. It is clearly seen that the crystals for $SR_{CaSO_4} = 1$ in figure 4.53 are a combination of calcium carbonate and calcium sulfate. The presence of calcium carbonate crystals at the end of the experiment in the reactor, can not be seen from a pH decrease in figure 4.60. The decrease in calcium concentration seen in figure 4.61 is small, but present, indicating that some calcium has precipitated. The XRD-plot shows that the crystals are expected to have both calcium sulfate, in the form of gypsum, and calcium carbonate present.

It is further seen that the crystals formed for $SR_{CaSO_4} = 2.5$ in figure 4.64 are a combination of calcium carbonate in vaterite form and calcium sulfate. The pH plot does not indicate the precipitation of calcium carbonate, but from the SEM picture it is clearly seen some calcium carbonate.

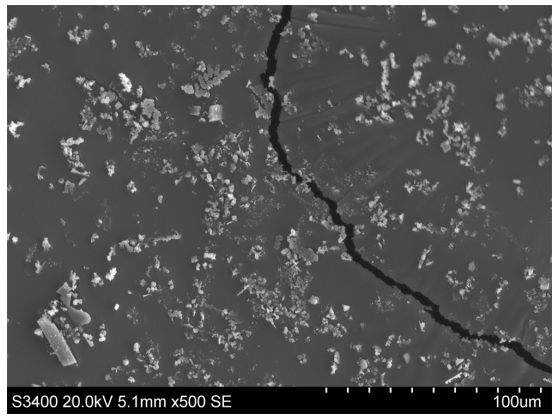

Figure 4.63 – SEM picture of the experiment with 90 wt % MEG, T = 30 °C at $SR_{CaSO_4} = 1$ after 6 hours. Scalebar is 100 µm and magnification is 500.

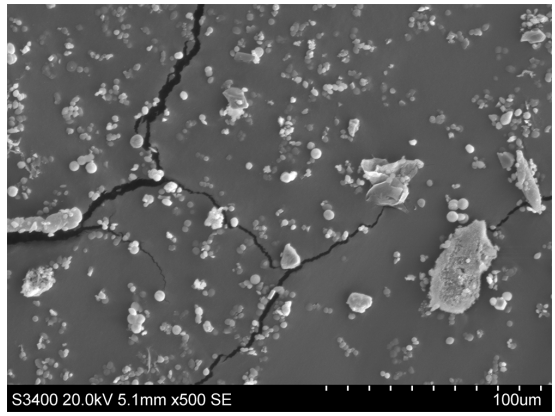

Figure 4.64 – SEM picture of the experiment with 90 wt % MEG, T = 30 °C at $SR_{CaSO_4} = 2.5$ after 6 hours. Scalebar is 100 µm and magnification is 500.

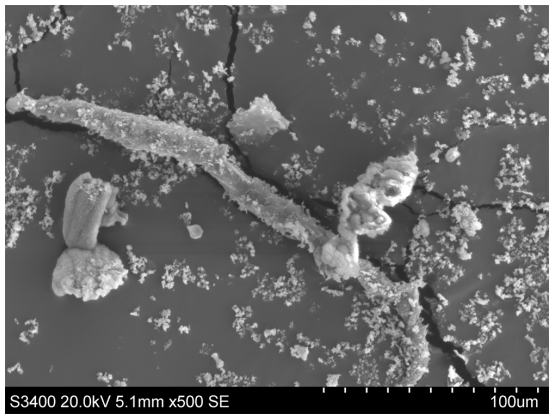

Figure 4.65 – SEM picture of the experiment with 90 wt % MEG, T = 30 °C at $SR_{CaSO_4} = 4$ after 6 hours. Scalebar is 100 µm and magnification is 500.

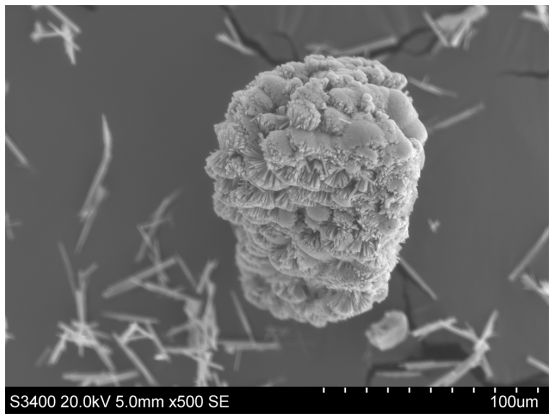

Figure 4.66 – SEM picture of the experiment with 90 wt % MEG, T = 30 °C at $SR_{CaSO_4} = 10$ after 6 hours. Scalebar is 100 µm and magnification is 500.

The crystals formed for $SR_{CaSO_4} = 4$ in figure 4.65 are calcium sulfate. The presence of calcium sulfate crystals in the reactor, correspond well to the

stable pH curve as seen in figure 4.60. The decrease in calcium concentration seen in figure 4.61 tells that some calcium has precipitated. The visible crystals correspond well to the XRD-plot for these conditions.

The crystals formed for $SR_{CaSO_4} = 10$ in figure 4.66 are small needle shaped anhydrite, which also have grown into larger crystals. This correspond well to the non existing pH decrease. The titration curve shows a large drop in calcium concentration, indicating that anhydrite precipitates faster at these conditions than for the other saturation ratios.

Experiments with 0 wt % MEG and T = 65 °C

Figure 4.67 and figure 4.68 show the measured pH values for experiments with $SR_{CaSO_4} = 1, 2.5, 4 \text{and} 10$ for 0 wt % MEG and T = 65 °C, and the titration curve for the same experiments, respectively.

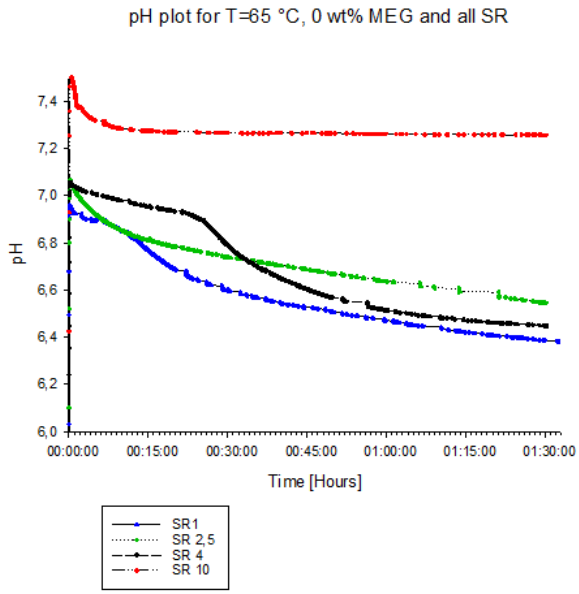

Figure 4.67 – pH-plot for experiments with T = 65 °C and 0 wt & MEG for all SR_{CaSO_4}.

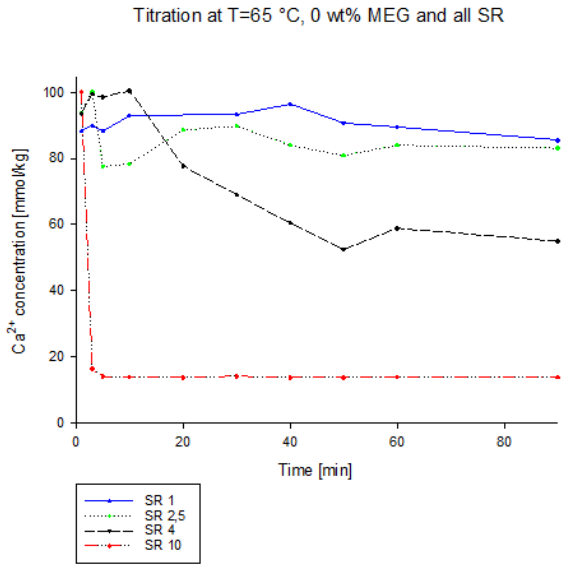

Figure 4.68 – Titration curves for experiments with T = 65 °C and 0 wt & MEG for all SR_{CaSO_4}. .

It is clearly a decrease in the pH for the three lowest saturation ratios, which indicates that calcium carbonate has precipitated. The decrease in pH for the experiments with the highest saturation ratios is small, or non existent, which indicates that calcium sulfate has precipitated. Comparing figure 4.67 and figure 4.68 gives a better understanding of what has happened in the reactor. For $SR_{CaSO_4} = 10$ a non existing pH decrease, is followed by a quite large drop in calcium concentration, indicating that a lot of calcium has precipitated in the first minutes of the experiment. As seen from figure 4.69, XRD analysis of the crystals for $SR_{CaSO_4} = 10$ is found to consist only of calcium sulfate.

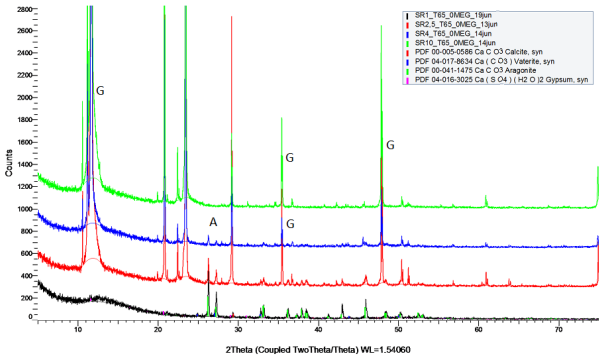

Figure 4.69 – XRD-plots for T = 65 °C and 0 wt & MEG for all SR_{CaSO_4}.

Figures 4.70 to 4.77 show the development of crystals for all experiments at 0 wt % MEG, T = 65 °C and all saturation ratios. It is clearly seen that the crystals formed after 11,5 minutes for $SR_{CaSO_4} = 1$ in figure 4.70 are a combination of all polymorphs of calcium carbonate but mostly aragonite and vaterite in the shape of flowers. The presence of calcium carbonate crystals at 11,5 minutes in the reactor, corresponds well to the pH decrease seen in figure 4.67 and the decrease in calcium concentration seen in figure 4.68. After 1,5 hours, the crystals have developed into more complex systems, consisting of a lot of aragonite, as seen in figure 4.71, but no gypsum has precipitated, which corresponds well to the XRD-plot.

It is further seen that the crystals formed after 13 minutes for $SR_{CaSO_4} = 2.5$ in figure 4.72 consist of calcium carbonate. This corresponds well to the measured pH decrease, which starts later than the one for $SR_{CaSO_4} = 1$. After 1,5 hours, the crystals in the reactor have developed into more complex crystals consisting of different polymorphs of calcium carbonate, seen in figure 4.73 on the edges of the gypsum crystals. The XRD-plot confirms that both gypsum and calcium carbonate is present at these conditions.

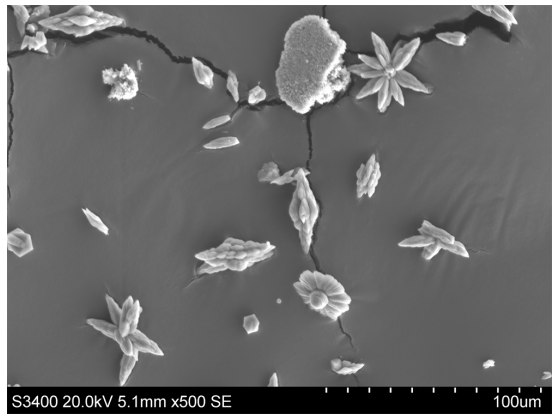

Figure 4.70 – SEM picture of the experiment with 0 wt % MEG, T = 65 °C at $SR_{CaSO_4} = 1$ after 11,5 minutes. Scalebar is 100 µm and magnification is 500.

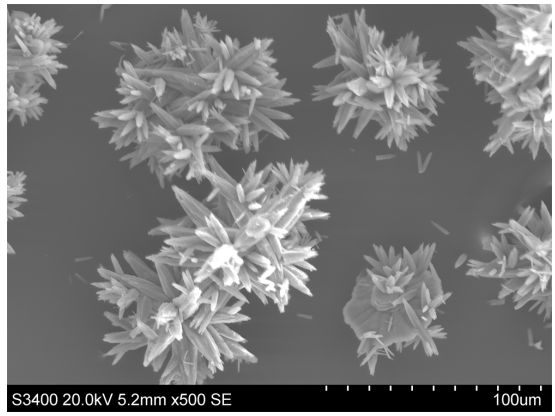

Figure 4.71 – SEM picture of the experiment with 0 wt % MEG, T = 65 °C at $SR_{CaSO_4} = 1$ after 1,5 hourss. Scalebar is 100 µm and magnification is 500.

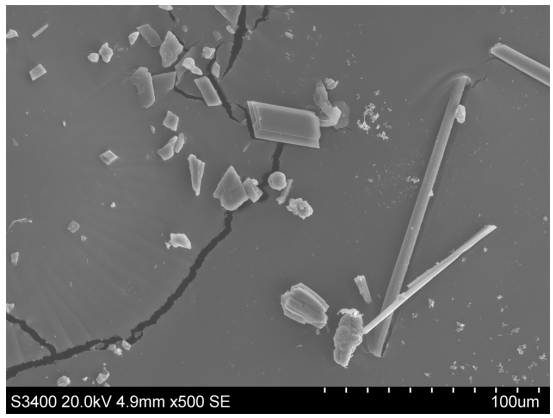

Figure 4.72 – SEM picture of the experiment with 0 wt % MEG, T = 65 °C at $SR_{CaSO_4} = 2.5$ after 13 minutes. Scalebar is 100 µm and magnification is 500.

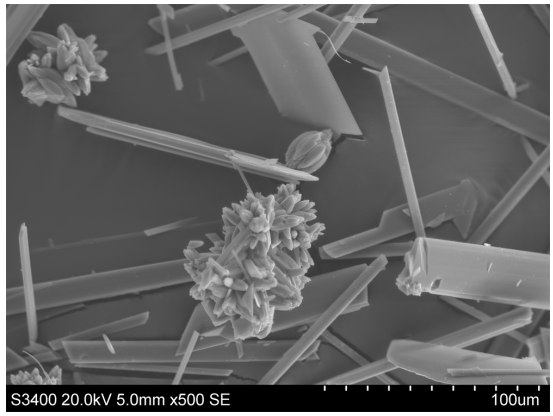

Figure 4.73 – SEM picture of the experiment with 0 wt % MEG, T = 65 °C at $SR_{CaSO_4} = 2.5$ after 1,5 hours. Scalebar is 100 µm and magnification is 500.

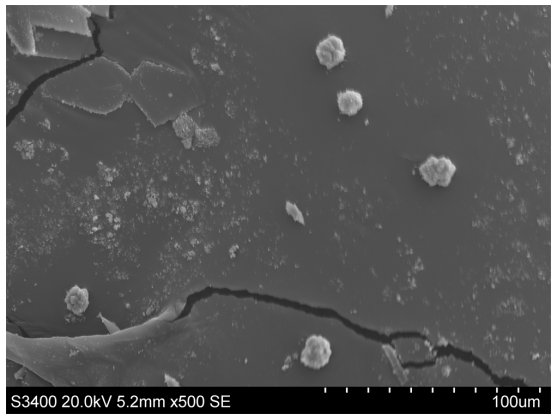

Figure 4.74 – SEM picture of the experiment with 0 wt % MEG, T = 65 °C at $SR_{CaSO_4} = 4$ after 12 minutes. Scalebar is 100 µm and magnification is 500.

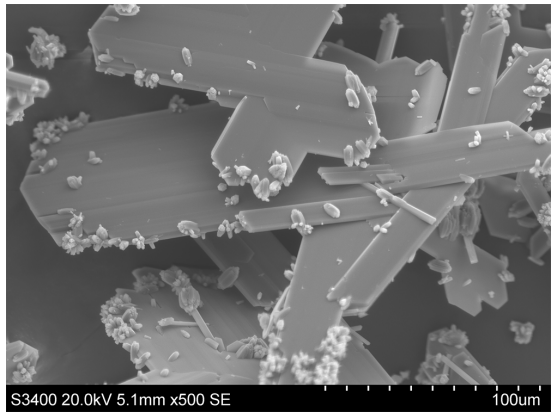

Figure 4.75 – SEM picture of the experiment with 0 wt % MEG, T = 65 °C at $SR_{CaSO_4} = 4$ after 1,5 hours. Scalebar is 100 µm and magnification is 500.

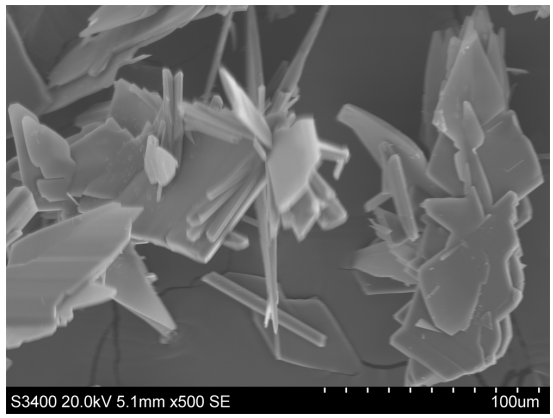

Figure 4.76 – SEM picture of the experiment with 0 wt % MEG, T = 65 °C at $SR_{CaSO_4} = 10$ after 3 minutes. Scalebar is 100 µm and magnification is 500.

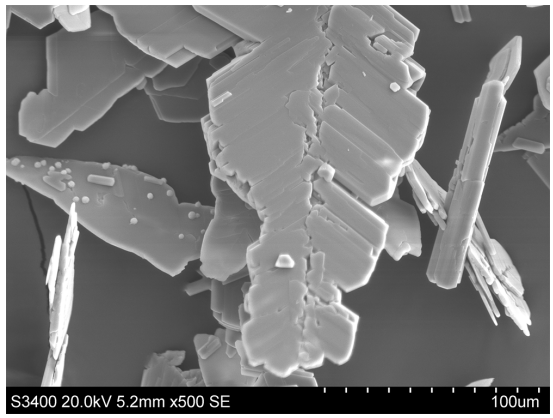

Figure 4.77 – SEM picture of the experiment with 0 wt % MEG, T = 65 °C at $SR_{CaSO_4} = 1$ after 1,5 hours. Scalebar is 100 µm and magnification is 500.

The crystals formed after 12 minutes for $SR_{CaSO_4} = 4$ in figure 4.74 are mostly plate like gypsum, but also some sphere like crystals of calcium car-

bonate can be seen. The presence of gypsum and calcium carbonate crystals at 12 minutes in the reactor, corresponds well to pH curve in figure 4.67. The decrease in calcium concentration seen in figure 4.68 tells that calcium has precipitated, and comparing pH and titration plots gives an assumption that both gypsum and calcium carbonate have precipitated. The titration curve is however steeper than the pH curve, which might indicate that gypsum has precipitated fast from the beginning of the experiment, and calcium carbonate has been slower, due to the small decrease in pH. After 1,5 hours, more crystals have become visible, and more calcium carbonate is seen in figure 4.75, indicating that the previous assumption for growth might be correct. The presence of both salts is also shown in the XRD-plot for these conditions.

The crystals formed after 3 minutes for $SR_{CaSO_4} = 10$ in figure 4.76 are gypsum plate shaped crystals of calcium sulfate. This corresponds well to the non exicting pH decrease. The titration curve shows a large drop in calcium concentration, indicating that gypsum has precipitated fast. After 1,5 hours, the crystals in the reactor have grown in size, see figure 4.77.

Experiments with 50 wt % MEG and T = 65 °C

Figure 4.78 and figure 4.79 show the measured pH values for experiments with $SR_{CaSO_4} = 1, 2.5, 4 \text{and} 10$ for 50 wt % MEG and T = 65 °C, and the titration curve for the same experiments, respectively.

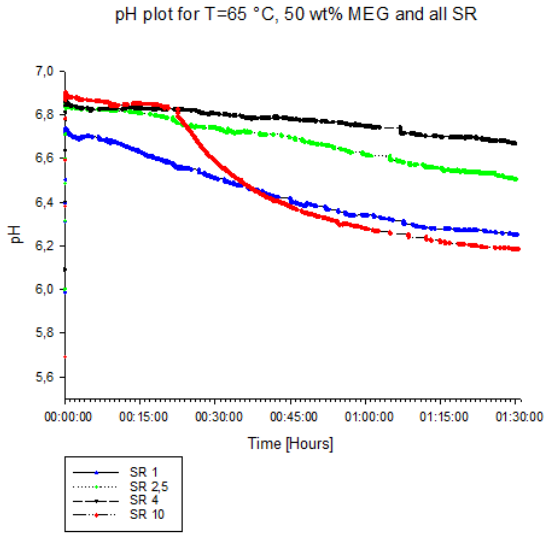

Figure 4.78 – pH-plot for experiments with T = 65 °C and 50 wt & MEG for all SR_{CaSO_4}.

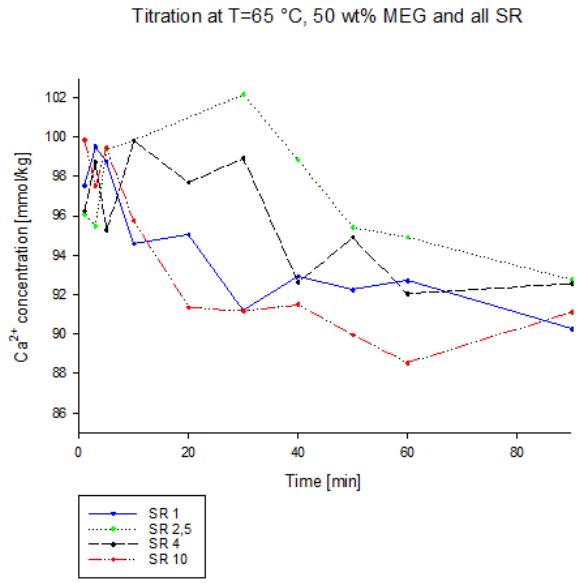

Figure 4.79 – Titration curves for experiments with T = 65 °C and 50 wt & MEG for all SR_{CaSO_4}.

It is clearly a decrease in the pH for all saturation ratios, which indicates that calcium carbonate has precipitated. Comparing figure 4.78 and figure 4.79 gives a better understanding of what has happend in the reactor. For $SR_{CaSO_4} = 10$ a quite large drop in calcium concentration, indicating that a lot of calcium has precipitated in the first minutes of the experiment. As seen from figure 4.80, XRD analysis of the crystals for $SR_{CaSO_4} = 10$ is found to consist of both gypsum and calcium carbonate.

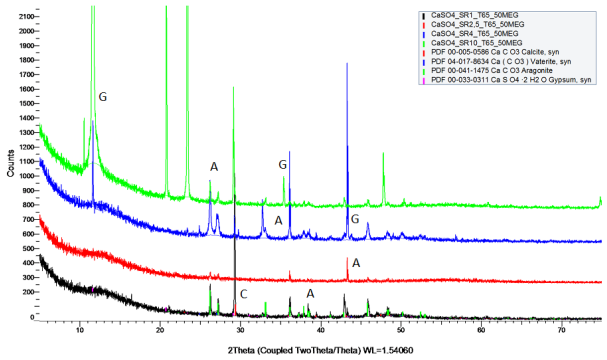

Figure 4.80 – XRD-plots for experiments with T = 65 °C and 50 wt & MEG for all SR_{CaSO_4}.

Figures 4.81 to 4.88 show the development of crystals for all experiments at 50 wt % MEG, T = 65 °C and all saturation ratios. It is clearly seen that the crystals formed after 12 minutes for $SR_{CaSO_4} = 1$ in figure 4.81 are a combination of all polymorphs of calcium carbonate. The presence of calcium carbonate crystals at 12 minutes in the reactor, corresponds well to the pH decrease seen in figure 4.78 and the decrease in calcium concentration seen in figure 4.79. After 1,5 hours, the crystals have developed into more complex systems, consisting of a lot of aragonite and vaterite, as seen in figure 4.82, but no gypsum has precipitated, which corresponds well to the XRD-plot.

It is further seen that the crystals formed after 18 minutes for $SR_{CaSO_4} = 2.5$ in figure 4.83 consist of calcium carbonate. This corresponds well to the meassured pH decrease. After 1,5 hours, the crystals in the reactor have developed into more complex crystals consisting of different polymorphs of calcium carbonate, seen in figure 4.84. The XRD-plot confirms that calcium carbonate is present at these conditions.

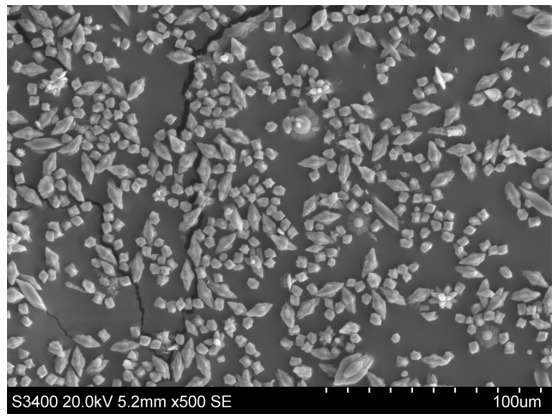

Figure 4.81 – SEM picture of the experiment with 50 wt % MEG, T = 65 °C at $SR_{CaSO_4} = 1$ after 12 minutes. Scalebar is 100 µm and magnification is 500.

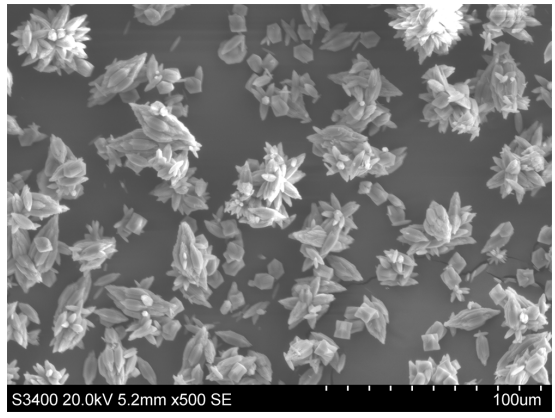

Figure 4.82 – SEM picture of the experiment with 50 wt % MEG, T = 65 °C at $SR_{CaSO_4} = 1$ after 1.5 hours. Scalebar is 100 µm and magnification is 500.

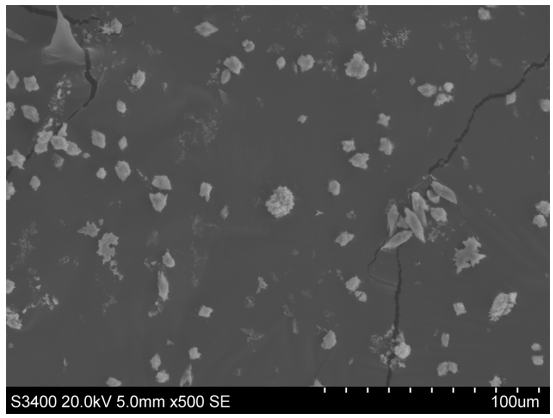

Figure 4.83 – SEM picture of the experiment with 50 wt % MEG, T = 65 °C at $SR_{CaSO_4} = 2.5$ after 18 minutes. Scalebar is 100 µm and magnification is 500.

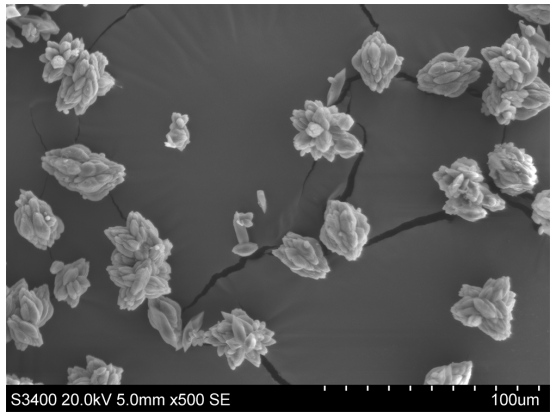

Figure 4.84 – SEM picture of the experiment with 50 wt % MEG, T = 65 °C at $SR_{CaSO_4} = 2.5$ after 1.5 hours. Scalebar is 100 µm and magnification is 500.

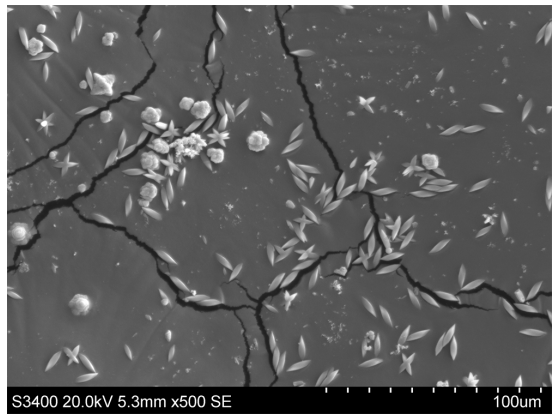

Figure 4.85 – SEM picture of the experiment with 50 wt % MEG, T = 65 °C at $SR_{CaSO_4} = 4$ after 33 minutes. Scalebar is 100 µm and magnification is 500.

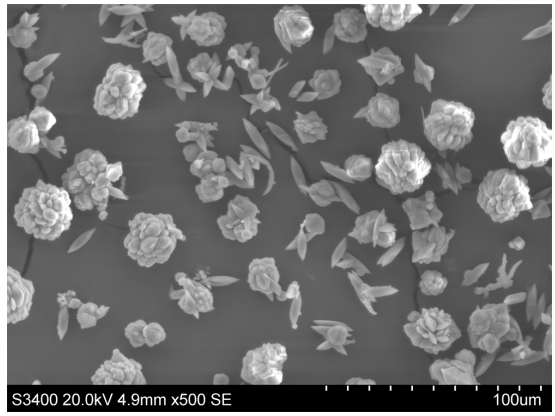

Figure 4.86 – SEM picture of the experiment with 50 wt % MEG, T = 65 °C at $SR_{CaSO_4} = 4$ after 1.5 hours. Scalebar is 100 µm and magnification is 500.

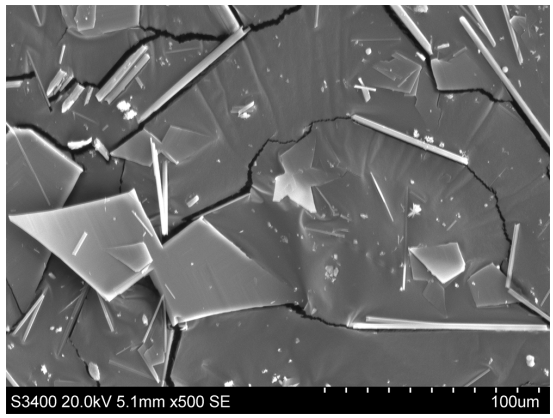

Figure 4.87 – SEM picture of the experiment with 50 wt % MEG, T = 65 °C at $SR_{CaSO_4} = 10$ after 8 minutes. Scalebar is 100 µm and magnification is 500.

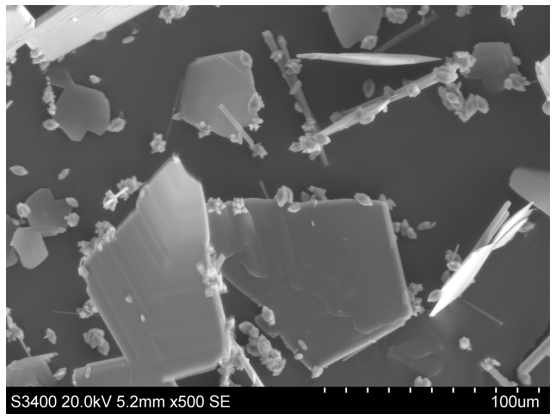

Figure 4.88 – SEM picture of the experiment with 50 wt % MEG, T = 65 °C at $SR_{CaSO_4} = 10$ after 1.5 hours. Scalebar is 100 µm and magnification is 500.

The crystals formed after 33 minutes for $SR_{CaSO_4} = 4$ in figure 4.74 are mostly small gypsum shaped as leafs, but also some vaterite crystals of calcium

carbonate can be seen. The presence of gypsum and calcium carbonate crystals at 33 minutes in the reactor, corresponds well to pH curve in figure 4.78. The decrease in calcium concentration seen in figure 4.79 tells that calcium has precipitated, and comparing pH and titration plots gives an assumption that both gypsum and calcium carbonate have precipitated. After 1,5 hours, more crystals have become visible, and more calcium carbonate in a more complex form is seen in figure 4.86. The presence of both salts is also shown in the XRD-plot for these conditions.

The crystals formed after 8 minutes for $SR_{CaSO_4} = 10$ in figure 4.87 are gypsum shaped as needles and plates. Some small crystals of calcium carbonate can also be seen. This corresponds well to the small pH decrease. The titration curve shows a large drop in calcium concentration, indicating that calcium has precipitated. After 1,5 hours, the crystals in the reactor have grown in size, seen in figure 4.88, and more calcium carbonate has precipitated on the edges of gypsum plates.

Experiments with 90 wt % MEG and T = 65 °C

Figure 4.89 and figure 4.90 show the measured pH values for experiments with $SR_{CaSO_4} = 1, 2.5, 4 \text{and} 10$ for 90 wt % MEG and T = 65 °C, and the titration curve for the same experiments, respectively.

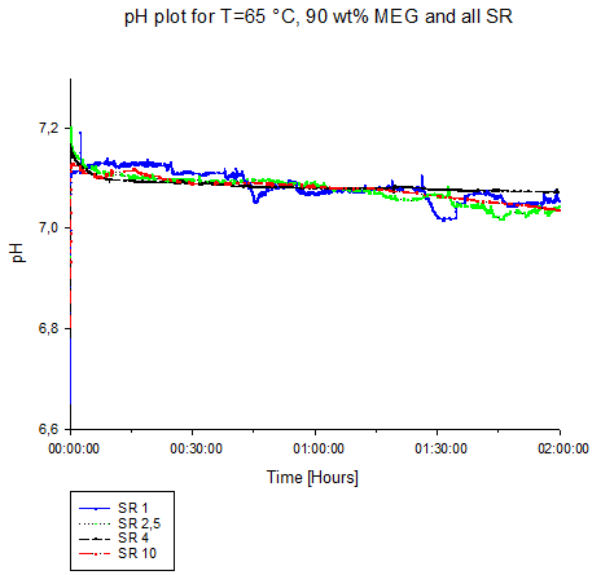

Figure 4.89 – pH-plot for experiments with T = 65 °C and 90 wt & MEG for all SR_{CaSO_4}.

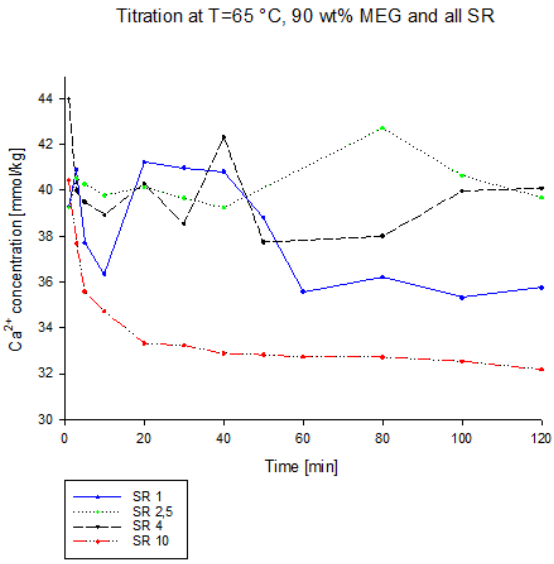

Figure 4.90 – Titration curves for experiments with T = 65 °C and 90 wt & MEG for all SR_{CaSO_4}.

A significant decrease in the pH for either of the saturation ratios, cannot be seen, which indicates that calcium sulfate is the dominating precipitate. Comparing figure 4.89 and figure 4.90 gives a better understanding of what has happened in the reactor. For $SR_{CaSO_4} = 10$ quite a large drop in calcium concentration, indicates that a lot of calcium has precipitated in the first minutes of the experiment. As seen from figure 4.91, XRD analysis of the crystals for $SR_{CaSO_4} = 10$ is found to consist only of calcium sulfate.

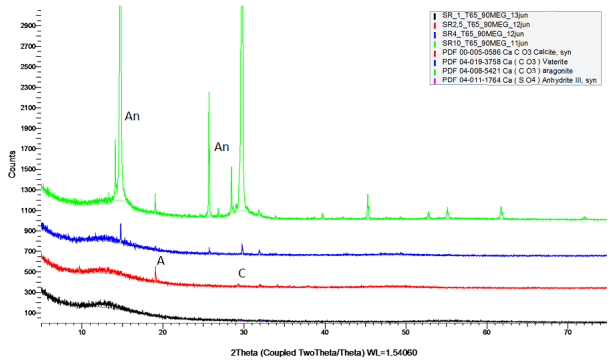

Figure 4.91 – XRD-plot for experiments with T = 65 °C and 90 wt & MEG for all SR_{CaSO_4}.

Figures 4.92 to 4.99 show the development of crystals for all experiments at 90 wt % MEG, T = 65 °C and all saturation ratios. It is assumed that the crystals formed after 32 minutes for $SR_{CaSO_4} = 1$ in figure 4.92 are a combination of all polymorphs of calcium carbonate. The presence of calcium carbonate crystals at 32 minutes in the reactor, does not show in the pH decrease in figure 4.89. A reason for seeing calcium carbonate crystals without a significant decrease in pH, might be an error in the pH measurements for 90 wt % MEG. A lot of disturbances can be seen in pH plots for both temperatures at 90 wt % MEG. The decrease in calcium concentration seen in figure 4.90 indicates precipitation of a calcium containing salt. After 2 hours, the crystals have developed into more complex systems, being covered with small crystals, as seen in figure 4.93, but no gypsum has precipitated, which corresponds well to the XRD-plot.

It is further seen that the crystals formed after 15 minutes for $SR_{CaSO_4} = 2.5$ in figure 4.94 consist of mostly calcium sulfate. This corresponds well to the measured pH. After 2 hours, the crystals in the reactor have developed into larger crystals consisting of smaller crystals, seen in figure 4.95. The XRD-plot confirms that calcium sulfate in anhydrite form is present at these conditions.

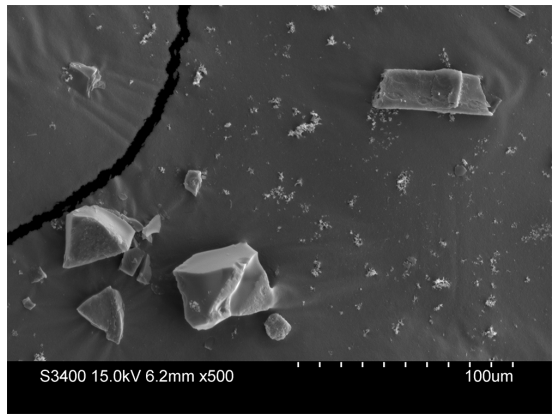

Figure 4.92 – SEM picture of the experiment with 90 wt % MEG, T = 65 °C at $SR_{CaSO_4} = 1$ after 32 minutes. Scalebar is 100 µm and magnification is 500.

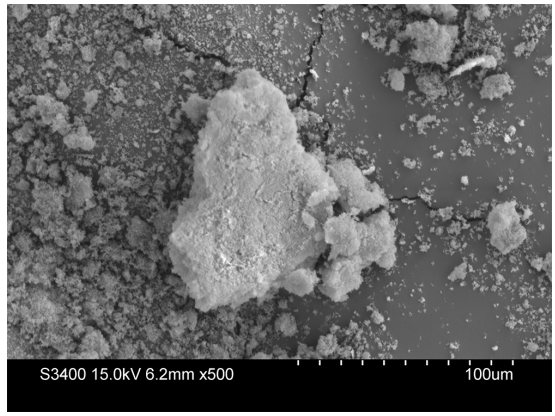

Figure 4.93 – SEM picture of the experiment with 90 wt % MEG, T = 65 °C at $SR_{CaSO_4} = 1$ after 2 hours. Scalebar is 100 µm and magnification is 500.

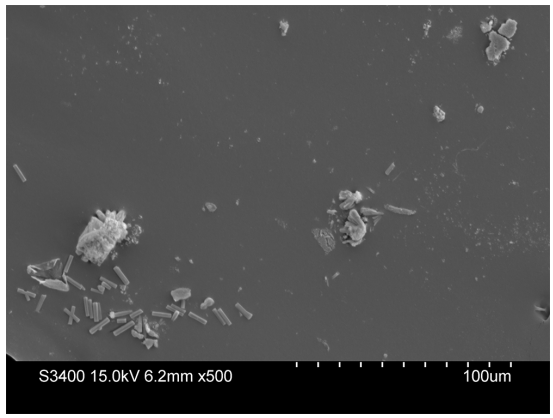

Figure 4.94 – SEM picture of the experiment with 90 wt % MEG, T = 65 °C at $SR_{CaSO_4} = 2.5$ after 15 minutes. Scalebar is 100 µm and magnification is 500.

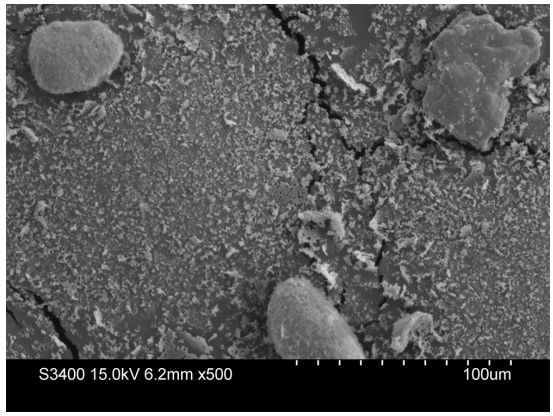

Figure 4.95 – SEM picture of the experiment with 90 wt % MEG, T = 65 °C at $SR_{CaSO_4} = 2.5$ after 2 hours. Scalebar is 100 µm and magnification is 500.

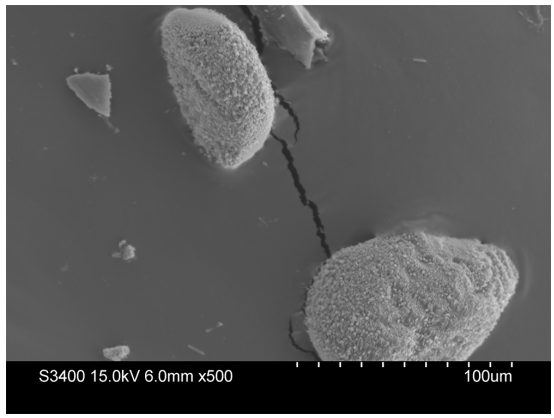

Figure 4.96 – SEM picture of the experiment with 90 wt % MEG, T = 65 °C at $SR_{CaSO_4} = 4$ after 32,5 minutes. Scalebar is 100 µm and magnification is 500.

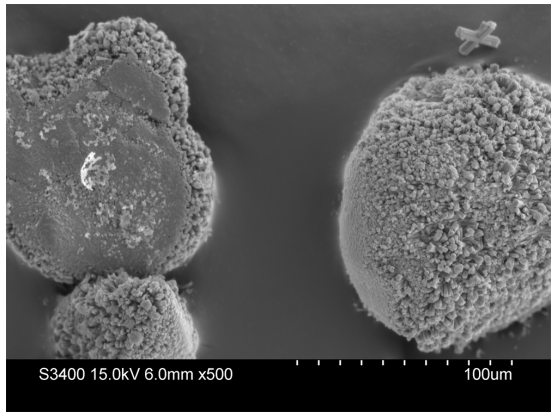

Figure 4.97 – SEM picture of the experiment with 90 wt % MEG, T = 65 °C at $SR_{CaSO_4} = 4$ after 2 hours. Scalebar is 100 µm and magnification is 500.

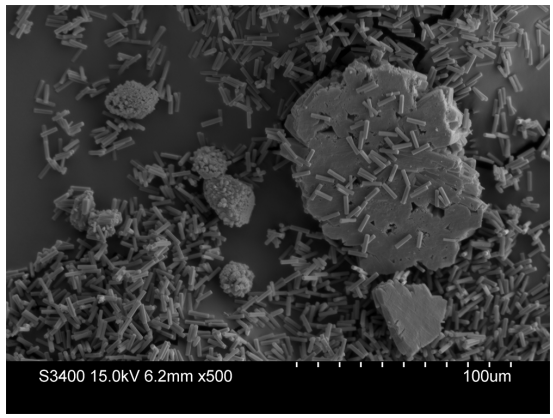

Figure 4.98 – SEM picture of the experiment with 90 wt % MEG, T = 65 °C at $SR_{CaSO_4} = 10$ after 7,5 minutes. Scalebar is 100 µm and magnification is 500.

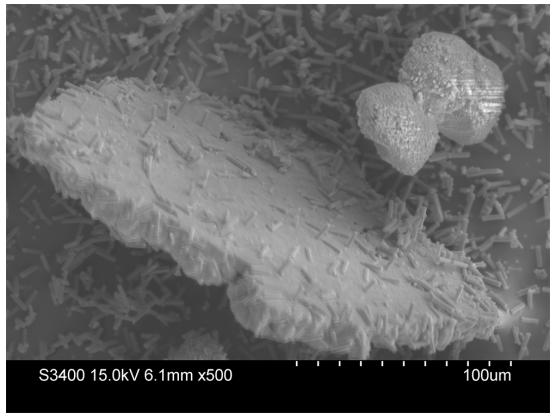

Figure 4.99 – SEM picture of the experiment with 90 wt % MEG, T = 65 °C at $SR_{CaSO_4} = 10$ after 2 hours. Scalebar is 100 µm and magnification is 500.

The crystals formed after 32,5 minutes for $SR_{CaSO_4} = 4$ in figure 4.96 are mostly large calcium sulfate crystals. The presence of calcium sulfate crystals

at 32,5 minutes in the reactor, corresponds well to pH curve in figure 4.89. The decrease in calcium concentration seen in figure 4.90 tells that calcium has precipitated, and comparing pH and titration plots gives an assumption that only calcium carbonate has precipitated. After 2 hours, more crystals have become visible, and the size of the calcium sulfate crystals have increased, see figure 4.97. The XRD-plot confirms that calcium sulfate has precipitated as anhydrite at these conditions.

The crystals formed after 7,5 minutes for $SR_{CaSO_4} = 10$ in figure 4.98 are small uniform anhydrite needles. This corresponds well to the non existent pH decrease. The titration curve shows a large drop in calcium concentration, indicating that calcium has precipitated fast, and at these conditions it is in anhydrite form. After 2 hours, more crystals with other shapes, such as rough spheres and plates have become visible and have increased their size. The small uniform needle shaped anhydrite has the same size as earlier, see figure 4.99. XRD analysis confirms that anhydrite is present.

4.6 Calculations from MultiScale

Thermodynamic calculations in MultiScale were investigated to get a better understanding of the relationship between supersaturation, expected yield and the concentrations of the precipitating ions, calcium, sulfate and carbonate (called alkalinity in the rest of the work). For temperature, T = 65 °C, calculations for 0, 50 and 90 wt % of MEG were conducted for all saturation ratios, SR_{CaSO_4}. For the saturation ratios in the table 4.3, a is a subscript for anhydrite, g is gypsum and h is hemihydrite. All solutions in the experiments, and in the calculations from MultiScale, had target values for gypsum equal to 1, 2.5, 4 or 10. Saturation ratio for calcium carbonate, SR_{CaCO_3}, was held constant in all calculations.

The effect of calcium concentration in the solution and expected yield for all saturation ratios, as well as all wt % of MEG and T = 65 °C were studied in from the table 4.3. Calcium concentration was held constant as the other

parameters shifted. The same study was performed with constant sulfate concentration.

From the table, it is clearly seen that when calcium concentration is held at 100 mmol kg^{-1}, the sulfate concentration needed to get the desired saturation ratio for gypsum decreases with decreasing saturation ratio. The amount of sulfate needed is drastically reduced with increasing MEG concentration. However, for 50 and 90 wt % MEG the sulfate needed, when calcium concentration is held constant, is relatively equal. This might indicate that sulfate solubility in MEG doesn't change that much in solvents with 50 wt % MEG or higher. The same effect can be seen for calcium when sulfate concentration is held constant at 100 mmol kg^{-1}. The concentration of calcium needed at 0 wt % MEG is much greater than the ones for 50 and 90 wt % MEG.

The expected yield, calculated from MultiScale, for calcium carbonate is seen to be held relatively constant at the same operating conditions. When calcium concentration, temperature and MEG concentration is held constant, the expected amount of precipitated calcium carbonate is the same for all saturation ratios of gypsum. With constant sulfate concentrations, the same relationship can not be seen. The expected yield for calcium carbonate when sulfate concentration is held constant varies a lot, and a clear trend can not be seen. It can however be seen an increase, with increasing saturation ratio for gypsum, in the alkalinity needed, when sulfate is held constant. In experiments with 90 wt % MEG, the expected yield of calcium carbonate is zero for all gypsum saturated solutions, and only $SR_{CaSO_{4g}} = 1$ gives an expected amount of precipitation of calcium carbonate.

The expected yield for calcium sulfate anhydrite corresponds well with the sulfate concentration needed when calcium is held constant for 50 and 90 wt % MEG. The higher the MEG concentration, the more similarity is found between expected yield for calcium sulfate and sulfate concentration. At 90 wt % MEG, the expected yield is almost the same as the sulfate concentration needed. Seeing this relationship, makes it possible to assume that sulfate is the limiting ion in precipitation of calcium sulfate when calcium concentration is held at

100 mmol kg^{-1}. It is also seen a decrease in expected yield with decreasing calcium concentration for all SR_{CaSO_4} when sulfate is held constant at 100 mmol kg^{-1}, indicating that at these conditions, calcium might be the limiting factor. For experiments with 50 wt % MEG and constant sulfate, only the highest saturation ratio are expected to give precipitation of calcium sulfate, indicating that the calcium concentration in the solution has to be higher than 6,8 mmol kg^{-1}.

T	wt% MEG	Initial pH	Equilibrium pH	SR_{CaCO_3}	Expected yield $CaCO_3$	$SR_{CaSO_{4a}}$	$SR_{CaSO_{4g}}$	$SR_{CaSO_{4h}}$	Expected yield $CaSO_{4a}$	Ca^{2+}	Alkalinity	SO_4^{2-}
°C	-	-	-	-	[mmol kg^{-1}]	-	-	-	[mmol kg^{-1}]	[mmol kg^{-1}]	[mmol kg^{-1}]	[mmol kg^{-1}]
65	0	6,6012	6,3005	50,0606	14,3259	16,2877	10,0553	2,9383	78,9815	51,55	100	250
65	0	6,5148	5,7424	50,0654	14,5924	6,3847	4,0112	1,1568	35,2686	34,25	100	43,5
65	0	6,4984	5,6823	50,0256	13,8559	3,3817	2,5057	0,7217	18,2929	32,2	100	25
65	0	6,4839	5,6454	50,0442	13,1907	1,6774	1,057	0,3042	4,02	30,57	100	10
65	0	6,4404	5,7011	50,0666	14,4227	16,1748	10,0436	2,9221	91,4866	33,85	176	100
65	0	6,6977	6,2306	50,0892	18,1967	6,5211	4,0911	1,1811	26,3689	52,8	52,4	100
65	0	6,8149	6,2836	50,0084	24,2815	3,9945	2,5083	0,7237	0,9157	67,7	32,15	100
65	0	7,0044	6,8722	50,0228	14,4651	1,69	1,0605	0,3061	0	103,85	15	100
65	50	6,6823	5,8449	50,0724	7,9067	17,9074	10,0604	0,143	10,3718	18,28	100	11
65	50	6,6752	5,831	50,086	7,7341	7,0557	4,0036	0,0565	3,6732	17,88	100	4,28
65	50	6,6733	5,8278	50,0537	7,69	4,4098	2,5084	0,0353	2,0678	17,78	100	2,67
65	50	6,6714	5,8248	50,0922	7,6456	1,8192	1,0373	0,0146	0,5021	17,68	100	1,1
65	50	7,1949	6,9866	50,0063	11,7518	18,4569	10,0735	0,144	2,486	59	15	100
65	50	7,3913	7,3302	50,039	6,6226	7,3907	4,0074	0,0574	0	92,5	6,8	100
65	50	7,4869	7,4554	50,0506	4,5926	4,6665	2,508	0,0359	0	115,5	4,7	100
65	50	7,6631	7,6335	50,0156	2,448	1,8551	1,0231	0,0148	0	174,75	2,5	100
65	90	7,1071	6,268	50,0692	5,6474	254,9065	10,0234	0,0285	10,6577	13,03	100	10,7
65	90	7,1004	6,2553	50,0719	5,5296	102,4307	4,0795	0,0113	4,1593	12,75	100	4,2
65	90	7,0989	6,2523	50,0623	5,4947	62,7282	2,5067	0,0069	2,5196	12,68	100	2,56
65	90	7,0971	6,2497	50,0644	5,4683	27,0535	1,0844	0,003	1,0599	12,62	100	1,1
65	90	7,6231	7,6432	50,0319	0	260,6313	10,0087	0,0299	14,4422	42,1	14,5	100
65	90	7,8186	7,8286	50,0158	0	105,447	4,0471	0,0121	6,4371	65,7	6,5	100
65	90	7,9165	7,9237	50,0747	0	65,6654	2,505	0,0076	4,3418	82,45	4,41	100
65	90	8,0797	8,0658	50,0698	2,3494	28,9124	1,0841	0,0034	0	121	2,4	100

Table 4.3 – Data obtained from calculations in MultScale, used to compare expected yield and concenatration of reactants.

CHAPTER 5

Conclusion

In this work, simultaneously precipitation of two salts with a common cation, has been investigated in a batch system with MEG-water solvent. Temperature, supersaturation and solvent concentration were varied to study the effect of which salt precipitates first, polymorphism and morphology, and induction time for precipitation of the two salts.

The experimental setup let the solutions containing the anions and the cations reach steady state before mixing and thus precipitation. The experimental setup and procedure were the same for all experiments performed.

The pH was found to only decrease with precipitation of calcium carbonate, and not for calcium sulfate, making it a good indicator for which salt precipitates at a given time.

It was found that 0 and 50 wt % MEG concentrations favor precipitation of gypsum at both temperatures. Solvents with 90 wt % MEG favoured precipitation of anhydrite for both temperatures.

The presence of MEG in the solvent was found to inhibit nucleation and growth of both calcium sulfate and calcium carbonate crystals. The size of the

crystals found with increasing concentration of MEG were found to decrease. So was the amount of crystals found in the bulk solution at the end of an experiment.

The effect of temperature was found to have an increase in amount of precipitate at an increase in temperature.

The transition between gypsum and anhydrite was found to favor anhydrite at 90 wt % MEG, and gypsum for lower MEG concentrations. For T = 65 °C the transition occurs between 90 and 50 wt % MEG. Anhydrite was only found at 90 wt % MEG for both temperatures.

The effect of supersaturation was investigated by performing each experiment at four different saturation ratios. High saturation ratios gives large crystals of calcium sulfate, and only small amounts of calcium carbonate. Low saturation ratios, $SR_{CaSO_4} = 1$ only resulted in calcium carbonate precipitation.

It was found from thermodynamical calculations in MultiScale that both calcium and sulfate concentrations effect the expected amount of precipitation of both calcium sulfate and calcium carbonate. Further it was found that both calcium and sulfate concentrations must be sufficiently high to give a desired yield of precipitate.

CHAPTER 6

Suggestions for future work

In this work the simultaneous precipitation of calcium carbonate and calcium sulfate was investigated at some chosen conditions. Further work with different operating conditions, such as T = 90 °C could be interesting. If possible, work with higher temperatures than this is also interesting to look at since higher temperatures and pressures are found in the production of oil and gas.

Higher temperatures might result in a different phase of calcium sulfate, which would be interesting to understand. High pressure studies should be performed if possible, since Total would like to know more about the operating conditions at their production sites.

This study focus only on the precipitation in the bulk liquid in the reactor. Future work should consider the formation of scale on a heated surface. A continuous setup, such as used by Nergaard [4], should be developed for the simultaneous precipitation and formation of scale for these two salts. The scale formation of two salts is complex, but an understanding of the structure of the scale layer would result in more knowledge in how to prevent it from forming, leading to less problems in the oil and gas industry.

Experiments with the opportunity to find the size distribution at a given time, such as experiments in the LabMax setup could be used. The large size difference in the precipitated crystals of calcium carbonate and calcium sulfate would be easy to separate in the LabMax, resulting in a better understanding of what happens in the reactor. The induction time should be determined.

Work with different impurities present in the reactor, such as magnesium, would effect the precipitation, and might be interesting to study further.

List of symbols

Symbol	Unit	Name
A	-	Proportional constant
A	varies	Pre-exponential kinetic parameter
A	m^2	Surface area
a	-	Activity
a^*	-	Activity at equilibrium
$a_\pm$	-	Mean ionic activity
B	varies	Pre-exponential kinetic parameter
b	-	Supersaturation dependance
C	$\mathrm{mol\,L^{-1}}$, $\mathrm{mmol/kg_{solvent}}$	Concentration
c	$\mathrm{mol\,L^{-1}}$, $\mathrm{mmol/kg_{solvent}}$	Concentration
c^*	$\mathrm{mol\,L^{-1}}$	Concentration at equilibrium
d	m	Distance
G	$\mathrm{J\,mol^{-1}}$	Gibbs free energy
G	$\mathrm{m\,s^{-1}}$	Growth rate
g	-	Growth order
I	-	Ionic strength
IAP	-	Ion activity product
J	$\mathrm{mol\,s^{-1}\,L^{-1}}$	Nucleation rate
j	-	Collision
K_g	-	Equilibrium solubility product
K_{SP}	-	Solubility constant
k	$\mathrm{J\,K^{-1}}$	Boltzman constant
k_d	-	Mass transfer coefficient for diffusion
k_r	-	Surface reaction rate coefficient
k_g	-	Growth order constant

Symbol	Unit	Name
L	m	Characteristic dimension
m	g	Mass
m	$\mathrm{mol\,kg^{-1}}$	Molality
M	$\mathrm{g\,mol^{-1}}$	Molecular weight
M_T	$\mathrm{mol\,L^{-1}}$	Concentration of the solids
n	mol	Moles
P	Pa	Pressure
R	$\mathrm{J\,K^{-1}\,mol^{-1}}$	Universal gas constant
r	m	Radius
S	-	Supersaturation
SR	-	Supersaturation ratio
T	K	Temperatur
t	s	Time
t_{ind}	s	Induction time
t_g	s	Growth time
t_{lp}	s	Latent period
t_n	s	Nucleation time
t_r	s	Relaxation time
v	-	Number of moles of ions in one mole of solution

Symbol	Unit	Name
γ	-	Activity coefficient
γ	-	Interfacial tension
Δ	-	Change
ϵ	-	Average power input from agitator
θ	-	Bragg's angle
θ	-	Contact angle
λ	nm	Wavelength
μ	-	Chemical potential
σ	-	Supersaturation
ϕ	-	Factor for nucleation

Bibliography

[1] Torunn Kvam, Jens-Petter Andreassen, and Ralf Beck. Precipitation in pre-treatment for regeneration of ethylene glycol, 2011.

[2] J. P. Andreassen. *Short course on precipitation and crystallization from solution.* Trondheim, NTNU.

[3] J. W. Mullin. *Crystallisation.* Chemical engineering series. Butterworths, London, 2nd ed. edition, 1972.

[4] Margrethe Nergaard, Jens-Petter Andreassen, and Ralf Beck. Scaling of calcium carbonate at heated surfaces in a continuous system, 2012.

[5] Ichiro Sunagawa. *Crystals : growth, morphology, and perfection.* Cambridge University Press, Cambridge, 2005.

[6] Takeshi Ogino, Toshio Suzuki, and Kiyoshi Sawada. The formation and transformation mechanism of calcium carbonate in water. *Geochimica et Cosmochimica Acta*, 51(10):2757–2767, 1987.

[7] Kristian Sandengen and materialteknologi Norges teknisk-naturvitenskapelige universitet Institutt for. *Prediction of mineral scale formation in wet gas condensate pipelines and in MEG (Mono Ethylene Glycol) regeneration plants.* Thesis, 2006. Avhandling (ph.d.) - Norges teknisk-naturvitenskapelige universitet, Trondheim, 2006.

[8] Baard Kaasa, Kristian Sandengen, and Terje Ostvold. Thermodynamic predictions of scale potential, ph and gas solubility in glycol containing systems, 2005/1/1/.

[9] Margrethe Hyllestad, Jens-Petter Andreassen, and Margrethe Nergaard. Scaling of calcium carbonate on a heated surface in a flow through system with mono ethylene glycol., 2013.

[10] T. H. Chong and R. Sheikholeslami. Thermodynamics and kinetics for mixed calcium carbonate and calcium sulfate precipitation. *Chemical Engineering Science*, 56(18):5391–5400, 2001.

[11] Ellen Marie Flaten, Marion Seiersten, and Jens-Petter Andreassen. Induction time studies of calcium carbonate in ethylene glycol and water. *Chemical Engineering Research and Design*, 88(12):1659–1668, 2010.

[12] Ellen Marie Flaten, Marion Seiersten, and Jens-Petter Andreassen. Polymorphism and morphology of calcium carbonate precipitated in mixed solvents of ethylene glycol and water. *Journal of Crystal Growth*, 311(13):3533–3538, 2009.

[13] Pavlos G. Klepetsanis, Evangelos Dalas, and Petros G. Koutsoukos. Role of temperature in the spontaneous precipitation of calcium sulfate dihydrate. *Langmuir*, 15(4):1534–1540, 1999.

[14] Therese Bache, Jens-Petter Andreassen, and Xiaoguang Ma. Scaling and precipitation risk of calcium sulfate in meg, 2015.

[15] S. Helbæk, M. Kjelstrup. *Fysikalsk Kjemi*. Fagbokforlaget, Bergen, 2. utgave. edition, 2009.

[16] Shilpa Seewoo, Rob Van Hille, and Alison Lewis. Aspects of gypsum precipitation in scaling waters. *Hydrometallurgy*, 75(1–4):135–146, 2004.

[17] Guozhong Cao. *Nanostructures And Nanomaterials : Synthesis, Properties And Applications*. Nanostructures And Nanomaterials: Synthesis,

Properties And Applications. World Scientific Publishing Company, Singapore, 2004.

APPENDIX A

Chemicals

The chemicals used in the experiments are listed in table A.1 below.

Chemical	Formula	Molecular weight [g mol^{-1}]	Purity [%]	Supplier
Calcium chloride dihydrate	$CaCl_2 \cdot 2H_2O$	147.02	99-103	Fluka Analytical Sigma-Aldrich
EDTA	$C_{10}H_{16}N_2O_8$	292.24	Titrisol(lll)[4]	Merck
Ethanol	C_2H_6O	46.10	96	Sigma-Aldrich
Hydrochloric acid	HCl	36.46	37	VWR International
Monoethylene glycol (MEG)	$C_2H_6O_2$	62.07	-	Fluka Analytical Sigma-Aldrich
Sodium bicarbonate	$NaHCO_3$	84.01	-	Sigma-Aldrich
Sodium sulfate	$NaSO_4$	142.04	-	Sigma-Aldrich
Ammonia	NH_3	17,03	> 25	VWR

Table A.1 – List of chemicals used in the project work.

APPENDIX B

Calculations

Supersaturation

From MultiScale, the concentration of each chemical is calculated to reach a specific supersaturation, and the calculated concentrations are given as mmol kg^{-1}. To calculate the necessary amount of chemicals needed in the experiements, the following equation is used for chemical A:

$$m_A[g] = c_A[\text{mmol}\,\text{kg}^{-1}] \cdot [\text{mol}/1000 \cdot \text{mmol}] \cdot M_A[\text{g}\,\text{mol}^{-1}] \cdot X_{tot}[\text{kg}_{\text{solvent}}] \quad \text{(B.1)}$$

The amount of solvent is the total amount of solvent used in the two solutions.

$$X_{tot} = X_A + X_B \quad \text{(B.2)}$$

Where X_A are the amount of solvent in solution 1, and X_B the amount of solvent in solution 2.

Titration with EDTA

From titration with EDTA, the amount of calcium ions in the reactor at a given time could be calculated. The amount of solution in the sample was calculated

using equation B.3.

$$\text{Amount of sample} = \text{Amount of sample cup and sample} - \text{Amount og sample cup} \tag{B.3}$$

When the equivalent point is reached in the titration, the amount of EDTA used is found. To determine the concentration of calcium ions in the sample, equation B.4 is used, with concentration of EDTA equal to 0,01 $\mathrm{mol\,L^{-1}}$.

$$[Ca^{2+}] = 1000 \cdot \frac{[EDTA] \cdot \text{Amount of EDTA in sample}}{\frac{\text{Amount of sample}}{1000}} \tag{B.4}$$

The equation above B.4 has the following units:

$$[\mathrm{mmol\,kg^{-1}}] = 1000 \cdot \frac{[\mathrm{mol\,L^{-1}}]}{\frac{[\mathrm{mmol}]}{1000}} \tag{B.5}$$

APPENDIX C

Experimental conditions

Table C.1 – Experimental conditions for all experiments.

Exp. no	T	wt% MEG	Initial pH	Equilibrium pH	SR_{CaCO_3}	Expected yield	$SR_{CaSO_4{}_a}$	$SR_{CaSO_4{}_g}$	$SR_{CaSO_4{}_h}$	Expected yield	Ca^{2+}	Alkalinity	SO_4^{2-}
-	°C	-	-	-	-	[mmol kg^{-1}]	-	-	-	[mmol kg^{-1}]	[mmol kg^{-1}]	[mmol kg^{-1}]	[mmol kg^{-1}]
1	65	0	5.8673	5.9184	1.4012	0	6.3804	4.0305	1.1589	40.4963	7.15	53	65
2	65	50	6.0560	6.0667	1.0209	0	6.0000	4.0949	0.0489	4.3024	3.3	20	5.2
3	65	0	6.6191	6.3403	50.0458	14.84	16.4836	10.0774	2.9529	74.9877	55.5	96	300
4	65	50	6.8370	6.0926	50.2889	9.6060	16.4389	10.1477	0.1325	13.1172	22.9	40	14.2
5	65	0	6.6036	5.8178	50.1870	15.3939	1.7238	1.0905	0.3129	4.5952	36.30	50	13.5
6	65	50	7.0642	6.7466	50.0991	9.2926	1.5084	1.0404	0.0122	0	33.70	10	2.30
7	65	0	6.6471	6.1360	50.0521	16.6296	6.5068	4.0893	1.1791	33.4102	45.7	60	75
8	65	50	6.9441	6.3311	50.0059	10.5149	6.1881	4.0846	0.0501	4.5535	33.6	40	48.5
9	65	50	6.9288	6.2429	50.1542	10.5461	3.7410	2.5044	0.0310	2.2922	27	20	6.8
10	65	50	6.7696	6.4886	50.002222	6.7698	240.8929	10.0197	0.0223	11.7458	26	20	3.9
11	65	90	7.2457	6.4248	50.0597	6.4069	93.3743	4.0708	0.0086	4.1541	15.9	40	11.8
12	65	90	7.2401	6.4130	50.0889	6.3203	56.4814	2.4969	0.0052	2.4553	14.89	40	4.2
13	65	90	7.2345	6.4032	50.0022	6.2343	22.8866	1.0226	0.0021	0.9363	14.67	40	2.5
14	65	90	6.4984	5.6822	50.0256	13.8559	3.9817	2.5057	0.7217	18.2929	14.46	40	1
15	65	0	6.4984	5.6822	50.0256	13.8559	3.9817	2.5057	0.7217	18.2929	32.30	100	25
16	65	0	6.5149	5.742	50.0949	14.5943	6.3727	4.0038	1.1547	35.1792	34.25	100	43.4
17	65	0	6.6012	6.3095	50.0606	14.3259	16.2877	10.0553	2.9383	78.9815	51.55	100	290
18	65	0	6.4838	5.6448	50.0807	13.1832	1.6283	1.0261	0.2953	3.7315	30.55	100	9.70
19	30	0	6.591167	6.1574	50.0922	32.0741	8.4568	10.0953	1.2693	91.4456	98.4	140	243.5
20	30	0	6.5039	5.7141	50.0522	28.9328	3.2967	4.0034	0.4969	30.4207	68.3	140	45.8
21	30	0	6.4901	5.6736	50.0169	27.7010	2.0591	2.5049	0.3105	13.1544	64.9	140	26.5
22	30	0	6.4781	5.6466	50.0980	26.5971	0.8320	1.0137	0.1255	0	62.1	140	10.1
23	30	50	6.7460	5.93	50.0849	18.8617	9.3855	10.0871	0.0620	11.4902	44.15	100	12.9
24	30	50	6.7365	5.9089	50.0809	18.35181	3.6932	4.0159	0.0245	3.5663	42.85	100	4.90
25	30	50	6.7343	5.9044	50.0795	18.2309	2.3008	2.5089	0.0152	1.7114	42.55	100	3.03
26	30	50	6.7319	5.9002	50.0464	18.1077	0.9173	1.0029	0.0029	0	42.25	100	1.2
27	30	90	7.2333	6.4113	50.0891	13.4102	164.2298	10.0838	0.0131	14.5138	31.1	100	14.6
28	30	90	7.2190	6.3856	50.0384	12.9312	64.0635	4.0657	0.0051	5.3181	30.12	100	5.4
29	30	90	7.2156	6.3801	50.0182	12.8189	39.2276	2.5094	0.0031	3.1889	29.85	100	3.27
30	30	90	7.2129	6.3754	50.0469	12.7279	16.9508	1.0920	0.0013	1.3195	29.63	100	1.4
31	30	90	6.6821	5.8449	50.0214	7.9017	17.9080	10.0607	0.1430	10.3718	18.27	100	11
32	65	50	6.6749	5.8319	50.0278	7.7290	7.0887	4.0223	0.0567	3.6931	17.87	100	4.3
33	65	50	6.6733	5.8278	50.0529	7.69	4.4098	2.5084	0.0353	2.0678	17.78	100	2.67
34	65	50	6.6714	5.8248	50.0022	7.6456	1.8192	1.0373	0.0149	0.5021	17.68	100	1.1
35	65	90	6.2488	6.2453	1.0277	0.0143	101.5071	4.0735	0.0112	3.9602	1.7	100	4
36	30	90	6.2309	6.2252	1.0368	0.0382	52.0787	4.0556	0.0048	4.2178	4	100	4.3
37	30	50	5.8851	5.8672	1.0949	0.1354	3.6367	4.0846	0.0256	3.3317	6	100	4.60
38	30	0	5.7109	5.7312	1.0619	0	3.3371	4.0818	0.5039	32.0456	10.5	100	47

APPENDIX D

Total

The thermodynamical data obtain from Total is attached below.

Case study: precipitation of CaCO3, CaSO4 and SrSO4 in presence of MEG and MEG+MDEA

Table 1: waters compositions SDX-3Y (SP3), SDX-4 (SP3), SDA-03Z and condensed water

Ion	SDX-3Y (SP3) (mg/l)	SDX- 4 (SP3) (mg/l)	SDA-03Z (mg/l)	Condensed water (mg/l)
Sodium	5454	8388	4752	159.51
Potassium	44.70	94	30	1.47
Calcium	323.03	1052.68	552.93	11.78
Magnesium	46.10	36	12.80	0.92
Barium	0.10	0.32	0	0.00
Strontium	14.00	47.65	24	0.53
Iron	0.2	8	0	0.00
Chloride	4900	12900	6500	194.44
Sulphate	5357.99	1945.48	2562.45	75.80
Bicarbonate	423.91	734.65	432.77	75.80
Bromide	24.20	99.5	0.00	0.00
Carboxylic acids	355	683.7	383	8.58
pH	6.85	7.74	6.71	7.26
TDS	16588.37	25299.53	14867.18	468.64

Table 2: CO2 and H2S content in the gas phase

CO_2	0.5 Molar %
H_2S	3ppm

Table 3: Production rates for the field

Year	Gas	Condensate	Water	Condensed water	MEG
	MMscf/d	STB/d	STB/d	STB/d	m^3/d
09/01/2027	551.44	34510.25	1947.43	286.27	240

Table 4: Reservoir and well pressure and temperature

Year	WH Pressure (bar)	WH temperature (°C)	Reservoir Temperature (°C)	Reservoir pressure (bar)
09/01/2027	143.66	71.06	318.06	507.77

Table 5: Saturation indexes for common scale deposits from manifold to surface units, early life (2027) Simulations performed with scalesoft Pitzer

Point in the process	Chemicals	Type of Scale	Results					
			SDX-3Y (SP3)		SDX-4 (SP3)		SDA-03Z	
			SI	mg/l	SI	mg/l	SI	mg/l
Heat exchangers (P=12bar; T=65°C)	Without MEG	$CaCO_3$	-0.86	0.00	-0.85	0.00	-0.86	0.00
		$BaSO_4$	0.00	0.00	0.00	0.00	0.00	0.00
		$Ca\ SO_4$	-0.10	0.00	-0.11	0.00	-0.10	0.00
		$SrSO_4$	0.15	8	0.18	29	0.17	14
	With MEG	$CaCO_3$	-0.76	0.00	-0.50	0.00	-0.63	0.00
		$BaSO_4$	0.00	0.00	0.00	0.00	0.00	0.00
		$Ca\ SO_4$	1.01	854	1.02	1855	1.00	1357
		$SrSO_4$	1.36	25	1.38	84	1.37	42
	With MEG and MDEA	$CaCO_3$	3.36	707	3.58	2296	3.51	1208
		$BaSO_4$	0.00	0.00	0.00	0.00	0.00	0.00
		$Ca\ SO_4$	0.48	610	0.54	1246	0.40	782
		$SrSO_4$	0.37	15	0.47	57	0.31	22
Heat exchangers (P=19bar; T=165°C)	Without MEG	$CaCO_3$	0.46	19	0.57	21	0.56	18
		$BaSO_4$	0.00	0.00	0.00	0.00	0.00	0.00
		$Ca\ SO_4$	1.12	878	1.14	1949	1.17	1440
		$SrSO_4$	0.94	23	0.83	74	0.93	39
	With MEG	$CaCO_3$	0.42	67	0.77	141	0.64	84
		$BaSO_4$	0.00	0.00	0.00	0.00	0.00	0.00
		$Ca\ SO_4$	2.64	959	2.68	2396	2.68	1636
		$SrSO_4$	1.73	25	1.63	85	1.73	43
	With MEG and MDEA	$CaCO_3$	3.95	707	4.14	2296	4.11	1208
		$BaSO_4$	0.00	0.00	0.00	0.00	0.00	0.00
		$Ca\ SO_4$	1.94	949	1.99	2322	1.86	1597
		$SrSO_4$	0.51	18	0.54	62	0.42	27
Heat exchangers (P=149bar; T=29°C)	Without MEG	$CaCO_3$	-1.39	0.00	-1.39	0.00	-1.39	0.00
		$BaSO_4$	0.00	0.00	0.00	0.00	0.00	0.00
		$Ca\ SO_4$	-0.56	0.00	-0.56	0.00	-0.55	0.00
		$SrSO_4$	-0.03	0.00	0.01	1	-1.01	0.00
	With MEG	$CaCO_3$	-1.49	0.00	-1.20	0.00	-1.34	0.00
		$BaSO_4$	0.00	0.00	0.00	0.00	0.00	0.00
		$Ca\ SO_4$	0.35	494	0.37	931	0.34	688
		$SrSO_4$	1.13	24	1.16	81	1.15	41
	With MEG and MDEA	$CaCO_3$	2.85	707	3.10	2296	3.02	1208
		$BaSO_4$	0.00	0.00	0.00	0.00	0.00	0.00
		$Ca\ SO_4$	-0.11	0.00	-0.05	0.00	-0.18	0.00
		$SrSO_4$	0.21	10	0.30	43	0.16	13

APPENDIX E

Calibration of titrator

The calibration of the Metler Toledo DL53 titrator was performed in the specialization work by Bache [14]. The titrator unit had some uncertainties in performance, and was calibrated to determine the per cent of uncertainty. Samples with approximately $0,5 \text{mmol kg}^{-1}$, calcium concentration were prepared, and weighed to get the weight of the sample. Titration with EDTA was performed and the table E.1 below shows the result from the calibration. The results were calculated using the equations in appendix B. The average concentration was

Table E.1 – Calibration of titrator unit

Parallells #	Volume of sample [mmol]	Equvalence point [mL]	Concentration [mmol kg^{-1}]
1	10,9443	0,578660	0,528732
2	10,5859	0,546061	0,515838
3	10,7328	0,549237	0,511736

calculated to 0,518 with a standard deviation 0,007. This gives an uncertainty of approximately 0,7 %.

APPENDIX F

Risk analysis

The risk assesment is attached below.

ID	1540	**Status**	**Dato**
Risikoområde	Risikovurdering: Helse, miljø og sikkerhet (HMS)	Opprettet	22.09.2015
Opprettet av	Therese Bache	Vurdering startet	22.09.2015
Ansvarlig	Jens-Petter Andreassen	Tiltak besluttet	
		Avsluttet	

EEART, Prosjekt/Master 2016, Therese Bache - Simultaneous precipitation of calcium sulfate and calcium carbonate during glycol regeneration

Gyldig i perioden:

9/21/2015 - 9/21/2018

Sted:

Laboratories IKP - K4-115 and K4-008

Mål / hensikt

Risk assessment of the work Therese Bache will perform related to laboratories at IKP.

Bakgrunn

Experimental work:
- Running a glass reactor
- Mechanical stirrer
- Waterbath
- Filtration with water vacuum
- Solution preparation and transportation
- Waste disposal

Beskrivelse og avgrensninger

Existing risk assessments for equipments and activities:
- Crystallization - growth of calcium carbonate and in water

Risk assessments for chemicals:
- CaCl2*2H2O
-NaHCO3
-Na2SO4
-MEG
-HCl
-NaOH

Water temperatures between 45 - 90 oC
Pressure in closed reactor is 1 atm

Forutsetninger, antakelser og forenklinger

Activities that does not include any dangers (chemicals, gases or high temperatures) does not need to be risk assessed.

Vedlegg

Risk assesment Crystallization (1).xlsx

Referanser

Preparation of solutions(https://avvik.ntnu.no/Risk/EditRiskAssessment/162)

Oppsummering, resultat og endelig vurdering

I oppsummeringen presenteres en oversikt over farer og uønskede hendelser, samt resultat for det enkelte konsekvensområdet.

Farekilde: **Waste disposal**

Uønsket hendelse: **Spill of waste on bench or floor**

Skal ikke analyseres.

Farekilde: **Preparation of solutions**

Uønsket hendelse: **Spill on bench or floor**

Skal ikke analyseres.

Uønsket hendelse: **Spill on humans**

Konsekvensområde: Helse Risiko før tiltak: Risiko etter tiltak:

Uønsket hendelse: **Breaking of glass equipment**

Konsekvensområde: Helse Risiko før tiltak: Risiko etter tiltak:

Farekilde: **Running the experiment**

Uønsket hendelse: **Hair into stirrer engine**

Konsekvensområde: Helse Risiko før tiltak: Risiko etter tiltak:

Uønsket hendelse: **scalding by hot water from the reactor jacket**

Konsekvensområde: Helse Risiko før tiltak: Risiko etter tiltak:

Uønsket hendelse: **Loss of cooling water**

Konsekvensområde: Helse Risiko før tiltak: Risiko etter tiltak:

Farekilde: **Preparation of samples for analysis**

Uønsket hendelse: **Spill on bench or floor**

Skal ikke analyseres.

Uønsket hendelse: **Spill on humans**

Konsekvensområde: Helse Risiko før tiltak: Risiko etter tiltak:

Farekilde: **Cleaning the equipment**

Uønsket hendelse: **Spill of acid on bench or floor**

Konsekvensområde: Helse Risiko før tiltak: Risiko etter tiltak:

Uønsket hendelse: **Spill of acid on humans**

Konsekvensområde: Helse Risiko før tiltak: Risiko etter tiltak:

Uønsket hendelse: **Hair into stirrer enginge**

Skal ikke analyseres.

Uønsket hendelse: **Hot glass reactor**

Konsekvensområde: Helse Risiko før tiltak: Risiko etter tiltak:

Endelig vurdering

Oversikt involverte enheter og personell

En risikovurdering kan gjelde for en, eller flere enheter i organisasjonen. Denne oversikten presenterer involverte enheter og personell for gjeldende risikovurdering.

Enhet /-er risikovurderingen omfatter

- Institutt for kjemisk prosessteknologi

Deltakere

Mikael Hammer

Gøril Flatberg

Lesere

Seniz Ucar

Xiaoguang Ma

Andre involverte/interessenter

[Ingen registreringer]

Følgende akseptkriterier er besluttet for risikoområdet Risikovurdering: Helse, miljø og sikkerhet (HMS):

Helse	Materielle verdier	Omdømme	Ytre miljø
			

Oversikt over eksisterende, relevante tiltak som er hensyntatt i risikovurderingen

I tabellen under presenteres eksisterende tiltak som er hensyntatt ved vurdering av sannsynlighet og konsekvens for aktuelle uønskede hendelser.

Farekilde	Uønsket hendelse	Tiltak hensyntatt ved vurdering
Preparation of solutions	Spill on humans	Personal protective equipment
	Spill on humans	Use of fume cupboard
	Spill on humans	HSE training
	Breaking of glass equipment	Personal protective equipment
	Breaking of glass equipment	Use of fume cupboard
	Breaking of glass equipment	HSE training
Running the experiment	Hair into stirrer engine	HSE training
	scalding by hot water from the reactor jacket	Personal protective equipment
	scalding by hot water from the reactor jacket	Equipment training and user manuals
	scalding by hot water from the reactor jacket	HSE training
	Loss of cooling water	Equipment training and user manuals
	Loss of cooling water	HSE training
Preparation of samples for analysis	Spill on humans	Personal protective equipment
	Spill on humans	Use of fume cupboard
	Spill on humans	Equipment training and user manuals
	Spill on humans	HSE training
Cleaning the equipment	Spill of acid on bench or floor	Personal protective equipment
	Spill of acid on bench or floor	Use of fume cupboard
	Spill of acid on bench or floor	Equipment training and user manuals
	Spill of acid on bench or floor	HSE training
	Spill of acid on humans	Personal protective equipment
	Spill of acid on humans	HSE training
	Hot glass reactor	Personal protective equipment
	Hot glass reactor	Equipment training and user manuals
	Hot glass reactor	HSE training

Eksisterende og relevante tiltak med beskrivelse:

Personal protective equipment
Goggles, labcoat and gloves. Covering shoes and heat glove when handeling hot equipment.

Use of fume cupboard
Preparation of solutions

Equipment training and user manuals

- SEM (Scanning electron microscope)
- XRD (X-ray diffraction)
- Titrator
- Microscope
- Coulter Counter

HSE training

HSE training has been given by the department.

Risikoanalyse med vurdering av sannsynlighet og konsekvens

I denne delen av rapporten presenteres detaljer dokumentasjon av de farer, uønskede hendelser og årsaker som er vurdert. Innledningsvis oppsummeres farer med tilhørende uønskede hendelser som er tatt med i vurderingen.

Følgende farer og uønskede hendelser er vurdert i denne risikovurderingen:

- **Preparation of solutions**
  - Spill on humans
  - Breaking of glass equipment
- **Running the experiment**
  - Hair into stirrer engine
  - scalding by hot water from the reactor jacket
  - Loss of cooling water
- **Preparation of samples for analysis**
  - Spill on humans
- **Cleaning the equipment**
  - Spill of acid on bench or floor
  - Spill of acid on humans
  - Hot glass reactor

Oversikt over besluttede risikoreduserende tiltak med beskrivelse:

Waste disposal (farekilde)

Transportation of waste canisters (25L) from the labs to the chemical waste storage.

Waste disposal/Spill of waste on bench or floor (uønsket hendelse)

Might spill waste

Samlet sannsynlighet vurdert for hendelsen: (0)

Kommentar til vurdering av sannsynlighet:

[Ingen registreringer]

Vurdering av risiko for følgende konsekvensområde: Helse

Vurdert sannsynlighet (felles for hendelsen): (0)

Vurdert konsekvens: ()

Kommentar til vurdering av konsekvens:

[Ingen registreringer]

Preparation of solutions (farekilde)

Preparation of solutions/Spill on humans (uønsket hendelse)

Samlet sannsynlighet vurdert for hendelsen: Svært sannsynlig (5)

Kommentar til vurdering av sannsynlighet:

Not harmful chemicals, will prepare a lot of solutions

Vurdering av risiko for følgende konsekvensområde: Helse

Vurdert sannsynlighet (felles for hendelsen): Svært sannsynlig (5)

Vurdert konsekvens: Liten (1)

Kommentar til vurdering av konsekvens:

Might spill NaOH?

Preparation of solutions/Breaking of glass equipment (uønsket hendelse)

Glass may shatter if i handel it wrong. Might get cut on glass if glass equipment is broken

Samlet sannsynlighet vurdert for hendelsen: Ganske sannsynlig (4)

Kommentar til vurdering av sannsynlighet:

Can be uncareful whhen preparing solutions, and might knock over the glass bottle so the glass breaks

Vurdering av risiko for følgende konsekvensområde: Helse

Vurdert sannsynlighet (felles for hendelsen): Ganske sannsynlig (4)

Vurdert konsekvens: Liten (1)

Kommentar til vurdering av konsekvens:

Will only use chemicals not very harmful to humans. A cut in the hand could happen when cleaning, but only solutions of different ubharmful salts will be in the glass equipment

Running the experiment (farekilde)

Running the experiment/Hair into stirrer engine (uønsket hendelse)

Samlet sannsynlighet vurdert for hendelsen: Lite sannsynlig (2)

Kommentar til vurdering av sannsynlighet:

Will have hair up.

Vurdering av risiko for følgende konsekvensområde: Helse

Vurdert sannsynlighet (felles for hendelsen): Lite sannsynlig (2)

Vurdert konsekvens: Liten (1)

Kommentar til vurdering av konsekvens:

Will have hair up, and a few starnd of hair is not that harmful to loose

Running the experiment/scalding by hot water from the reactor jacket (uønsket hendelse)

Samlet sannsynlighet vurdert for hendelsen: Sannsynlig (3)

Kommentar til vurdering av sannsynlighet:

have been some spill before

Vurdering av risiko for følgende konsekvensområde: Helse

Vurdert sannsynlighet (felles for hendelsen): Sannsynlig (3)

Vurdert konsekvens: Stor (3)

Kommentar til vurdering av konsekvens:

Might get burned

Running the experiment/Loss of cooling water (uønsket hendelse)

evaporation of MEG when heated

Samlet sannsynlighet vurdert for hendelsen: Lite sannsynlig (2)

Kommentar til vurdering av sannsynlighet:

Sjekk slangen for skader, ikke sannsynlig at vannet ryker

Vurdering av risiko for følgende konsekvensområde: Helse

Vurdert sannsynlighet (felles for hendelsen): Lite sannsynlig (2)

Vurdert konsekvens: Liten (1)

Kommentar til vurdering av konsekvens:

Evaporation of MEG, not harmful

Preparation of samples for analysis (farekilde)

Preparation of samples for analysis/Spill on humans (uønsket hendelse)

Might spill EDTA and NH3/NH4 + buffer

Samlet sannsynlighet vurdert for hendelsen: Ganske sannsynlig (4)

Kommentar til vurdering av sannsynlighet:

Know that i might work with more harmful chemicals, and will therfore be more aware when preparing the solutions. Spill of solutions happen.

Vurdering av risiko for følgende konsekvensområde: Helse

Vurdert sannsynlighet (felles for hendelsen): Ganske sannsynlig (4)

Vurdert konsekvens: Liten (1)

Kommentar til vurdering av konsekvens:

Might get some chemicals on the skin, but know how to handle. and the chemicals will be dilluted?

Cleaning the equipment (farekilde)

Cleaning the equipment/Spill of acid on bench or floor (uønsket hendelse)

Might spill HCl

Samlet sannsynlighet vurdert for hendelsen: Ganske sannsynlig (4)

Kommentar til vurdering av sannsynlighet:

Solutions will get on the bench or floor if i spill, know that im working with acid, and will therfore be careful

Vurdering av risiko for følgende konsekvensområde: Helse

Vurdert sannsynlighet (felles for hendelsen): Ganske sannsynlig (4)

Vurdert konsekvens: Middels (2)

Kommentar til vurdering av konsekvens:

dilluted acid, will use safety equipment, will clean up if i spill.

Cleaning the equipment/Spill of acid on humans (uønsket hendelse)

Might spill HCl

Samlet sannsynlighet vurdert for hendelsen: Ganske sannsynlig (4)

Kommentar til vurdering av sannsynlighet:

Know it is acid, will be careful and use safety equipment

Vurdering av risiko for følgende konsekvensområde: Helse

Vurdert sannsynlighet (felles for hendelsen): Ganske sannsynlig (4)

Vurdert konsekvens: Middels (2)

Kommentar til vurdering av konsekvens:

will be careful and use safety equipment

Cleaning the equipment/Hot glass reactor (uønsket hendelse)

Hot due to high temperature in water jacket

Samlet sannsynlighet vurdert for hendelsen: Sannsynlig (3)

Kommentar til vurdering av sannsynlighet:

Might get burned, but will use heat gloves when handleing hot equipment

Vurdering av risiko for følgende konsekvensområde: Helse

Vurdert sannsynlighet (felles for hendelsen): Sannsynlig (3)

Vurdert konsekvens: Middels (2)

Kommentar til vurdering av konsekvens:

Might get burned. Will use safety equipment, and handle hot equipment with care

Oversikt over besluttede risikoreduserende tiltak:

Under presenteres en oversikt over risikoreduserende tiltak som skal bidra til å reduseres sannsynlighet og/eller konsekvens for uønskede hendelser.

Oversikt over besluttede risikoreduserende tiltak med beskrivelse: